

8-12-2016

Synthesis and Characterization of Amphiphiles for Mammalian Cell Transfection and Antimicrobial Activity

Joseph William Meisel

University of Missouri-St. Louis, jwmeisel@gmail.com

Follow this and additional works at: <https://irl.umsl.edu/dissertation>



Part of the [Chemistry Commons](#)

Recommended Citation

Meisel, Joseph William, "Synthesis and Characterization of Amphiphiles for Mammalian Cell Transfection and Antimicrobial Activity" (2016). *Dissertations*. 65.

<https://irl.umsl.edu/dissertation/65>

This Dissertation is brought to you for free and open access by the UMSL Graduate Works at IRL @ UMSL. It has been accepted for inclusion in Dissertations by an authorized administrator of IRL @ UMSL. For more information, please contact marvinh@umsl.edu.

Synthesis and Characterization of Amphiphiles for Mammalian Cell Transfection and Antimicrobial Activity

Joseph W. Meisel

Master of Science in Chemistry, University of Missouri-St. Louis, 2013

Bachelor of Science in Biochemistry, Indiana University, 2009

Bachelor of Science in Human Biology, Indiana University, 2009

A Dissertation Submitted to the Graduate School at the

University of Missouri-St. Louis

in Partial Fulfillment of the Requirements for the Degree of

DOCTOR OF PHILOSOPHY

in

CHEMISTRY

August 2016

Dissertation Committee

George W. Gokel, Ph.D.

Chairperson

James K. Bashkin, Ph.D.

Michael R. Nichols, Ph.D.

Christopher D. Spilling, Ph.D.

ABSTRACT OF THE DISSERTATION

Synthesis and Characterization of Amphiphiles for Mammalian Cell Transfection and Antimicrobial Activity

by

Joseph W. Meisel

Doctor of Philosophy in Chemistry

University of Missouri-St. Louis, 2016

Dr. George W. Gokel, Advisor

Amphiphiles are molecules that contain both hydrophilic and hydrophobic components. The dual nature of these molecules engenders remarkable properties including the ability to self-assemble into ordered structures. Cell membranes are composed of amphiphilic phospholipids that organize into a bilayer motif. Synthetic amphiphiles can interact with natural membranes and influence the transport of molecules across the cell membrane. The work elaborated in this report employs amphiphiles to co-assemble with DNA and transport the genetic material across cell membranes.

First, a simplified method for interacting DNA with amphiphiles was developed. Typically, a liposome containing cationic lipids and often helper lipids is prepared in a multistep process. Then, the liposome is mixed with DNA to spontaneously form a lipid-DNA complex. An abbreviated method was developed by dissolving lipids in an aqueous-miscible organic solvent and mixing directly with DNA. The lipid-DNA complexes formed by this method had similar properties as assessed by agarose gel electrophoresis, dynamic light scattering, and electron microscopy. The complexes were compared against the standard procedure in the transfection of two different mammalian epithelial cell lines with plasmid DNA encoding a green fluorescent protein. The different methods yielded comparable results. This direct-mixing method obviates a liposomal intermediate thereby broadening the range of chemical structures that can be tested in transfection.

Second, a series of known ion-transporting compounds were assayed for their interaction with DNA. Hydraphile and lariat ethers are ionophoric compounds consisting of diaza-18-crown-6 subunits. The former act as ion channels in lipid membranes and the latter are putative ion carriers. Utilizing the direct-mixing method established herein, the effects of hydrocarbon chain length, DNA counter-cation, and buffer pH were assessed by agarose gel electrophoresis. The results support a model wherein protonated diazacrown ethers interact with the negatively charged phosphate backbone of DNA. The hydrophobic aliphatic chains then self-associate resulting in a condensed DNA nanoparticle.

Third, a new class of DNA-binding molecules was designed and characterized. The molecules consist of two amino acids coupled via their carboxy-termini to a diamine linker. The remaining amino termini are exposed and are protonated at physiological pH. Arylene and alkylene linkers were investigated, as were various amino acids. *Bis*(aminoamide) compounds containing the hydrophobic amino acid tryptophan and the cationic amino acid lysine were the most efficient in binding and condensing DNA. Studies at varying pH indicated different mechanisms for DNA interactions with the tryptophan- and lysine-based compounds. The resultant complexes with plasmid DNA were examined by electron microscopy. A *bis*(tryptophan) compound begat nanoparticles markedly different from lipid-DNA complexes. Results obtained from the aforementioned three DNA-focused studies have application in biological research and potentially in gene therapy to cure disease.

In addition to DNA binding, some of the *bis*(tryptophan) molecules described in this work were found to have antimicrobial properties. The compounds were shown to reverse antimicrobial resistance when co-administered with another antibiotic. The compounds were found to be non-toxic at low and antimicrobially active concentrations to three mammalian epithelial cell lines. Confocal microscopy studies suggest that the compounds are membrane-active, which implies a more general strategy for combating antibiotic resistance.

Both the DNA and antimicrobial studies employed a uniquely supramolecular perspective in the design of methods and compounds that are biologically functional and aim to treat disease. Together, this work represents a structure-based approach to the understanding of how amphiphilic small molecules interact within biologically relevant systems.

Summary and Contributions

The majority of the work reported herein was conceived of and performed by the author. This section details contributions to the experiments elaborated in this dissertation.

Chapter 2. I performed all lipid manipulations, agarose gel electrophoresis, and dynamic light scattering experiments. I prepared electron microscopy samples, which were examined with the assistance of Dr. David Osborn in the Center for Nanoscience. I performed all mammalian cell culturing and confocal microscopy studies. Flow cytometry experiments were carried out with the assistance of the Flow Cytometry Core at the Saint Louis University School of Medicine. The plasmid DNA used in the experiments was amplified and preliminarily purified by Mohit Patel, a co-worker in the Gokel Laboratory.

Chapter 3. I performed all agarose gel electrophoresis and dynamic light scattering experiments. Hydraphiles and lariat ethers were prepared by Dr. Sergey Sedinkin and Nichole Curvey, co-workers in the Gokel Laboratory. I prepared electron microscopy samples, which were examined with the assistance of Dr. David Osborn. The plasmid DNA used in the experiments was amplified and preliminarily purified by Mohit Patel.

Chapter 4. I performed all chemical syntheses, agarose gel electrophoresis, and circular dichroism studies. An undergraduate, Ryan A. Stanton, prepared electron microscopy samples under my direction, which were examined with the assistance of Dr. David Osborn. The plasmid DNA used in the experiments was amplified and preliminarily purified by Mohit Patel.

Chapter 5. I performed all chemical syntheses and directed the structure-based approach. Biological testing was performed by Mohit Patel.

Acknowledgements

There is hardly enough space to acknowledge every person for which I am grateful and to adequately convey the extent of my gratitude. I must first express my tremendous appreciation for Dr. George W. Gokel, my research advisor and mentor. I owe a great deal of my personal and professional development to this man. Dr. Gokel cares deeply about the intellectual development of his students and without him I most certainly would not have the scientific understanding and perspective I have today.

In the course of my graduate work at the University of Missouri-St. Louis I have come to know and respect a great deal of the faculty in the Department of Chemistry & Biochemistry and the Center for Nanoscience. I must mention Dr. Chris Spilling, Dr. Mike Nichols, and Dr. Jim Bashkin, who form my dissertation committee and with whom I have enjoyed many enlightening scientific discussions. Dr. Rudi Winter and Mr. Joe Kramer in the mass spectrometry facility, Dr. Nigam Rath in X-ray crystallography, and Dr. David Osborn in electron microscopy have been of tremendous assistance in their respective areas of expertise.

In addition to my many research interests, I am especially dedicated to advocating for scientific literacy. To this end, I engaged in various outreach presentations, demonstrations, and designed and instructed a course for non-science majors on the chemistry of beer brewing. I must thank the Departmental and University administration in supporting these efforts. I am especially grateful for the patience of my advisor, Dr. Gokel, in allowing me to pursue these endeavors.

Throughout my time at UMSL I have enjoyed valuable discussions and meaningful friendships with my graduate colleagues—truly, too many to thank. I am especially indebted to my coworkers, past and present, in the Gokel Laboratory: Dr. Sergey Sedinkin, Dr. Saeedeh Negin, Mohit Patel, Mike Gokel, and Ryan Cantwell. I have also had the pleasure of working with a number of undergraduate students who have enlivened the lab and have contributed to the work reported herein.

Finally, I would be remiss in not mentioning the unwavering support of my parents, family, and friends. Their enduring love and encouragement have proved critical to my success and happiness.

Table of Contents

	Page
Dissertation Abstract	ii
Summary and Contributions	iv
Acknowledgements	v
Table of Contents	vi
List of Figures and Tables	viii
Chapter 1. Introduction	1
Chapter 2. A Simplified Direct Lipid Mixing Lipoplex Preparation	7
Introduction.....	7
Results and Discussion	8
<i>Agarose gel electrophoresis studies</i>	9
<i>Dynamic light scattering studies</i>	15
<i>Electron microscopy studies</i>	17
<i>Mammalian cell transfection studies</i>	19
Conclusion	25
Experimental Section	26
References	29
Chapter 3. Condensation of Plasmid DNA by Benzyl Hydraphiles and Lariat Ethers	33
Introduction.....	33
Results and Discussion.....	35
<i>Agarose gel electrophoresis studies of DNA with benzyl hydraphiles</i>	35
<i>Agarose gel electrophoresis studies of DNA with lariat ethers</i>	41
<i>Electron microscopy studies</i>	44
Conclusion	45
Experimental Section	45
References	46
Chapter 4. De Novo Design, Synthesis, and Biophysical Characterization of Bis(aminoamides) that Bind and Condense Plasmid DNA	50
Introduction.....	50

Results and Discussion	51
<i>Electrophoresis studies of simple amines</i>	51
<i>Structure-based design of DNA-binding structures</i>	56
<i>Structures and DNA-binding of bis(aminoamide)s</i>	61
<i>Structure-activity assay of bis(tryptophan)s</i>	68
<i>Electron microscopy studies</i>	73
<i>Circular dichroism studies</i>	76
Conclusion	77
Experimental Section	78
References	91
Chapter 5. Reversal of Tetracycline Resistance in <i>Escherichia coli</i> by Non-cytotoxic Bis(Tryptophan)s	95
Introduction.....	95
Results and Discussion	95
<i>Compounds studied</i>	96
<i>Antimicrobial activity</i>	98
<i>Cytotoxicity to mammalian cells</i>	100
<i>Recovery of antimicrobial activity against a resistant strain</i>	102
<i>Confocal microscopy study of <i>E. coli</i> membrane permeability</i>	105
<i>Confocal microscopy study of mammalian cell membrane permeability</i>	106
Conclusion	107
Experimental Section	108
References	115

List of Figures and Tables

Chapter 1

Figure 1.1	Amphiphile publications per year	1
Figure 1.2	Amphiphile geometry and self-assembly	2

Chapter 2

Figure 2.1	Chemical structure of DOTAP.....	9
Figure 2.2	Electrophoresis apparatus and structures.....	10
Figure 2.3	Agarose gel matrix model	11
Figure 2.4	Typical agarose gel image.....	12
Figure 2.5	Topological isomers of plasmid DNA	13
Figure 2.6	Electrophoresis of DOTAP-DNA complexes.....	14
Figure 2.7	Particle size of DOTAP-DNA complexes	17
Figure 2.8	Electron microscopy of DOTAP-DNA complexes.....	19
Figure 2.9	Transfected HEK-293 cells – high DNA concentration.....	20
Figure 2.10.....	Transfected HEK-293 cells – low DNA concentration	21
Figure 2.11.....	HEK-293 cells transfected with commercial reagents	22
Figure 2.12.....	Flow cytometry evaluation of transfection and toxicity	23
Figure 2.13.....	Flow cytometry of transfected COS-7 cells	24
Figure 2.14.....	Summary of transfection methodologies.....	25

Chapter 3

Figure 3.1	Structures of lariat ethers and hydraphiles studied.....	34
Figure 3.2	Electrophoresis of DNA with benzyl C8 and C14 hydraphiles	36
Figure 3.3	Models of azacrown ether complexes with DNA backbone.....	37
Figure 3.4	Summary of pH effect on DNA-hydraphile complexation.....	39
Figure 3.5	Structures tested for DNA-hydraphile complex prevention	40
Figure 3.6	Electrophoresis DNA-hydraphile prevention	41
Figure 3.7	Chain length dependence of lariat ether-DNA complexation	42
Figure 3.8	Proposed models of lariat ether-DNA structures	44
Figure 3.9	Electron micrograph of hydraphile-DNA particles	45

Chapter 4

Figure 4.1	Structures of simple amines studied	52
------------------	---	----

Figure 4.2	Electrophoresis of DNA complexed with simple amines.....	53
Figure 4.3	DNA complexation with aryl amines and diamines.....	55
Figure 4.4	B-form DNA structure with interphosphate distances	57
Figure 4.5	Conformations of protonated aminoamides	58
Figure 4.6	Models of <i>bis</i> (glycylamido)benzene isomers	59
Figure 4.7	Crystal structures of <i>bis</i> (amido)benzene isomers	60
Figure 4.8	Structures of the 20 genetically coded amino acids	62
Table 4.1	Structures of <i>bis</i> (aminoamide) compounds 1-13	63
Figure 4.9	Crystal structures of <i>bis</i> (glycylamido)benzene compounds.....	64
Figure 4.10.....	Electrophoresis of DNA with <i>bis</i> (alanylamido)benzene.....	65
Table 4.2.....	Summary of electrophoresis of DNA with compounds 1-13	67
Table 4.3	Summary of electrophoresis of DNA with compound 14-18	69
Figure 4.11.....	Electrophoresis of DNA with <i>bis</i> (tryptophan)s 19-22	71
Table 4.4	Summary of electrophoresis of DNA with compounds 19-22	72
Figure 4.12.....	Effect of pH on <i>bis</i> (lysine)-DNA and <i>bis</i> (tryptophan)-DNA.....	73
Figure 4.13.....	Electron micrographs of a <i>bis</i> (tryptophan)-DNA complex.....	74
Figure 4.14.....	Electron micrographs of a <i>bis</i> (lysine)-DNA complex.....	74
Figure 4.15.....	Scanning electron micrograph of a <i>bis</i> (trp)-DNA complex.....	75
Figure 4.26.....	Circular dichroism spectrum of a <i>bis</i> (lys)-DNA complex	77
Chapter 5		
Figure 5.1	Structures of tryptophan-based compounds 1-11	97
Table 5.1	Minimum inhibitory concentrations of 1-11	98
Figure 5.2	Mammalian cytotoxicity of <i>bis</i> (trp)s at the MIC concentration ..	101
Figure 5.3	Cytotoxicity of <i>bis</i> (trp)s at twice the MIC concentration.....	102
Table 5.2.....	Recovery of tetracycline against resistant <i>E. coli</i>	103
Figure 5.4	Tetracycline recovery at constant <i>bis</i> (trp) concentration	105
Figure 5.5	Confocal micrographs of <i>E. coli</i> membrane permeability	106
Figure 5.6	Confocal micrographs of HEK-293 membrane permeability.....	107

Chapter 1

Introduction and background.

1.1. *Amphiphiles and membranes.* Amphiphiles are molecules with both hydrophilic (water-loving) and hydrophobic (water-hating—sometimes called lipophilic or lipid-loving) components. These molecules were first termed *amphipathic* (from the Greek *amphi*, meaning both) by G. S. Hartley in 1936 when describing the aggregation properties of paraffin-chain salts in water.¹ The term *amphiphilic* became popular about 20 years later, employing the *philic* suffix for continuity.² Figure 1.1 clearly shows an escalating interest in amphiphiles demonstrated by the number of publications per year on the subject.³

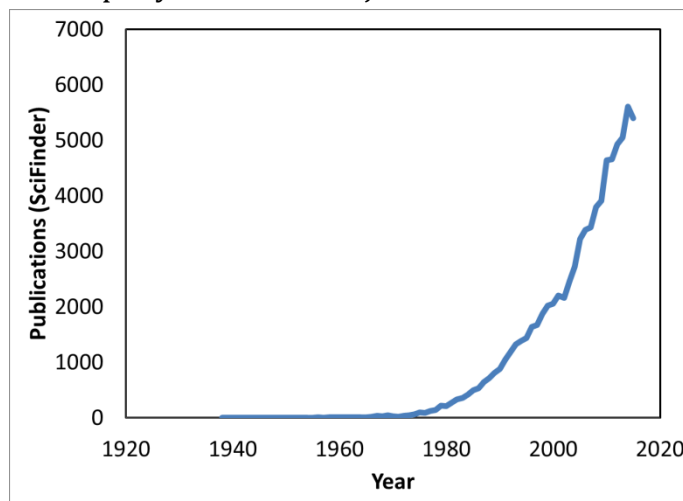


Figure 1.1. Publications per year indexed in SciFinder® containing the term *amphiphilic*, *amphipathic*, or derivatives thereof.

Much of the early work on amphiphilic molecules describes their ability to form aggregates in aqueous solutions.^{1,2,4} Amphiphiles that consist of a relatively small hydrophilic head group and a longer hydrophobic tail will undergo self-assembly to exclude water from the hydrophobic portion of the molecule. Figure 1.2 shows the chemical structure (left panel) and aggregation/self-assembly behavior (right panel) of two common amphiphiles.⁵ The particle that is formed from the assembly of amphiphiles in water depends on the geometry of the amphiphile.⁶ The hydrophilic head group is hydrated in aqueous solution, making it wider than an aliphatic chain. This results in a conical geometry for single-chained amphiphiles. The cones assemble into a sphere with the hydrophobic tails pointing toward the center and the head groups facing outward to the solution. This maximizes the interaction of hydrophilic groups with water and minimizes the contacts between hydrophobic tails and the solvent. The resulting structure is called a micelle. Twin-chained amphiphiles have a cylindrical geometry and typically aggregate into bilayers (lamellae). Micellar and bilayer structures are just two examples of the

different amphiphile polymorphisms in aqueous solution. Additional liquid crystalline phases are accessible to amphiphiles of varying composition and under different solution conditions.

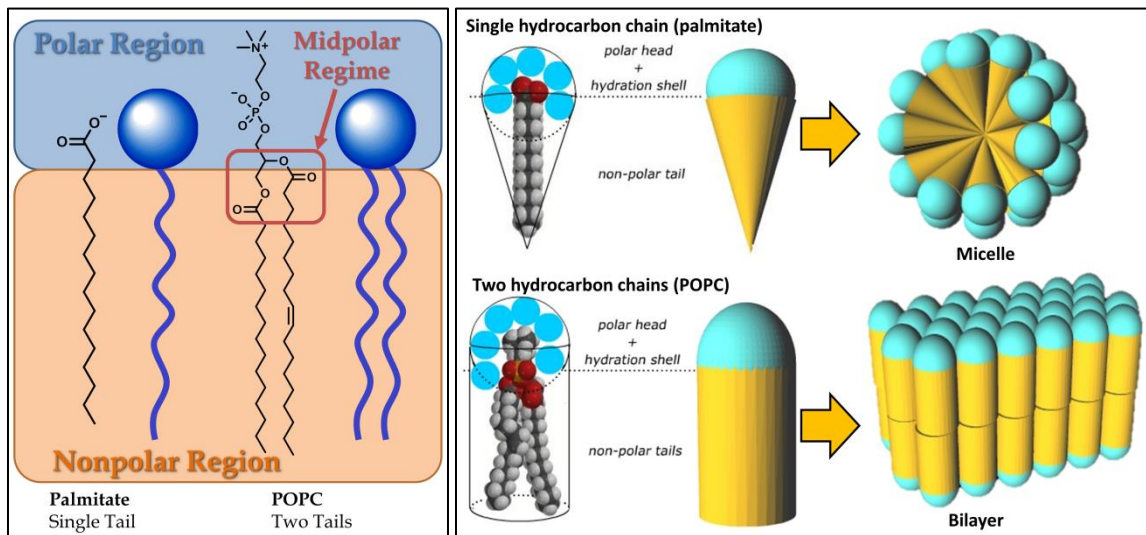


Figure 1.2. The left panel shows chemical structures and cartoon 'lollipop' representations of representative single- (left) and twin-chained (right) amphiphiles. The right panel shows the geometry of hydrated single-chained (top) amphiphiles and micellar aggregates. Twin-chained amphiphiles (bottom) are shown forming a bilayer structure.⁵

Phospholipids comprise a class of amphiphiles that typically consist of phosphorylated diacylglycerols. They are ubiquitous in living organisms and as twin-chained amphiphiles, they form bilayer structures. Synthetic spherical bilayer structures can be formed from phospholipids. The resulting structure is called a *liposome* or a *vesicle* and can contain a single bilayer (unilamellar) or many bilayers (multilamellar). The key difference between micelles and liposomes is that the latter contains an aqueous interior compartment. Liposomes can therefore transport hydrophilic cargo in their interior as well as hydrophobic molecules embedded in the lipid bilayer. Liposomes may be considered the simplest representation of the membranes of living cells; however, the latter is considerably more complex in both composition and structure.

Cellular membranes are two-dimensional fluids of various lipids interspersed with proteins. This perspective of membrane structure was elaborated in 1972 by Singer and Nicolson as the *fluid-mosaic model* of cell membranes.⁷ While nonpolar small molecules such as O₂ and CO₂ can diffuse through the membrane, ions and larger

hydrophilic compounds cannot. Hydrophobic compounds of low molecular weight can diffuse through the membrane. Water diffusion through the membrane is assisted by transmembrane proteins called aquaporins.⁸ Passive and active transport of ions and other compounds is often achieved by highly specific protein channels.

1.2 Nucleic acids and genetic transformation. Nucleic acids consist of planar heteroaromatic rings fused to a ribose-phosphate backbone. DNA and RNA differ in that the former does not contain the 2'-hydroxyl group on the ribose subunit. Both are polyanionic, arising from the acidic phosphate groups on the backbone. Neither is capable of simple diffusion through a phospholipid bilayer. As the carrier of genetic information, nucleic acids have been studied for their ability to carry their encoded protein-making instructions between organisms. This *transforming principle* was observed in bacteria before the structure and function of nucleic acids was even discovered.^{9,10} The ability to transfer genetic material into eukaryotes in general and mammalian cells in particular was first observed with viral nucleic acids and was called *transfection*.¹¹ Soon thereafter, it was discovered that various cationic polymers¹² and calcium aggregates¹³ enhanced the transfection efficiency of nucleic acids.

Viral transfection methods are highly efficient. However, the safety of the method is of concern. The use of certain viral vectors to transport genetic material results in the random insertion of the exogenous DNA into the host genome. In a 2002 gene therapy clinical trial this resulted in the alteration of oncogenes and caused leukemia in four patients, one of whom did not survive.¹⁴ Certain viral vectors, such as adeno-associated viral vectors, are safer because their genome insertion is non-random.¹⁵ Nevertheless, the immune response to viral vectors can still pose a threat, as was the case in the tragic death of 18 year old Jesse Gelsinger in 1999.¹⁴

In response to the safety concerns of viral vectors in gene therapy, non-viral methods have been developed. Perhaps the more promising of these methods is the use of cationic lipids for transfection. This technique was pioneered by Felgner and coworkers, who called it *lipofection*.¹⁶ The process involves preparing a liposome containing cationic lipids. Neutral helper lipids are often included to manipulate the lipid packing, a commonly used example is dioleoylphosphatidylethanolamine (DOPE). Once formed, the liposomes are then mixed with DNA, which causes spontaneous assembly into lipid-DNA complex called a *lipoplex*. The aim of the experiments in Chapter 2 was to assess a simplified method for preparing the lipoplex. The results elaborated in Chapter 3 utilized the method elaborated in the preceding chapter to characterize complexes formed from azacrown ethers and

plasmid DNA. In Chapter 4, amino acid-based compounds were synthesized and assessed for DNA binding ability.

A long-term goal of the effort to design novel DNA binding compounds is to engender sequence-specificity into the structures. The ability to target a particular DNA or RNA sequence has tremendous potential for research and clinical applications. New technologies in RNA interference (RNAi)¹⁷ and gene editing (CRISPR)¹⁸ are especially promising. Both techniques require the transport of nucleic acids across a cellular membrane. Synthetic chemicals are also being studied for their ability to bind DNA in a sequence-specific manner¹⁹ and have recently shown promise²⁰ in curing infectious diseases.

1.3 Antimicrobial resistance. The necessity for developing new classes of antimicrobial chemotherapies can hardly be overstated. Resistance to current antibiotics continues to increase while the approval of new antibiotics is in decline.²¹ The results elaborated in Chapter 5 show that new amino acid-based small molecules show broad-spectrum antimicrobial activity. Even more interesting was the discovery that these molecules are capable of recovering antibiotic potency in a tetracycline-resistant strain of *E. coli*. The membrane activity of these molecules is implicated in these observations, suggesting a more general strategy for combating a particular class of antibiotic resistance.

Whether DNA-binding and transport or antimicrobial activity was investigated, the unifying theme of the work reported in this document is the structure and function of amphiphiles in biologically relevant systems. This work represents a uniquely supramolecular perspective as it applies to binding, aggregation, and transport phenomena influenced by chemical structure.

1.2. References

- 1 Hartley, G. S., Aqueous solutions of paraffin-chain salts; a study in micelle formation. Hermann: Paris. 1936. 69 p.
- 2 Winsor, P., Hydrotropy, solubilisation, and related emulsification processes. Parts I-IV. *Trans. Faraday. Soc.* **1948**, *44*, 376-398.
- 3 SciFinder search for publications containing the terms amphiphilic or amphipathic or derivatives thereof. Accessed 12 May, 2016.
- 4 (a) Winsor, P. A., Binary and multicomponent solutions of amphiphilic compounds. Solubilization and the formation, structure, and theoretical significance of liquid crystalline solutions. *Chem. Rev.* **1968**, *68*, 1-40. (b)

- Ekwall, P. Composition, properties, and structures of liquid crystalline phases in systems of amphiphilic compounds. *Adv. Liq. Cryst.* **1975**, *1*, 1-142.
- 5 Caflisch, A., Membranen, Enzymatische Katalyse, Serinpeptidasen, Kinasen, Enzymhemmung. <http://www.biochem-caflisch.uzh.ch/static/Biochemistry/1Membranen.pdf>. Accessed 19 May, 2016.
- 6 Israelachvili, J. N., Mitchell, D. J. & Ninham, B. W. Theory of self-assembly of hydrocarbon amphiphiles into micelles and bilayers. *J. Chem. Soc., Faraday Trans. 2* **72**, 1525-1568 (1976).
- 7 Singer, S. J.; Nicolson, G. L., The fluid mosaic model of the structure of cell membranes. *Science* **1972**, *175*, 720-731.
- 8 Murata, K.; Mitsuoka, K.; Hirai, T.; Walz, T.; Agre, P.; Heymann, J. B.; Engel, A.; Fujiyoshi, Y., Structural determinants of water permeation through aquaporin-1. *Nature* **2000**, *407*, 599-605.
- 9 Griffith, F., The significance of pneumococcal types. *J. Hygiene* **1928**, *27*, 113-159.
- 10 Avery, O. T.; Macleod, C. M.; McCarty, M., Studies on the chemical nature of the substance inducing transformation of pneumococcal types : induction of transformation by a desoxyribonucleic acid fraction isolated from pneumococcus type III. *J. Exp. Med.* **1944**, *79*, 137-158.
- 11 (a) Weil, R., A quantitative assay for a subviral infective agent related to polyoma virus. *Virology* **1961**, *14*, 46-53. (b) Szybalska, E. H.; Szybalski, W., Genetics of human cell lines, IV. DNA-mediated heritable transformation of a biochemical trait. *Proc. Natl. Acad. Sci. U. S. A.* **1962**, *48*, 2026-2034.
- 12 (a) Vaheri, A.; Pagano, J. S., Infectious poliovirus RNA: a sensitive method of assay. *Virology* **1965**, *27*, 434-436. (b) McCutchan, J. H.; Pagano, J. S., Enhancement of the infectivity of Simian Virus 40 deoxyribonucleic acid with diethylaminoethyl-dextran. *JNCI J. Natl. Canc. Institut.* **1968**, *41*, 351-357. (c) Benzinger, R.; Kleber, I.; Huskey, R., Transfection of Escherichia coli spheroplasts I. general facilitation of double-stranded deoxyribonucleic acid infectivity by protamine sulfate. *J. Virol.* **1971**, *7*, 646-650. (d) Henner, W. D.; Kleber, I.; Benzinger, R., Transfection of Escherichia coli spheroplasts III. facilitation of transfection and stabilization of spheroplasts by different basic polymers. *J. Virol.* **1973**, *12*, 741-747.
- 13 Graham, F. L.; van der Eb, A. J., A new technique for the assay of infectivity of human adenovirus 5 DNA. *Virology* **1973**, *52*, 456-467.
- 14 Sheridan, C., Gene therapy finds its niche. *Nat. Biotechnol.* **2011**, *29*, 121-128.

- 15 Nussbaum, R. L.; McInnes, R. R.; Willard, H. F., Thompson & Thompson Genetics in Medicine. Elsevier: Canada; 2015. 278 pp.
- 16 Felgner, P. L.; Gadek, T. R.; Holm, M.; Roman, R.; Chan, H. W.; Wenz, M.; Northrop, J. P.; Ringold, G. M.; Danielsen, M., Lipofection: A highly efficient, lipid-mediated DNA-transfection procedure. *Proc. Natl. Acad. Sci. U.S.A.* **1987**, *84*, 7413-7417.
- 17 Hannon, G. J.; RNA interference. *Nature* **2002**, *418*, 244-251.
- 18 Cong, L.; Ran, F. A.; Cox, D.; Lin, S.; Barretto, R.; Habib, N.; Hsu, P. D.; Wu, X.; Jiang, W.; Marraffini, L. A.; Zhang, F., Multiplex genome engineering using CRISPR/Cas systems. *Science* **2013**, *339*, 819-823.
- 19 White, S.; Szewczyk, J. W.; Turner, J. M.; Baird, E. E.; Dervan, P. B., Recognition of the four Watson–Crick base pairs in the DNA minor groove by synthetic ligands. *Nature* **1998**, *391*, 468-471.
- 20 Edwards, T. G.; Koeller, K. J.; Slomczynska, U.; Fok, K.; Helmus, M.; Bashkin, J. K.; Fisher, C., HPV episome levels are potently decreased by pyrrole-imidazole polyamides. *Antiviral Res.* **2011**, *91*, 177-186.
- 21 (a) Center for Disease Control and Prevention, Antibiotic resistance threats in United States, 2013. (b) World Health Organization, Antimicrobial resistance global report and surveillance, 2014.

Chapter 2

A Simplified Direct Lipid Mixing Lipoplex Preparation: Comparison of Liposomal-, Dimethylsulfoxide-, and Ethanol-Based Methods

2.1. Introduction.

The tetravalent polyamine spermine was among the first reagents successfully employed in the transfection of mammalian cells over fifty years ago.¹ Shortly thereafter, DEAE-dextran, protamine, and other cationic polymers were found to increase the genetic transforming activity of viral DNA and RNA on bacterial and mammalian cells.^{2,3,4,5} A technique utilizing the co-precipitation of calcium phosphate with DNA marked one of the first chemical transfection methods not using polyamines.⁶

Since these earliest studies, numerous procedures have been developed for non-viral mammalian cell transfection. Several physical techniques for transfection have been explored. These include gene gun,⁷ electrospray,⁸ electroporation,⁹ sonoporation,¹⁰ and magnetofection.¹¹ Chemical approaches typically involve the use of cationic polymers,¹² calcium phosphate,⁶ inorganic nanoparticles,¹³ and lipids.^{14,15}

The formation of stable and condensed particles containing DNA is the most common strategy used for *in vitro* transfection. When such a complex is formed using a cationic polymer it is called a *polyplex*, whereas cationic lipids beget a *lipoplex*. While cationic polymers are typically water soluble, cationic lipids are not. The latter must therefore be pre-formed into liposomes.¹⁶ The lipoplex is then generated by the addition of an aqueous solution of cationic liposomes to an aqueous solution of DNA. The spontaneously formed lipoplex transfects cells in the process known as *lipofection*.¹⁵

The lipoplex structure does not resemble that of the small unilamellar liposomes from which they derive. Instead, the lipoplex is a multilamellar liquid crystal consisting of hydrated DNA layers alternating with cationic lipid bilayers.¹⁷ A structural variant consists of a columnar hexagonal phase in which the DNA helix comprises the axis. Cationic lipid head groups face the DNA and the hydrophobic tails interdigitate between the hexagonally packed columns excluding water.¹⁸ The dynamics of lipoplex assembly are poorly understood, but it has been shown that lipid packing parameters¹⁹ dictate the structure's organization.

In most reports involving transfection, lipoplex formation was predominantly achieved by mixing plasmid DNA with cationic liposomes formed by the well-

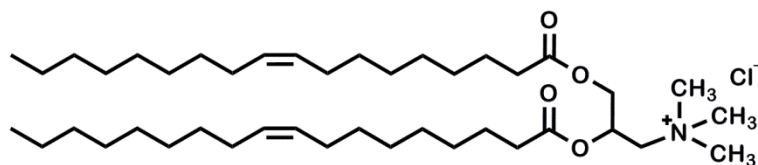
established lipid film hydration method.²⁰ Small unilamellar vesicles are achieved by sonication and/or extrusion²¹ of the hydrated lipid. An ethanol-injection method has also been reported for liposome formation²² and used in transfection.²³ These and other lipoplex preparation methods based on a liposomal intermediate require the use of lipids or lipid mixtures that form stable liposomes. Unless an amphiphile can form liposomes, it cannot be tested for DNA interaction or transfection using these methods.

Lipoplex preparation methods have been developed that eliminate the liposomal intermediate. One method requires the use of a T-shaped mixing chamber to add an ethanolic solution of lipids to aqueous DNA.²⁴ Another method utilizes 50% aqueous ethanol to dissolve both lipids and DNA and the resulting particles have been called *Genospheres*TM.²⁵ Both methods require rotary evaporation or dialysis to remove ethanol before the lipoplex is delivered to cells.

The results presented here demonstrate that lipids dissolved in dimethylsulfoxide (DMSO) or ethanol (EtOH) may be added directly to aqueous DNA to form a lipoplex. We call this technique *direct lipid mixing* (DLM) and denote the solvent by subscript, *i.e.* DLM_{DMSO} or DLM_{EtOH}. This method is fast, simple, and requires neither specialized equipment nor removal of the organic solvent. The method enables facile optimization of multi-lipid mixtures and lipid-DNA ratios. The absence of a liposomal intermediate enables the investigation of a greater diversity of chemical structures for transfection ability.

2.2. Results and Discussion.

2.2.1. Model cationic lipid transfection agent. The studies presented here use the cationic lipid 1,2-dioleoyl-3-trimethylammoniumpropyl chloride (DOTAP, see Figure 1). This lipid is widely used as an *in vitro* transfection agent,^{26,27} its lipoplex with DNA has been characterized,^{18,28} and it is commercially available. Liposomes can easily be prepared from DOTAP alone without the need for a helper lipid (such as dioleoylphosphatidylethanolamine, DOPE). DOTAP is also soluble in the water-miscible organic solvents DMSO and ethanol. This property makes it possible to assess if DOTAP functions differently in lipoplex formation depending on whether the lipid is initially isotropically dispersed in a solvent (DLM) or the lipid is in the form of aqueous liposomes. Such differences in lipoplex formation could affect DOTAP's activity as a transfection agent. It is this question that is addressed herein.



DOTAP

Figure 2.1. Chemical structure of model cationic lipid transfection reagent 1,2-dioleoyl-3-trimethylammoniumpropyl chloride (DOTAP)

2.2.2. *Introduction to agarose gel electrophoresis.* DNA migrates through an agarose gel matrix by the action of an electric field according to its charge, length, and morphology. Successful transfection reagents, whether polymers or lipids, inhibit the migration of plasmid DNA through the gel. This retardation may result from aggregate formation, which cannot pass through the pores in the gel, and/or by screening the charge on the DNA phosphates from the influence of the electric field.

A typical agarose gel electrophoresis experiment is run with a gel prepared from 0.5-1.0% agarose in tris-acetate buffer. The gel is cast into a slab measuring approximately 1 x 12 x 13 cm for our apparatus. A *comb* is used to create regularly spaced and sized holes in the gel. These holes are termed *wells* and upon removal of the comb they are used to load samples into the gel. The comb may be placed at one end of the gel or in the middle. The gel is submerged under aqueous *running buffer*, which is typically the same composition as the buffer used to cast the gel. Figure 2.2 shows an image of our gel apparatus in panel A, a side-view schematic of the apparatus in panel B, and the chemical structures of agarose polymer, tris-acetate (TA), and ethylenediaminetetraacetic acid (EDTA) in panel C. The metal ion chelating agent EDTA is often included in the buffer. EDTA prevents DNA damage from metal-dependent nuclease enzymes by binding the divalent metals (calcium, magnesium) necessary for the function of the enzyme. We have omitted EDTA from our buffer preparations in order to avoid any interaction between the polyanionic EDTA and our cationic DNA-binding reagents. We do not see nuclease activity in our system as the buffer and DNA are highly purified.

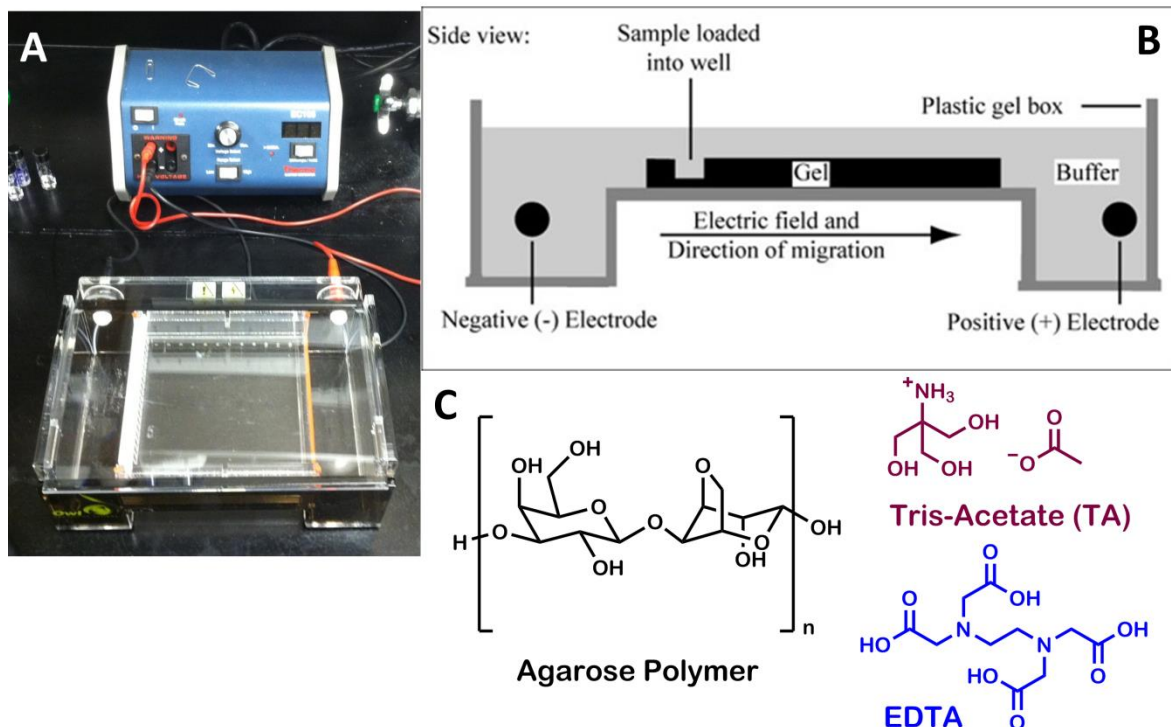


Figure 2.2. A) Electrophoresis apparatus. B) Side-view schematic of electrophoresis chamber. C) Chemical structures of the agarose polymer, tris-acetate, and ethylenediaminetetraacetic acid (EDTA).

The formation of a gel from the agarose polymer powder creates a porous matrix through which the DNA can migrate under an electric current. The pore size of the matrix is dependent on the concentration of the polymer used, with lesser amounts of agarose leading to larger pores. Under our conditions (0.5% agarose w/v) the pore size ranges from 200-1000 nm in diameter. A 2007 study analyzed gels formed from a similar material, sepharose, by using transmission electron microscopy to generate a computer model of the gel matrix.²⁹ The computer-generated image of a gel matrix is shown in Figure 2.3. If a chemical binds DNA and condenses it into a nanoparticle that is too large to efficiently move through the pores of the gel, then it will not be observed to migrate on the gel.

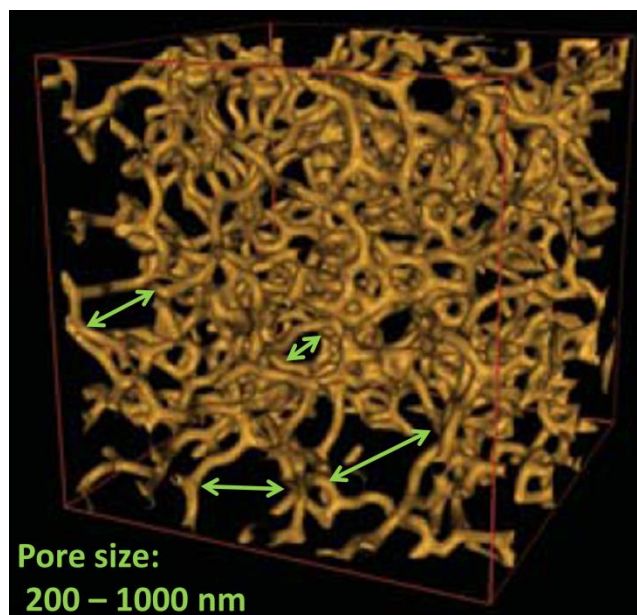


Figure 2.3. Computer model of an agarose gel matrix. The agarose fibers create pores of various sizes depending on the concentration of agarose used.

The DNA migrates as the gel is run at ~ 100 V for 1.5 hours. The gel is then stained to visualize the location of the DNA. The fluorescent dye ethidium bromide is used for this purpose. Ethidium bromide is known to intercalate between the base pairs of DNA and upon intercalation a large increase in its fluorescence intensity is observed.³⁰ The gel is stained in a solution of running buffer containing the dye and imaged on a UV trans-illuminator. An image of a typical gel is presented with annotations in Figure 2.4. The external-most lanes in the gel consist of a 1 kilobase *ladder* (Promega). The 1 kb ladder is a reference that consists of linear double stranded DNA from 250 base pairs in length to 10,000 base pairs. The second and next-to-last lanes consist of control plasmid DNA. The control plasmid DNA is mixed with the solvent in which the experimental compound is dissolved (in most cases dimethyl sulfoxide). The sixteen lanes between the ladder and plasmid controls are the experimental lanes. Their contents are typically shown above the lane and the equivalent of compound to DNA phosphate is also shown. The direction of DNA migration through the gel is from the top of the image to the bottom. Dark rectangles can be seen at the top of the gel. These are the wells in which the sample is placed. Fluorescent material can sometimes be observed in the wells. In many cases this is retained DNA. However, certain aggregates of insoluble compounds can also create this effect, as can deformed wells. Therefore, the appearance of fluorescent material in the well must be assessed in conjunction with the migration of DNA in order to conclude whether DNA was retained.

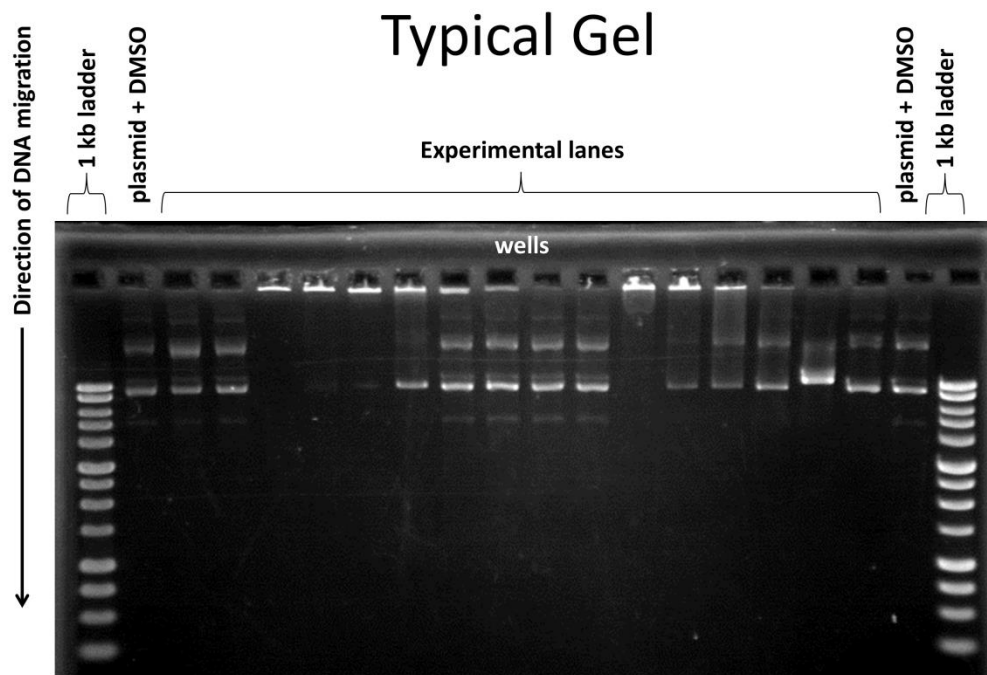


Figure 2.4. A typical image of an agarose gel stained by ethidium bromide. The image is obtained by UV trans-illumination.

Plasmids are circular, double-stranded DNA. The plasmid used in electrophoresis experiments was a 9,988 base pair plasmid (pKLMF-FX, New England Biolabs) that was amplified in and extracted from the bacterium *Escherichia coli*. We have usually rounded the plasmid size to 10 kilobase pairs (10 kb) in this document. Often, more than one band is observed for a single plasmid on a gel. The multiple bands arise from the different topological isomers (topoisomers) plasmids can form. The most prevalent bands observed are, in order of fastest migration, *supercoiled*, *linear*, and *open-circular* (nicked) plasmid DNA. The different topoisomers of plasmid DNA are shown in Figure 2.5. The supercoiled DNA is more compressed than the other forms and therefore migrates the fastest. The linear DNA is a plasmid that has been cut through both strands. The pKLMF-FX plasmid shown in the Figure was cut with the BamHI enzyme to form a linear strand. The linear DNA migrates slightly slower than the supercoiled DNA and is seen to co-migrate with the 10,000 bp linear reference ladder DNA. Open-circular DNA is a plasmid that has been cut only through one strand of the double-helix. This allows the supercoiled DNA to relax by winding about the other intact strand to form an open circle. The nicked DNA migrates slower than supercoiled and linear DNA.

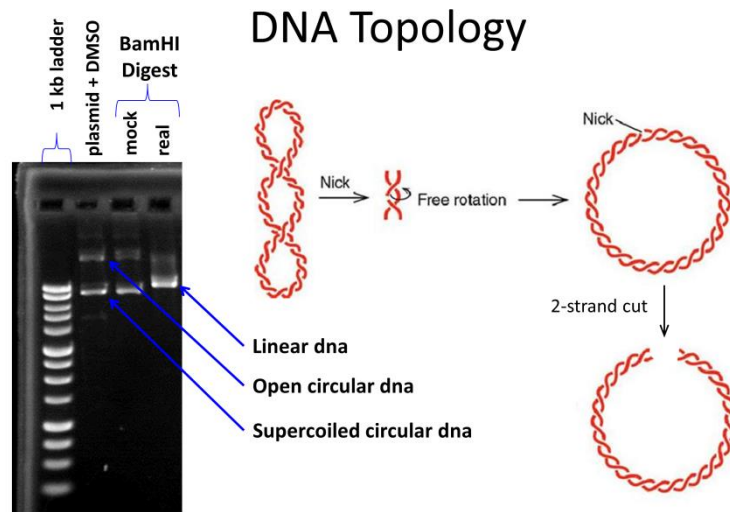
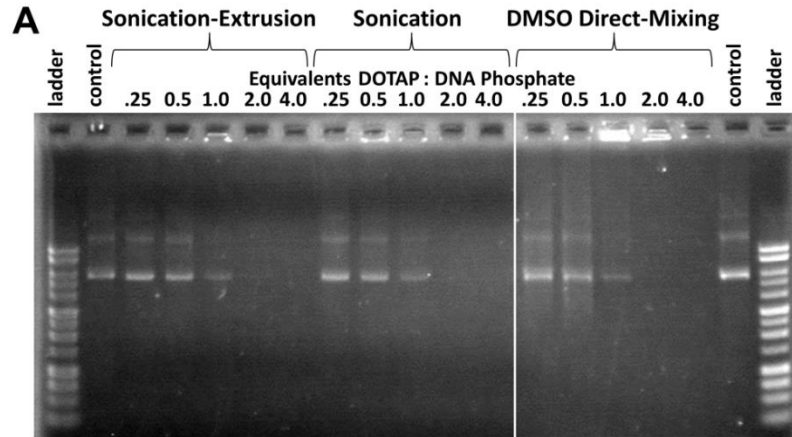


Figure 2.5. The topological isomers of DNA are shown and identified on an agarose gel. The enzyme BamHI was used to make a double-strand cut in the DNA.

2.2.3. Assessment of DOTAP-DNA interaction by agarose gel electrophoresis. We compared the effects of concentration and the physical state of DOTAP on the migration of plasmid DNA in an agarose gel in order to assess whether DLM or liposomal methods influence the DNA-lipid interaction. Lipoplex solutions were formed either by the addition of aqueous liposomal DOTAP or DMSO-dissolved DOTAP (DLM_{DMSO}) to an aqueous solution of 10 kilobase-pair (10 kb) plasmid DNA. Aqueous liposomes were prepared by two methods: by sonication or sonication-extrusion (hereafter referred to only as “extrusion”). Lipoplex solutions of DOTAP:DNA phosphate (+/- charge) ratios from 0.25 to 4 were prepared and added to the wells of an agarose gel. We were unable to test ethanol-dissolved DOTAP (DLM_{EtOH}) because the mixture is less dense than water. This precludes the loading of the mixture into the wells. The electrophoretic mobility of the DNA was observed by ethidium bromide staining.

We found that the DNA-lipid interaction as assessed by electrophoretic mobility was independent of the initial lipid physical state. The gel image in Figure 2.6A shows that both liposomal and DLM_{DMSO} DOTAP interact with DNA to the same extent. At DOTAP:DNA phosphate ratios of 1-2, nearly all of the DNA was retained independent of the initial lipid physical state. Substoichiometric amounts of cationic lipid resulted in some DNA retention. The absence of significant streaking suggested the presence of minor amounts of intermediate structures, *i.e.* partially formed lipoplexes. The latter result suggested that lipoplex formation may be cooperative.

The graph in Figure 2.6B confirms that the concentration-retention profile for each lipid form is nearly identical. Together, these data suggest that the primary function of preparing a liposomal form of lipofection reagents is to make the lipids water-soluble. Once the liposomes and DNA interact, the liposomal structure collapses and the lipids and DNA co-assemble into a distinct lipoplex structure. By dissolving the lipid in DMSO or ethanol, the liposome preparation step can be eliminated.



B DOTAP-DNA Binding by Agarose Gel Electrophoresis

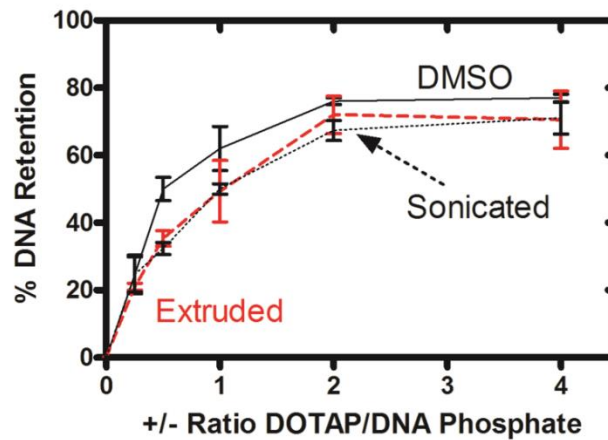


Figure 2.6. (A) Agarose gel electrophoresis of 10 kb plasmid DNA-DOTAP lipoplexes formed with liposomes (sonicated or extruded) or by DLM_{DMSO}. The image represents a single gel; the gap in the image omits a control plasmid lane for clarity. (B) Percent retention of DNA by DOTAP as a function of +/- charge ratio and initial lipid form calculated by densitometric transformation of agarose gel images. Error bars represent the standard deviation of three trials.

The stability of transfection reagents is an important consideration when assessing the convenience of methods. Liposomes are often stored at 4 °C with a shelf life from weeks to months with many factors contributing to their stability.³¹ The chemical degradation of phospholipids by oxidation or hydrolysis and the physical stability of liposomes in suspension can be responsible for lower transfection efficiency or higher toxicity. The DLM method possesses major advantages relevant to stability. First, DLM lipid solutions may be prepared immediately prior to use much more rapidly than liposome solutions. Second, because DLM lipid solutions are isotropically dispersed they are not susceptible to the physical stability (*i.e.* aggregation) issues encountered with liposomes. Finally, DLM_{DMSO} solutions may be particularly stable as DMSO readily freezes at 4 °C. In order to assess stability, the DNA retention of sonicated, extruded, and DLM_{DMSO} solutions stored at 4 °C for 6 months was tested by electrophoresis and found no difference in DNA mobility was apparent when compared to fresh solutions.

2.2.4. Lipoplex characterization by dynamic light scattering (DLS). Both liposomes and lipoplex particles were studied in aqueous solution by dynamic light scattering. DOTAP liposomes were prepared by sonication or extrusion and diluted to a concentration of 30 μM in water. DLS showed that the average particle size was 350 nm for the sonicated lipid, whereas extrusion resulted in 180 nm particles (corresponding well to the 0.2 μm (200 nm) membrane filter pore). The size distribution for liposomes formed by sonication alone was broader than for liposomes formed by extrusion. When DMSO-dissolved lipids were diluted with water to 30 μM, 90 nm particles were observed and fewer particles were apparent than was recorded for either liposomal method. In the latter case, some lipids may be dispersed as monomers or aggregates that were too small to be detected.

A so-called “simple injection” technique for liposome formation that was reported some years ago involves ethanol-dissolved lipids.²³ A DLS analysis of particle sizes obtained by using this technique found too few particles to measure. Presumably, the lipids were mostly dispersed as monomers or perhaps as aggregates too small to be detected. Based on the specifications of the instrument used in our analyses, the former seems more likely. The simple-injection procedure requires rapid injection of ethanol-dispersed lipids into water with simultaneous vortexing to form liposomes. Notwithstanding its potential convenience, this method has been used only occasionally in transfection studies during the past two decades.

The charge affinity between the cationic lipids and the DNA phosphate groups drives the self-assembly. It is also likely that solvent exclusion from the complex

also fosters its formation. DLS showed that directly mixing DMSO-dissolved lipids with DNA (DLM_{DMSO}) resulted in monodisperse lipoplex structures.

Figure 2.7 shows particle size (DLS) data for lipoplexes formed by each of the four methods discussed here. They are (1) sonication, (2) extrusion, and the present method using (3) DMSO or (4) ethanol as the lipid solvent. Lipoplexes were formed using DOTAP and 6.2 kb or 10 kb plasmid DNA. The results demonstrate that methods 2-4 afford lipoplex particles that are similar in size. However, aqueous lipids that were sonicated formed larger liposomes. Comparing the results of similar experiments conducted with 6.2 kb and 10 kb plasmids show that the lipoplex reflects the initial liposome size rather than the length of the DNA included within it.

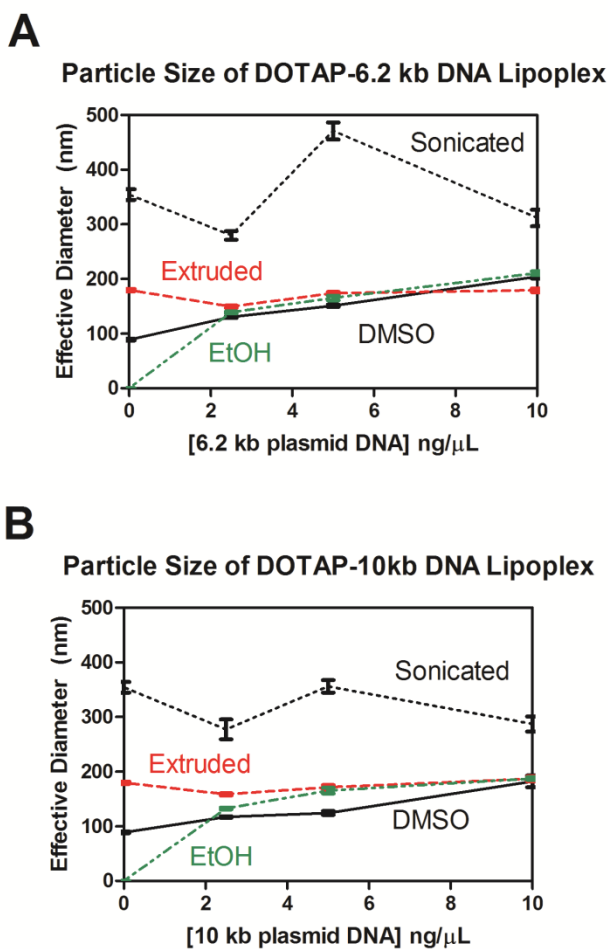


Figure 2.7. Assessment of particle size variations for 30 μ M DOTAP with varying amounts of plasmid DNA. Sonicated and extruded DOTAP are liposomal methods. EtOH and DMSO DOTAP are direct lipid mixing methods. Data shown represent the average of 10 measurements.

The size range of lipoplexes measured was relatively monodisperse across all preparation methods. The polydispersity index (PDI) was less than 0.25 for all methods with sonication giving the widest size distribution (PDI \sim 0.25). DLM methods had a typical PDI of 0.15. Unsurprisingly, extruded liposomes produced the most uniform lipoplexes, which had a PDI of \sim 0.1. Under our preparation conditions, both the size and polydispersity of lipoplexes were reproducible in repeated trials.

2.2.5. Transmission electron microscopy of DOTAP-DNA lipoplex. The size and morphology of DOTAP-DNA lipoplexes prepared by extrusion or by DLM_{DMSO} were examined by using transmission electron microscopy. Lipoplexes were adhered to formvar/carbon-coated copper grids and negatively stained with uranyl acetate. Both extrusion and DLM_{DMSO} methods resulted in multilamellar structures. Lamellar spacings in extrusion samples were 4.7 ± 1.2 nm. A similar lamellar spacing (4.6 ± 0.5 nm) was observed in samples prepared by the DLM_{DMSO} method. These spacings correspond to lamellae consisting of DNA alternating with DOTAP bilayers.

We clearly observe lamellar structures for the lipoplexes formed by using the DLM_{DMSO} method. The lamellar spacing is approximately 5 nm (50 Å). Lamellar spacings recorded in other lipoplex formation reports are larger than this, but reflect different experimental conditions. Talmon and coworkers reported a spacing of 4.9 nm for DOTAP with single-stranded oligonucleotides measured by cryo-TEM and by small angle X-ray scattering (SAXS).³² Safinya and coworkers reported lamellar spacings of 3.72 nm (37.2 Å) for DOTAP in the absence of DNA.³³ This finding implies lipid tail interdigitation, as our estimation of the length of a DOTAP monomer is 2.6 nm (26 Å). In the present case, the lipoplexes are supported (formvar backing) and are neither in solution nor suspension. If we estimate the DNA cylindrical diameter to be 2 nm (20 Å), the lipids must occupy \sim 3 nm (30 Å). The repeating unit must therefore include 20 Å + 15 Å + 15 Å to account for the spacing of 50 Å. This seems possible only if the lipids are interdigitated. Such compression seems reasonable because the solid TEM sample is unlikely to be hydrated.

Despite the similarity in lamellar spacing, extrusion lipoplexes maintain a concentric lamellar structure (see Figure 2.8A), whereas DLM_{DMSO} lipoplexes have a stacked lamellar arrangement (Figure 2.8B). It is unclear whether the lipoplex preparation method or the TEM grid preparation accounts for the difference in morphology. We speculate that lipoplex formation from liposomes may be templated by the liposome, resulting in the curvature observed in the concentric lamellae. However,

lipoplex formation from dissolved lipids may be templated by the DNA or by small lipid assemblies. The latter could result in a lipoplex lamellar structure that is influenced by the lipid packing parameters. This comports with DOTAP (a low-curvature lamellae-forming lipid) forming the stacked lamellar structure. Interestingly, Lehn and coworkers observed stacked lamellar structures for lipoplexes derived from a water-soluble guanidinium-cholesterol reagent (BGTC) by cryo-TEM.³⁴ However, when BGTC was formulated with DOPE as a liposome, concentric lamellar structures were observed for the corresponding lipoplex. This comports with our speculation above on liposome-templation versus DNA-templation or small lipid assembly-templation.

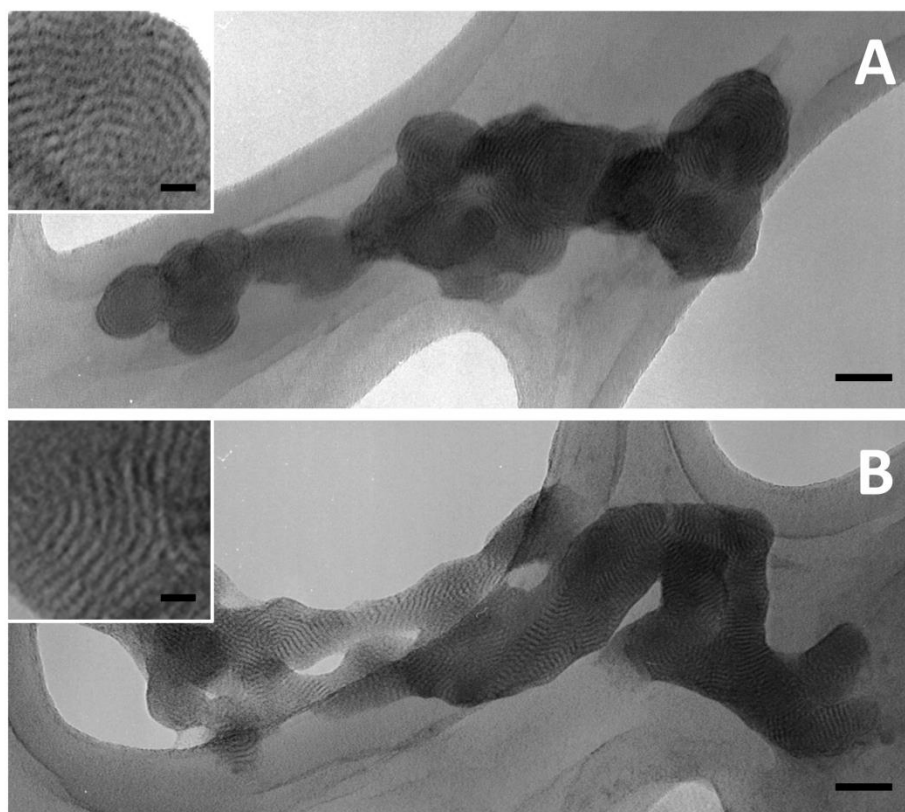


Figure 2.8. (A) Aggregated lipoplex particles formed from extruded DOTAP liposomes (B) Aggregated and partially-fused lipoplex particles formed from DMSO-dissolved DOTAP. The lamellar spacing is approximately 5 nm (50 Å) and is shown in the magnified inset. Scale bars represent 50 nm, inset scale bars represent 10 nm.

2.2.6. Transfection using DMSO-dissolved lipids. An application study was undertaken to determine if the similarities in lipoplex structures on electrophoretic, light scattering, and electron microscopic evidence were reflected in cells. Transfection

studies were conducted on HEK-293 human embryonic kidney cells. The 6.2 kb plasmid pCDNA3-EGFP encoding the enhanced green fluorescent protein (EGFP) was used to visually identify transfected cells. Confocal microscopy was used to assay transfection efficiency. Transfection studies were run in triplicate and data was derived from representative confocal micrographs. Micrographs were analyzed using ImageJ software for cell counting (~2,500 cells per sample). Hand counting and computer analysis agreed within $\pm 7\%$, represented by error bars in Figures 2.9B and 2.10B.

Both the DLM_{DMSO} and liposomal methods resulted in transfected cells. The first transfection study used 1000 ng of DNA per well and lipoplexes were formed from a 1:1 +/- ratio of DOTAP to DNA phosphate. The amount of DNA and DOTAP lipid used in each experiment was identical and is unoptimized for this cell line. Figure 2.10 shows the results of this study, which compared both liposomal methods and the DLM_{DMSO} transfection method. The micrographs shown qualitatively demonstrate comparable transfection rates between methods. Quantitative analysis by cell-counting corrects for variable cell density and confirms that transfection efficiencies are similar.

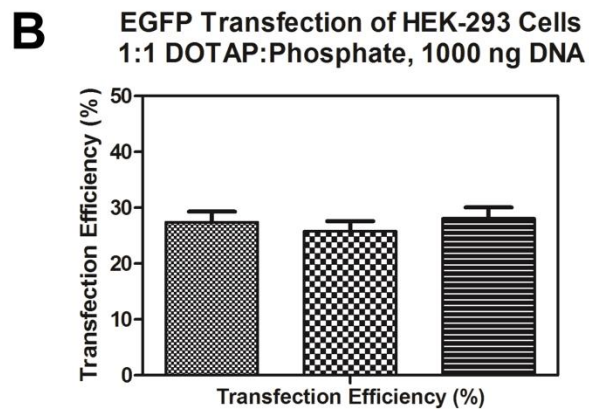
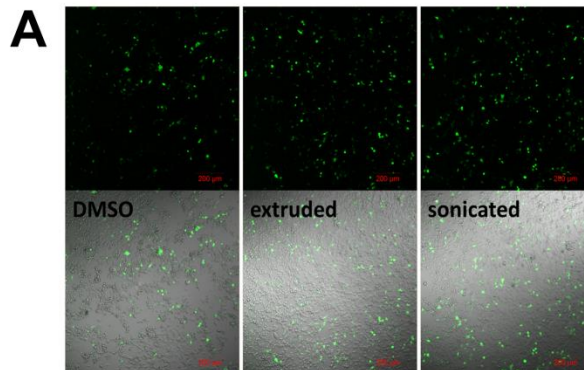


Figure 2.9. (A) Confocal micrographs of DOTAP-transfected HEK-293 cells using DMSO-solvated DOTAP (left), aqueous extruded liposomal DOTAP (middle), and aqueous sonicated liposomal DOTAP (right). The top darkfield images show EGFP fluorescence alone, bottom images are of the same cells with the fluorescence channel overlaid with brightfield to show cell density. (B) Transfection efficiency as determined by cell counting, expressed as a percentage of transfected cells. Error bars represent a $\pm 7\%$ error associated with cell counting.

In order to confirm that similar transfection efficiency was observed under different conditions, we performed an additional transfection at a lower DNA concentration (250 ng per well) and a greater DOTAP:DNA ratio (4:1). The amount of DOTAP per well was the same as in the previous experiment. Lipoplexes in this experiment were prepared by DLM_{EtOH} as well as the previously studied DLM_{DMSO} and sonicated liposome methods. The results from this study are shown in Figure 2.10. Transfected cells were observed for each lipoplex preparation method. The rates of transfection for this DNA and DOTAP concentration regime were uniformly higher than in the previous transfection. The transfection efficiency was similar across all lipid formulation methods. These data suggest that DLM methods and liposomal methods give comparable transfection results under varied transfection conditions.

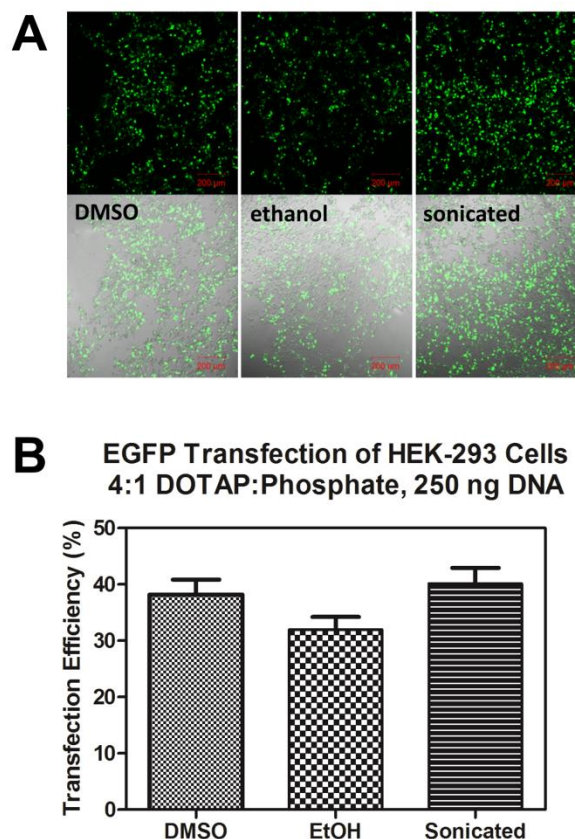


Figure 2.10. (A) Confocal micrographs of DOTAP-transfected HEK-293 cells using DMSO-solvated DOTAP (left), ethanol-solvated DOTAP (middle), and aqueous sonicated liposomal DOTAP (right). The top darkfield images show EGFP fluorescence alone, bottom images are of the same cells with the fluorescence channel overlaid with brightfield to show cell density. (B) Transfection efficiency as determined by cell counting, expressed as a percentage of transfected cells. Error bars represent a $\pm 7\%$ error associated with cell counting.

After obtaining transfection results for the direct-mixing lipoplex formation method with model lipid DOTAP, we examined its applicability to commercial lipofection reagents. The Lipofectamine™ reagents have been used to transfect a variety of cell lines. Viafect™ is a relatively new formulation that claims low cell toxicity. The exact formulations of the reagents are proprietary, but both are aqueous lipid-based solutions. A known volume of the commercial transfection reagent was dried by lyophilization and reconstituted in the same volume of DMSO. This dissolves the liposome assembly, leading to an isotropic solution. The DMSO-dissolved lipids were then mixed with DNA in the same ratio as the aqueous solutions and the resulting lipoplexes were used to transfect HEK-293 cells. Confocal micrographs of

the transfected cells are displayed in Figure 2.11. A quantitative determination of transfection efficiency or fluorescence intensity was not possible in this study due to high cell density. The DNA amount and lipid ratio have not been optimized for this cell line, but in each case both the aqueous and DLM_{DMSO} reagents successfully transfected the cells.

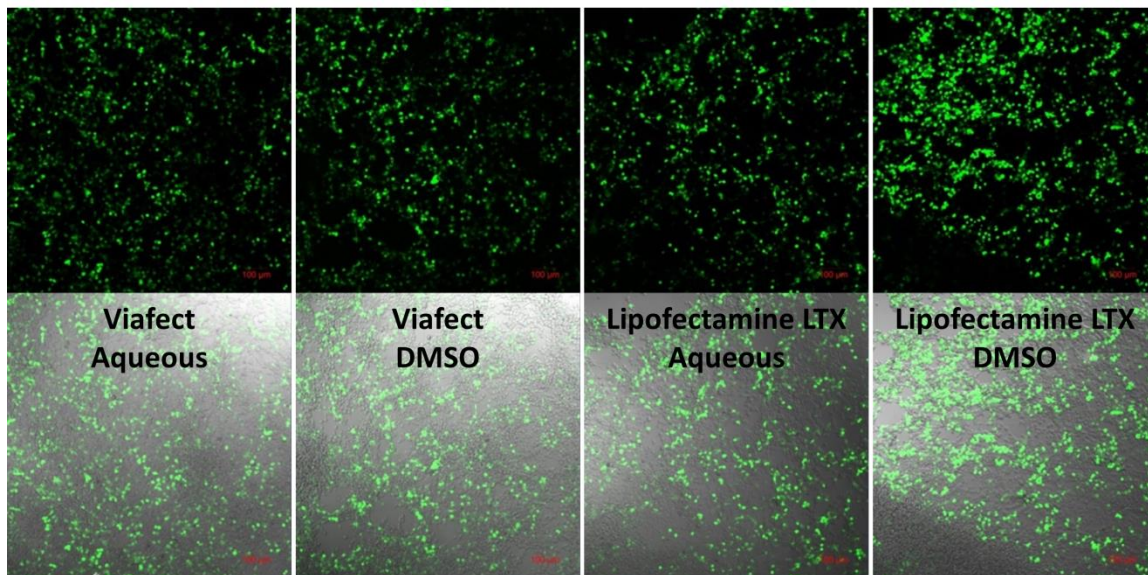


Figure 2.11. Confocal microscopy images of EGFP transfected cells. Top row is darkfield and bottom is brightfield image. Transfection was performed using the commercial reagent Viafect™ as an aqueous liposomal solution (far left) and as a DMSO solution (middle left) and the commercial transfection reagent Lipofectamine LTX™ as an aqueous liposomal solution (middle right) and as a DMSO solution (far right).

2.2.7. Transfection and toxicity assessed by flow cytometry. In order to demonstrate the utility and versatility of the direct lipid mixing method we performed additional transfection experiments using flow cytometry to determine transfection efficiency and toxicity. Transfection efficiency was assessed by EGFP fluorescence and toxicity was determined using the cell impermeant dye propidium iodide (PI).³⁵ For the widespread applicability of this method, it must be useful with multicomponent lipid mixtures in addition to single lipid formulations. The top panel of Figure 2.13 shows the results of the transfection of HEK-293 cells with lipoplexes derived from DOTAP (left) or from 1:1 DOTAP:DOPE (right). In each case the molar ratio of total lipid to DNA phosphate was 4:1. Three DNA concentrations were tested: 1.0, 2.5, and 5.0 $\mu\text{g}/\text{mL}$. The associated toxicities of these methods are represented in the bottom panel of Figure 2.12. In each case, the toxicity of the DLM methods is similar to or less than that observed by using the liposomal methods. The transfection efficiency

of DLM methods with DOTAP were similar to liposomal methods at 2.5 $\mu\text{g/mL}$ DNA, but slightly lower at 5.0 $\mu\text{g/mL}$. The toxicity of DLM methods was less than the liposomal methods when cationic lipids were combined with a helper lipid DOPE. In transfection with the binary lipid system, DLM_{EtOH} was less toxic under these conditions but resulted in low transfection efficiency at 5 $\mu\text{g/mL}$ DNA. DLM_{DMSO} performed significantly better than all other methods having both the highest transfection efficiency and lowest toxicity.

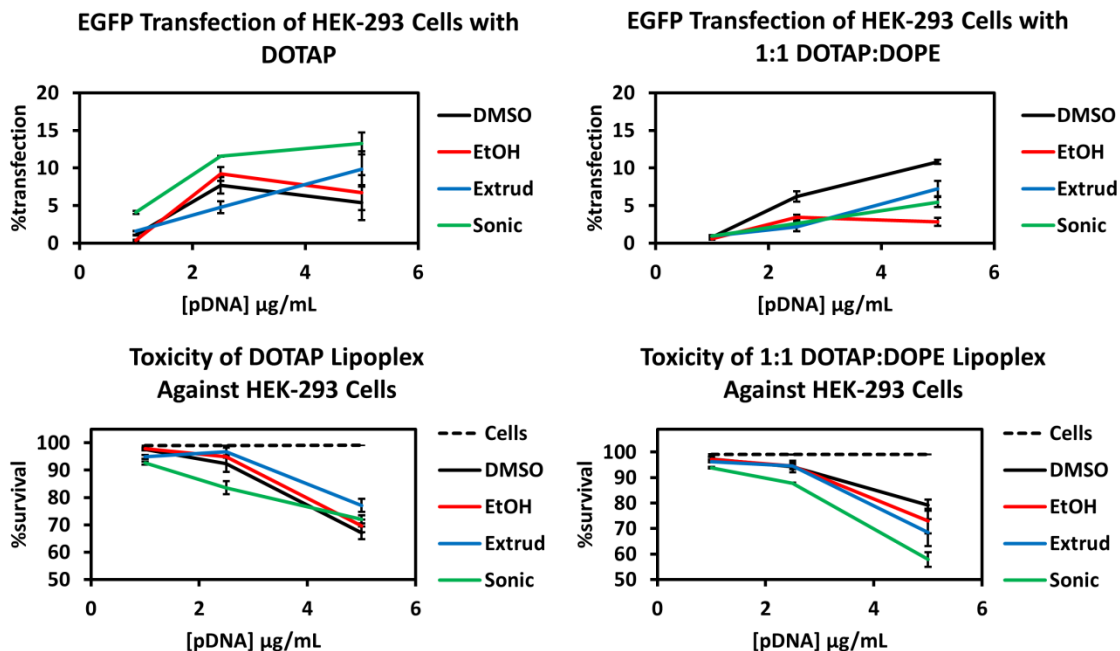


Figure 2.12. Transfection (top) and toxicity (bottom) of DLM and liposomal methods in human embryonic kidney cells. Single-lipid (left) and binary lipid (right) mixtures were assayed.

In addition to assessing transfection efficiency and toxicity for DLM and liposomal methods with different lipid mixtures and various DNA concentrations, the application of DLM in a different cell line was also tested. The COS-7 cell line was chosen because of its widespread use in transfection for the preparation of recombinant proteins.³⁶ The transfection was carried out at 5.0 $\mu\text{g/mL}$ DNA, 4:1 total lipid to DNA phosphate, and with DOTAP or DOTAP:DOPE lipid mixtures. The results are shown in Figure 2.13.

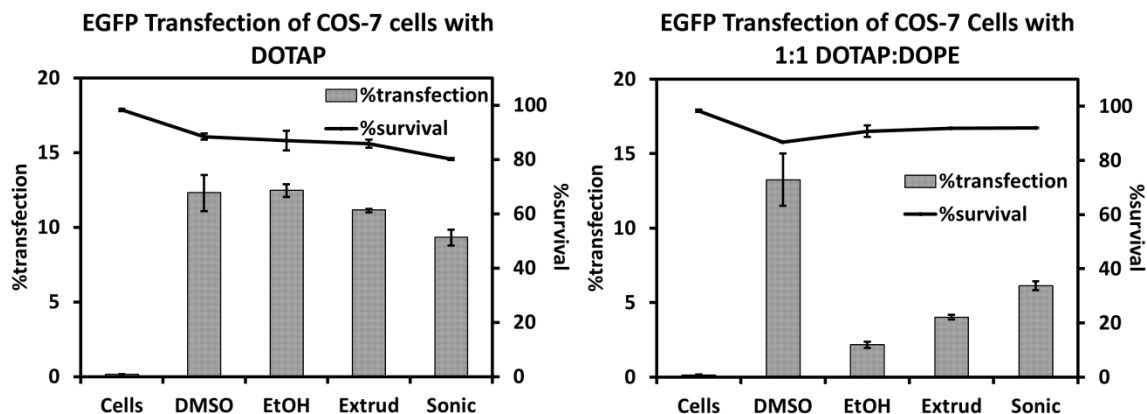


Figure 2.13. Transfection (bars) and toxicity (lines) of DLM and liposomal methods in COS-7 monkey kidney cells. Single-lipid (left) and binary lipid (right) mixtures were assayed.

The transfection of COS-7 (monkey kidney) cells by DLM or liposomal methods with DOTAP or DOTAP:DOPE lipoplexes at 5.0 $\mu\text{g}/\text{mL}$ DNA showed generally lower toxicity than the same transfection conditions in HEK-293 cells. When DOTAP was used alone, DLM and liposomal methods transfected COS-7 cells with similar efficiency and toxicity. For the binary lipid system the transfection results were similar to those found with HEK cells. DLM_{DMSO} was the most efficient, liposomal methods were intermediate, and DLM_{EtOH} was the least effective. The appearance of this trend across two cell lines suggests that DMSO is the preferred solvent for direct lipid mixing for multi-lipid systems at higher DNA concentrations.

The use of DMSO in this procedure deserves comment. Since this solvent's introduction into biological studies, the reports of its effects have varied from extremely favorable in certain applications to those uses where its presence was inimical to the desired outcome. We recently showed that the application of DMSO in a series of related systems showed some variation in outcome under similar conditions.³⁷ Notwithstanding, the studies presented here show that when used as prescribed, the transfection outcomes are reproducible and comparable to procedures that require greater manipulation.

The primary utility of this method, and indeed the conditions under which it has been tested, is for *in vitro* transfection with plasmid DNA. The application of the method to *in vitro* oligonucleotide delivery is under investigation. While not currently being tested, the extension of this method to *in vivo* transfection studies is not precluded. Organic solvents have long been used safely to solubilize drugs for parenteral applications and as embolic liquids themselves.³⁸ While the initial mixing of lipid and DNA in the DLM method results in a solution of 15-50% by volume of

organic solvent, the solution delivered to cells consisted of only 1% organic solvent or less and was effective in media with or without serum. DMSO is listed as an inactive ingredient in approved drugs in the United States for topical administration in three FDA applications and for a single intravenous application (lyophilized powder, DMSO content not specified).³⁹ Ethanol is listed as an inactive ingredient in many topical applications and at least 15 intravenous or intramuscular applications with intravenous injection concentrations as high as 92%.

2.3. Conclusion.

The present approach is a simplification of established methodology. It uses known lipids to form lipoplexes that are successfully transfected into mammalian cells. The studies presented here are side-by-side comparisons of two previous methods with the present approach. The key advantages of the method described here are convenience, cost, and efficiency. The comparative data confirm that the present approach affords transfection results that are comparable to those obtained by using methods that are in more common use. A summary diagram comparing the known and present methods is shown as Figure 2.14.

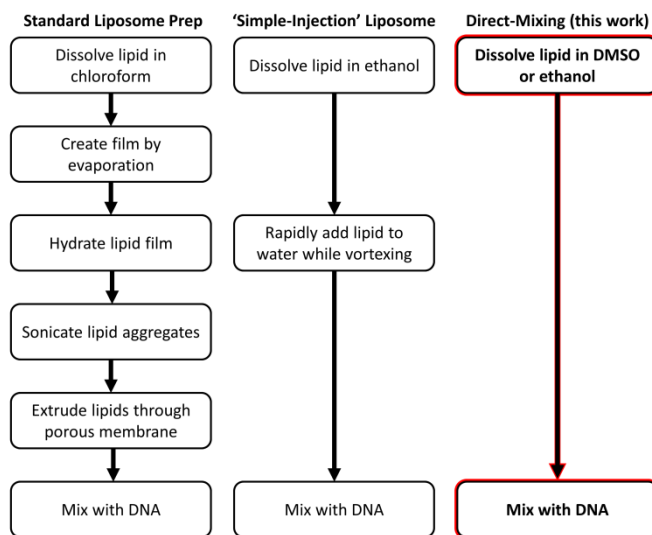


Figure 2.14. Flow chart demonstrating lipoplex methods compared herein. Depicted are the liposomal methods of standard lipid film hydration-sonication-extrusion (left), simple-injection method (middle), and the non-liposomal direct lipid mixing (DLM) method featured in this work (right).

Taken together, the results reported in this work demonstrate that the liposomal structure itself is not a necessary prerequisite to lipoplex formation. Liposome formation can be bypassed by dissolving lipids in an aqueous-miscible organic

solvent and mixing directly with an aqueous solution of DNA. The resulting lipoplexes transfected HEK-293 and COS-7 mammalian cells with efficiencies comparable to the standard protocol. This was demonstrated with the model lipid DOTAP dissolved either in dimethylsulfoxide or in ethanol. Our results suggest that the DLM_{DMSO} method is advantageous in binary or multi-lipid systems. We also provide evidence that the DLM_{DMSO} method works with the commercial lipid formulations Lipofectamine LTX™ and Viafect™.

By obviating the necessity for liposome-forming lipids, this work greatly expands the range of chemical structures that can be tested for transfection ability.

Furthermore, the process of optimizing lipid formulations to a particular cell line is simplified. Of course, the choice of solubilizing solvent is an important consideration. While DMSO and ethanol were the solvents tested in this study, other solvents might be used. Minimally, the solvent must dissolve the transfection reagents and be miscible with water. The biological effects of such solvents on their own should also be examined and controlled for, with our results indicating that DMSO and ethanol have no observable effect on toxicity at the concentrations used. We anticipate that the development of the DLM method, while modest, may potentiate the pursuit of higher efficiency, more selective transfection reagents for biological research and gene therapy.

2.4. Experimental.

Lipofectamine™ and Viafect™ were obtained from commercial sources as aqueous suspensions. DOTAP was obtained from Avanti Polar Lipids (Alabaster, AL, USA) in solid form as the chloride salt. Plasmid DNA (pKLMF-FX, 9.988 kb, New England Biolabs or pCDNA3-EGFP, 6.160 kb, Addgene # 13031) was amplified in *E. coli*, extracted using Zyppy™ Maxiprep spin columns, purified by NaCl/ethanol precipitation, and dissolved in 18.2 MΩ purified water.

2.4.1. Lipid preparations.

Sonicated and extruded DOTAP liposomes. A 1.0 mL solution of 6.06 mM (or 24.24 mM for transfection) DOTAP-Cl in chloroform was prepared in a clean glass vial. Chloroform was removed by rotary evaporation to leave a thin film of lipid. The lipid film was hydrated with 1.0 mL 18.2 MΩ purified water, vortexed, and sonicated to homogeneity. Extruded liposomes were prepared from sonicated lipids by passing the solution through a 0.2 μm Whatman filter membrane 11 times.

DMSO (or ethanol)-dissolved DOTAP lipid. A 1.0 mL solution of 6.06 mM (24.24 mM for transfection) DOTAP-Cl in dimethyl sulfoxide (or ethanol) was prepared in a clean glass vial. The solution was incubated at 37 °C on an orbital shaker at 50 rpm and vortexed to ensure complete dissolution.

DMSO-Dissolved commercial transfection solutions. A 100 μL solution of Lipofectamine LTX™ or Viafect™ formulation was lyophilized on a Labconco Lyph Lock 6 freeze dryer. The residue was then dissolved in 100 μL DMSO and used as directed.

2.4.2. Transfection procedure. Transfection was carried out on HEK-293 cells in antibiotic-free media on black Nunc™ 96-well optical-bottom plates (Thermo Scientific). Plates were seeded with 20,000 cells/well in antibiotic-free Dulbecco's modified Eagle's medium (DMEM), 10% fetal bovine serum (FBS) and grown to approximately 70% confluency before transfection. DOTAP-pCDNA3-EGFP lipoplexes of 1:1 +/- ratio were prepared by mixing 5 μL 6.06 mM DOTAP (sonicated, extruded, DMSO-dissolved, or EtOH-dissolved) with 100 μL of 100 ng/ μL plasmid DNA. Lipoplex-containing media was prepared by adding 42 μL lipoplex solution to 400 μL DMEM (FBS-free). Lipoplexes of 4:1 +/- ratio were formed by the same procedure using 24.24 μM lipid and diluted 4-fold with 18.2 M Ω H₂O, controlling for DMSO or ethanol content for DLM methods. Cell media was removed and 110.5 μL lipoplex media was added to cells and incubated 90 min, 37 °C, 5% CO₂ before 200 μL DMEM (containing blasticidin and 10% FBS) was added. Cells received either 1000 ng DNA at 1:1 +/- ratio or 250 ng DNA at 4:1 +/- ratio. The final concentration of DMSO or ethanol was less than 0.5%. After 36 h, cell media was replaced with phosphate-buffered saline and cells were imaged on a Zeiss LSM 700 confocal microscope.

2.4.3. Flow Cytometry. Transfection for flow cytometry experiments was performed in 24-well plates treated for cell culture. Cells were seeded in 1 mL aliquots at 50,000 cells per well in DMEM with 10% FBS and grown to about 70% confluency overnight. Lipoplexes were prepared as described above for a 4:1 total lipid to DNA phosphate molar ratio. DOTAP trials were performed in triplicate and DOTAP:DOPE trials were performed in duplicate. Transfection was performed in 0.5 mL DMEM (FBS-free) containing the lipoplex for 90 min, 37 °C, 5% CO₂ before 0.5 mL DMEM (10% FBS) was added. The DNA concentration before the DMEM+FBS supplement for HEK-293 transfection was 1.0, 2.5, or 5.0 $\mu\text{g}/\text{mL}$; COS-7 cells were transfected in an identical manner at 5.0 $\mu\text{g}/\text{mL}$ DNA. After 24 h, the cell media was removed and centrifuged at 100 x g for 5 min to collect dead cells (for toxicity assay) and the supernatant was removed. Adherent cells were collected by washing with 0.3 mL PBS, adding 0.3 mL 0.25% trypsin-EDTA solution and incubating 5 min at 37 °C, then 0.7 mL DMEM+FBS was added and the cells were combined with dead cells and centrifuged at 100 x g for 10 min. The supernatant was removed and cells were resuspended in 300 μL DMEM+FBS. To stain dead cells 0.5 μL 0.5 mg/mL propidium

iodide (PI) solution was added. Cells were analyzed on a BD Biosciences FACSCanto II. EGFP was detected by excitation at 488 nm using a 530/30 nm filter, 520 LP mirror; PI was detected by excitation at 488 nm using a 670 nm filter, 655 LP mirror. Toxicity and transfection efficiency were determined by gating out cell debris and establishing a quadrant analysis based on PI +/- and EGFP +/- . Toxicity is reported as %survival = (PI-/EGFP- + PI-/EGFP+)/total cells. Transfection efficiency is reported as %transfection = (PI-/EGFP+)/total cells. After gating out debris each analysis contained about 30,000 cells on average.

2.4.4. Agarose Gel Electrophoresis. Agarose powder was obtained from Sigma Aldrich. Purified water with 18.2 M Ω resistivity (Milli-Q) was used in all cases. Gels were cast by heating a 0.5% w/v solution of agarose in 40 mM tris-acetate buffer (pH 7.2) until fully dissolved, then cast by cooling the solution to room temperature in an Owl B2 horizontal electrophoresis chamber with a centrally placed 20-well comb. The gel was submerged under 40 mM tris-acetate (pH 7.2) running buffer, samples were added to the wells, and the gel was run 90 minutes at 105 \pm 3 volts. Gels were stained in 2.5 μ g/mL ethidium bromide for 15 minutes at 37 $^{\circ}$ C, 50 rpm, and destained in Milli-Q water for 5 minutes at 37 $^{\circ}$ C, 50 rpm. Ethidium bromide-stained DNA was visualized using a UV trans-illuminator.

Gel images were analyzed by densitometry using ImageJ software.⁴⁰ Lane profile plots were generated and integrated (data not shown). Using manual baselines, the control plasmid was set as 100% DNA migration. The inverse of the DNA migration in experimental wells relative to control DNA migration gave a measure of percent DNA retention. Results presented are the average of three gels.

2.4.5. Dynamic Light Scattering. Measurements were performed on a Brookhaven Instruments Corp. ZetaPALS instrument at 37 $^{\circ}$ C using a 660 nm laser and correlating scattering at 90 $^{\circ}$. Samples were prepared by adding 10 μ L 6.06 mM lipid solution to 200 μ L of 25, 50, or 100 ng/ μ L pKLMF-FX or pCDNA3-EGFP in a pre-cleaned glass vial. The mixture was vortexed and incubated at room temperature for 5 minutes then diluted to 2.0 mL with 37 $^{\circ}$ C 18.2 M Ω H₂O, transferred to a clean glass cuvette and equilibrated in the instrument for 5 min at 37 $^{\circ}$ C. Ten measurements consisting of two-minute runs were made on each sample. The average effective diameter was calculated with the standard deviation reported as the error.

2.4.6. Transmission Electron Microscopy. The samples from dynamic light scattering measurements were also used for TEM. A 10 μ L sample was applied to lacey formvar/carbon 300 mesh copper TEM grids (Ted Pella, Inc.) for 60 seconds and the grid was washed with 18.2 M Ω H₂O (30 s), stained with 2 % uranyl acetate (30 s),

and washed twice with H₂O (15 s each). The above solutions were applied at a volume of 10 µL, wicked away between each application, and the grid was finally dried with a gentle N₂ stream. Specimens were examined on a JEOL JEM-2000 FX transmission electron microscope operated at 300 keV. Lamellae measurements were performed by ImageJ analysis of electron micrographs. Briefly, density profiles perpendicular to lamellae were generated from a minimum of 6 lipoplex structures per sample. Lamellar spacings were obtained by taking the first derivative of the density profile function.

2.5. References.

- 1 Szybalska, E. H.; Szybalski, W., Genetics of human cell lines, IV. DNA-mediated heritable transformation of a biochemical trait. *Proc. Natl. Acad. Sci. U. S. A.* **1962**, *48*, 2026-2034.
- 2 Vaheri, A.; Pagano, J. S., Infectious poliovirus RNA: a sensitive method of assay. *Virology* **1965**, *27*, 434-436.
- 3 McCutchan, J. H.; Pagano, J. S., Enhancement of the infectivity of Simian Virus 40 deoxyribonucleic acid with diethylaminoethyl-dextran. *JNCI J. Natl. Canc. Institut.* **1968**, *41*, 351-357.
- 4 Benzinger, R.; Kleber, I.; Huskey, R., Transfection of Escherichia coli spheroplasts I. general facilitation of double-stranded deoxyribonucleic acid infectivity by protamine sulfate. *J. Virol.* **1971**, *7*, 646-650.
- 5 Henner, W. D.; Kleber, I.; Benzinger, R., Transfection of Escherichia coli spheroplasts III. facilitation of transfection and stabilization of spheroplasts by different basic polymers. *J. Virol.* **1973**, *12*, 741-747.
- 6 Graham, F. L.; van der Eb, A. J., A new technique for the assay of infectivity of human adenovirus 5 DNA. *Virology* **1973**, *52*, 456-467.
- 7 Fynan E. F.; Webster, R. G.; Fuller, D. H.; Haynes, J. R.; Santoro, J. C.; Robinson, H. L., DNA vaccines: protective immunizations by parenteral, mucosal, and gene-gun inoculations. *Proc. Natl. Acad. Sci. U. S. A.* **1993**, *90*, 11478-11482.
- 8 Ikemoto, K.; Sakata, I.; Sakai, T., Collision of millimetre droplets induces DNA and protein transfection into cells. *Sci. Rep.* **2012**, *2*, 289.
- 9 Neumann, E.; Schaefer-Ridder, M.; Wang, Y.; Hofschneider, P. H., Gene transfer into mouse lyoma cells by electroporation in high electric fields. *EMBO J.* **1982**, *7*, 841-845.
- 10 Marmottant, P.; Hilgenfeldt, S., Controlled vesicle deformation and lysis by single oscillating bubbles. *Nature* **2003**, *423*, 153-156.
- 11 Scherer, F.; Anton, M.; Schillinger, U.; Henke, J.; Krüger, A.; Gänsbacher, B.; Plank, C., Magnetofection: enhancing and targeting gene delivery by magnetic force in vitro and in vivo. *Gene Ther.* **2002**, *9*, 102-109.

- 12 De Smedt, S. C.; Demeester, J.; Hennink, W. E., Cationic polymer based gene delivery systems. *Pharm. Res.* **2000**, *17*, 113-126.
- 13 Sokolova, V.; Epple, M., Inorganic nanoparticles as carriers of nucleic acids into cells. *Angew. Chem. Int. Ed.* **2008**, *47*, 1382-1395.
- 14 Fraleyt, R.; Subramani, S.; Berg, P.; Papahadjopoulos, D., Introduction of liposome-encapsulated SV40 DNA into cells. *J. Biol. Chem.* **1980**, *255*, 10431-10435.
- 15 Felgner, P. L.; Gadek, T. R.; Holm, M.; Roman, R.; Chan, H. W.; Wenz, M.; Northrop, J. P.; Ringold, G. M.; Danielsen, M., Lipofection: A highly efficient, lipid-mediated DNA-transfection procedure. *Proc. Natl. Acad. Sci. U.S.A.* **1987**, *84*, 7413-7417.
- 16 Li, W.; Szoka Jr., F. C., Lipid-based nanoparticles for nucleic acid delivery. *Pharm. Res.* **2007**, *24*, 438-449.
- 17 Rädler, J. O.; Koltover, I.; Salditt, T.; Safinya, C. R., Structure of DNA-cationic liposome complexes: DNA intercalation in multilamellar membranes in distinct interhelical packing regimes. *Science* **1997**, *275*, 810-814.
- 18 Safinya, C., Structures of lipid-DNA complexes: supramolecular assembly and gene delivery. *Curr. Opin. Struct. Biol.* **2001**, *11*, 440-448.
- 19 Israelachvili, J. N.; Mitchell, D. J.; Ninham, B. W., Theory of self-assembly of hydrocarbon amphiphiles into micelles and bilayers. *J. Chem. Soc. Faraday Trans. 2* **1976**, *72*, 1525-1568.
- 20 Bangham, A. D.; Standish, M. M.; Watkins, J. C., Diffusion of univalent ions across the lamellae of swollen phospholipids. *J. Mol. Biol.* **1965**, *13*, 238-252.
- 21 Olson, F.; Hunt, C. A.; Szoka, F. C.; Vail, W. J.; Papahadjopoulos, D., Preparation of liposomes of defined size distribution by extrusion through polycarbonate membranes. *Biochim. Biophys. Acta.* **1979**, *557*, 9-23.
- 22 Batzri, S.; Korn, E. D., Single bilayer liposomes prepared without sonication. *Biochim. Biophys. Acta.* **1973**, *298*, 1015-1019.
- 23 Campbell, M. J., Lipofection reagents prepared by a simple ethanol injection technique. *Biotechniques* **1995**, *18*, 1027-1032.
- 24 Jeffs, L. B.; Palmer, L. R.; Ambegia, E. G.; Giesbrecht, C.; Ewanick, S.; MacLachlan, I., A scalable, extrusion-free method for efficient liposomal encapsulation of plasmid DNA. *Pharm. Res.* **2005**, *22*, 362-372.
- 25 Hayes, M. E.; Drummond, D. C.; Kirpotin, D. B.; Zheng, W. W.; Noble IV, C. O.; Park, J. W.; Marks, J. D.; Benz, C. C.; Hong, K., Genospheres: self-assembling nucleic acid-lipid nanoparticles suitable for targeted gene delivery. *Gene Ther.* **2006**, *13*, 646-651.

- 26 Stamatatos, L.; Leventis, R.; Zuckermann, M. J.; Silvius, J. R., Interactions of cationic lipid vesicles with negatively charged phospholipid vesicles and biological membranes. *Biochemistry* **1988**, *27*, 3917-3925.
- 27 Leventis, R.; Silvius, J. R., Interactions of mammalian cells with lipid dispersions containing novel metabolizable cationic amphiphiles. *Biochim. Biophys. Acta* **1990**, *1023*, 124-132.
- 28 Simberg, D. *et al.* Phase behavior, DNA ordering, and size instability of cationic lipoplexes. *J. Biol. Chem.* **276**, 47453-47459 (2001).
- 29 Nisslert, R.; Kvarnström, M.; Lorén, N.; Nydén, M.; Rudemo, M., *J. Microscopy*, **2007**, *225*, 10-21.
- 30 Bangham, A. D.; Standish, M. M.; Watkins, J. C., Diffusion of univalent ions across the lamellae of swollen phospholipids. *J. Mol. Biol.* **1965**, *13*, 238-252.
- 31 Grit, M.; Crommelin, D. J., Chemical stability of liposomes: implications for their physical stability. *Chem. Phys. Lipids* **1993**, *64*, 3-18.
- 32 Weisman, S.; Hirsch-Lerner, D.; Barenholz, Y.; Talmon, Y., Nanostructure of cationic lipid-oligonucleotide complexes. *Biophys. J.* **2004**, *87*, 609-614.
- 33 Rädler, J. O.; Koltover, I.; Jamieson, A.; Salditt, T.; Safinya, C. R., Structure and interfacial aspects of self-assembled cationic lipid-DNA gene carrier complexes. *Langmuir* **1998**, *14*, 4272-4283.
- 34 Pitard, B.; Oudrhiri, N.; Vigneron J.-P.; Hauchecorne, M.; Aguerre, O.; Toury, R.; Airiau, M.; Ramasawmy, R.; Scherman, D.; Crouzet, J.; Lehn, J.-M.; Lehn, P., Structural characteristics of supramolecular assemblies formed by guanidinium-cholesterol reagents for gene transfection. *Proc. Natl. Acad. Sci. U.S.A.* **1999**, *96*, 2621-2626.
- 35 Petrunka, A. M.; Harrison, R. A. P., Mathematical analysis of mis-estimation of cell subsets in flow cytometry: viability staining revisited. *J. Immunol. Methods* **2011**, *368*, 71-79.
- 36 Blasey, H. D.; Aubry, J.-P.; Mazzei, G. J.; Bernard, A. R., Large scale transient expression with COS cells. *Cytotechnology* **1996**, *18*, 183-192.
- 37 Negin, S.; Gokel, M. R.; Patel, M. B.; Sedinkin, S. L.; Osborn, D. C.; Gokel, G. W., The aqueous medium-dimethyl sulfoxide conundrum in biological studies. *RSC Adv.* **2015**, *5*, 8088-8093.
- 38 Mottu, F.; Laurent, A.; Rüfenacht, D. A.; Doelker, E., Organic solvents for pharmaceutical parenterals and embolic liquids: a review of toxicity data. *PDA J. Pharm. Sci. Technol.* **2000**, *54*, 456-469.
- 39 United States Food and Drug Association Center for Drug Evaluation and Research, Inactive Ingredient Database, <http://www.accessdata.fda.gov/scripts/cder/iig/index.cfm> (Feb. 29, 2016), accessed April 30, 2016.

40 Rasband, W.S. ImageJ 1.47v. U. S. National Institutes of Health, Bethesda, Maryland, USA, (1997-2015) Available at: <http://imagej.nih.gov/ij/> (Accessed: 21st October 2015)

Chapter 3

Condensation of Plasmid DNA by Benzyl Hydraphiles and Lariat Ethers: Dependence on pH and Chain Length

3.1. Introduction.

Deoxyribonucleic acids are vast stacks of planar heterocycles linked by a sugar phosphate backbone. The large size of DNA, coupled with the ionized phosphates, comprises a barrier that prevents passage of these molecules through phospholipid membranes. The emergence of gene therapy has engendered the search for agents that can overcome these impediments and permit DNA to enter cells. The obvious goal is to find inexpensive, non-toxic, and efficient transformation and transfection agents.¹ Viruses,² polyamines,³ and even mechanical devices (gene gun)⁴ have been used to facilitate DNA transport into cells. A standard methodology for delivering DNA in transfection experiments is to form a lipoplex in which DNA is within a complex consisting of at least lipid monomers.⁵ Liposomal delivery methods are increasingly common, especially those utilizing such commercial reagents as Lipofectamine.[®]

We have long been interested in binding⁶ and transporting both cations⁷ and anions.⁸ We surmised that the lariat ether⁹ and hydraphile¹⁰ amphiphiles that we had previously developed might be applicable in this context. In particular, we sought to characterize DNA complexation by either lariats or hydraphiles by using gel electrophoresis. The metric for this experiment would be to determine how much of the amphiphile was required to condense DNA. Complexing or neutralizing the surface phosphates would diminish the DNA plasmid's response to an electric field and reduce or prevent its mobility on agarose gel.

A recent report¹¹ describes the incorporation of steroidal lariat ethers¹² into liposomes prepared from 3β [*N,N'*-dimethylaminopropyl]carbonyl]cholesterol and dioleoylphosphatidylethanolamine (DOPE). These liposomes included plasmid DNA within them and the lipoplexes were used to transfect human embryonic kidney (HEK-293) cells. We were intrigued by this report for three reasons. First, we originally reported the two steroidal carbamate lariat ethers chosen for the study.¹³ Second, we have recently reported a new and simplified direct mixing lipoplex preparation method.¹⁴ Third, we have a long-standing interest in the complexation and transport properties of various lariat ethers and pore-forming hydraphiles.¹⁵ The compounds used in the Sewbalas *et al.* study¹¹ are shown in the upper left of Figure 3.1. The amphiphilic lariat ether family that we have extensively studied¹⁶ is shown in the upper right of the Figure and the pore-forming hydraphiles that are the subject of the present report are illustrated in the bottom panel.

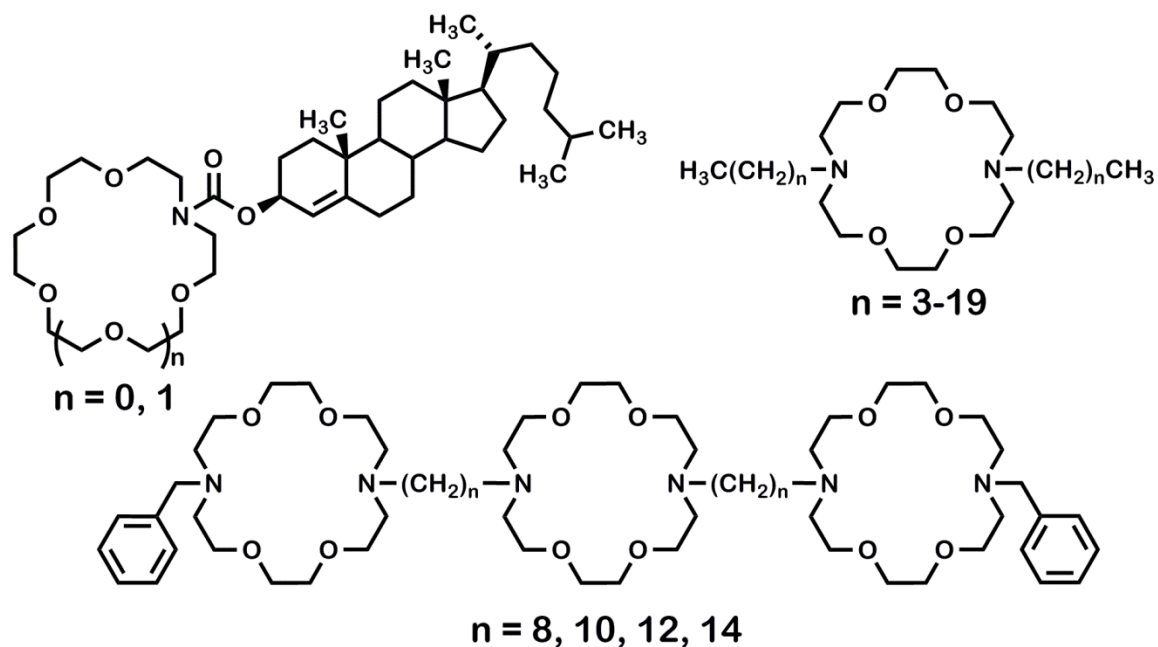


Figure 3.1. 15- and 18-membered ring cholesteryl lariat ethers reported as transfection agents in reference 11 (upper left). Dialkyl lariat ethers previously studied whose binding constants are noted herein (upper right). Lower structure shows hydraphiles studied for the present report.

The lariats in the above cited report¹¹ were chosen for a transfection application because they are amphiphiles and they insert in membranes.¹⁷ The cholesteryl residue obviously imparts membrane solubility to the mixture and likely enhances the stability of the liposomes in this three-component mixture. A significant difference between the carbamoylated lariat ethers and either dialkyl lariats or hydraphiles is that the latter two compounds can be protonated at nitrogen. Amidic and carbamoyl lariat ethers cannot be readily protonated and the amidic links to the macrocyclic ring rigidifies them. Moreover, amidic and carbamoyl lariat ethers are typically poor cation binders.¹⁸ Notwithstanding, the macrocyclic ring is polar enough to comprise an amphiphilic head group whether or not its polarity is augmented by binding a cation.¹⁹

The compounds that we call hydraphiles are synthetic amphiphiles that insert into phospholipid bilayer membranes and mediate the passage of cations by pore formation.²⁰ Moreover, they are multiple cation binders.²¹ We envisioned that hydraphiles and amphiphilic, alkyl side-chained lariat ethers could interact with DNA in either or both of two possible ways. The DNA polyphosphate ladder is negatively charged, but associated with cations. Both lariat ethers and hydraphiles could form complexes with cations that are further associated with DNA. Alternately,

the amine nitrogen atoms present in either type of structure could undergo protonation at physiological pH and the di- or polyammonium salts could associate with DNA. In either case, DNA mobility across a phospholipid bilayer—and ultimately the potential to transfect mammalian cells—might be enhanced.

In the work reported here, we have found that alkyl side armed lariat ethers and hydraphiles do, indeed, form assemblies with DNA that lead to diminished mobility under electrophoretic conditions on agarose gels. We report below the effects of compound structure, variations in cations, and changes in pH on DNA mobility and present evidence from electron microscopy that complexes of significant size form between the amphiphiles and DNA.

3.2. Results and Discussion.

3.2.1. Compounds studied. Plasmid DNA (pKLMF-FX, 10 kilobase)²² was obtained from New England Biosciences and amplified in *E. coli* and extracted by using standard protocols (*see* Experimental Section). This plasmid was used in all studies reported herein. Two types of closely related compounds that we anticipated would interact with this plasmid are the lariat ether²³ derivatives based on 4,13-diaza-18-crown-6 derivatives in which each macroring nitrogen is substituted by an alkyl group: *n*-butyl, *n*-hexyl, *n*-octyl, *n*-decyl, *n*-dodecyl, *n*-tetradecyl, *n*-hexadecyl, and *n*-octadecyl. The hydraphiles are *tris*(macrocycle)s that form cation-conducting pores in phospholipid bilayer membranes.¹⁰ Four hydraphiles were prepared and studied for the present report.²⁴ Figure 3.1 shows both lariat ethers and hydraphiles. The latter have benzyl side arms on the distal macrocycles and the internal spacer chains are octylene, decylene, dodecylene, or tetradecylene.

3.2.2. Assay of DNA complex gel mobility (gel retardation). DNA polymers are rich in phosphate anions and accompanying cations. Both lariat ethers²⁵ and hydraphiles²¹ bind cations. Moreover, both are membrane active, albeit by different mechanisms.^{4,19} The lariat ethers are typically carriers²⁶ whereas hydraphiles of appropriate length form ion-conducting pores.²⁷ The lariat ethers and the hydraphiles that are the subject of this study not only bind and transport cations, they have protonatable nitrogen atoms. Any ammonium salt is expected to interact with phosphate anions present in DNA chains.

One means by which the interaction of DNA with another compound can be assayed is a change in electrophoretic mobility. In this study, the mobility of the amphiphile•DNA complex on an agarose gel was compared to migration of DNA alone. DNA migration was visualized by using ethidium bromide.²⁸ This dye intercalates in DNA, which enhances its fluorescence. Typically, the macrocyclic

complexing agent will not interact with ethidium bromide to enhance fluorescence and no signal will be observed absent the dye's interaction with DNA. In control experiments, no fluorescent enhancement was observed when ethidium bromide was present in solutions containing either lariat ethers or hydraphiles at concentrations similar to those used with gels.

The presence of either benzyl C₈ or benzyl C₁₄ hydraphile admixed with the DNA plasmid was found to inhibit DNA plasmid mobility. The study was conducted on an agarose gel in the presence of tris-acetate (TA) buffer. The divalent cation chelating agent ethylenediaminetetraacetic acid (EDTA) was omitted without affecting DNA stability. Figure 3.2 shows an image of the stained gel obtained by UV transillumination. The compound mixture was placed in wells which are clearly illuminated upon staining after the gel was run. This suggested that the amphiphile•DNA complexes were either too large to move through the pores in the gel or the surface charge of the complex was too low to respond to the applied potential. The effect on mobility is dependent on the amount of hydraphile used and on the length of the hydraphile spacer chain. Benzyl C₈ hydraphile prevented the migration of plasmid DNA at a ratio of 5.0 equivalents of amphiphile to DNA phosphate. The longer chained benzyl C₁₄ hydraphile retained DNA more effectively, requiring a ratio of 3.5 equivalents. Better retention by hydraphiles having longer spacer chains implies at least some hydrophobic effect in DNA complexation by these compounds.

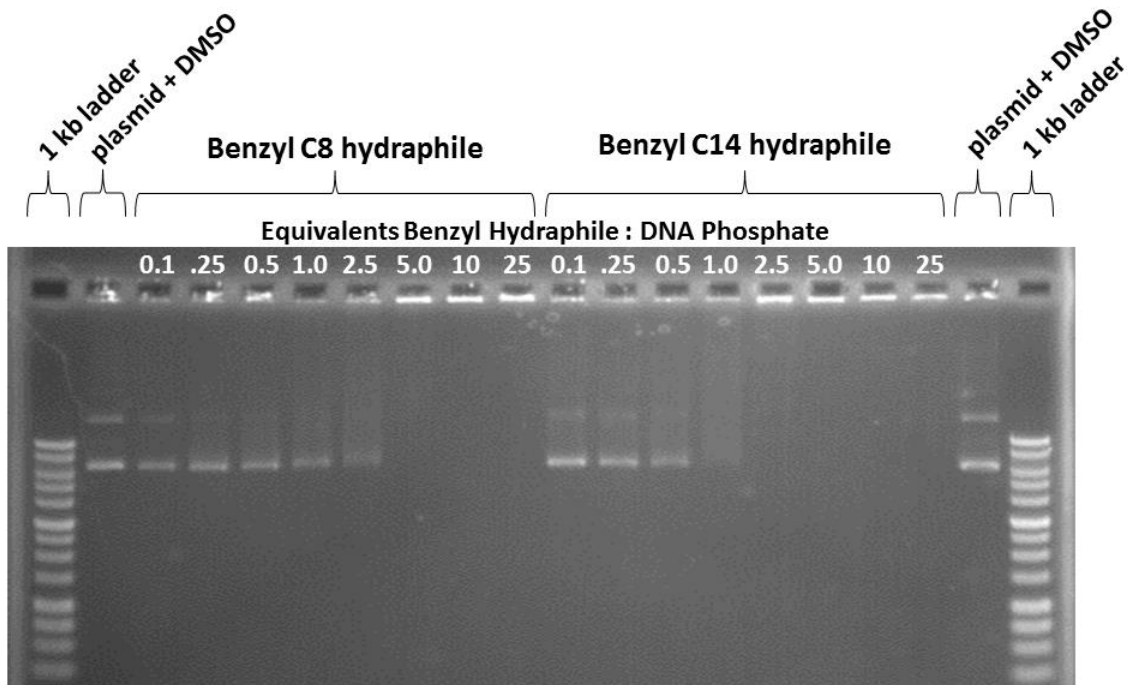


Figure 3.2. Electrophoretic mobility assay for increasing concentrations of benzyl C₈ hydrophile and benzyl C₁₄ hydrophile mixed with 10 kb plasmid DNA at pH 8.5 in tris-acetate buffer.

It is interesting to note that the shift in DNA mobility is observed as complete immobility of DNA. In other words, the DNA either migrates normally or is retained in the well. The absence of major bands of DNA between the plasmid control and the well suggests that complexation is cooperative.

Based on our experience in crown ether²⁹ and cation complexation⁶ chemistry as well as ion transport, we envisaged a tripartite crown-sodium cation-DNA phosphate sandwich complex. Figure 3.3 shows two 4,13-diaza-18-crown-6 structures complexed in different ways to a DNA fragment. Typically, a crown ether will complex an alkali metal cation such as K⁺ within the macroring and the four oxygen and two nitrogen atoms will contact the ion, disperse the charge, and stabilize the assembly.³⁰ Thus, we anticipated that complexation would be cation dependent. To test this hypothesis, we performed agarose gel electrophoresis³¹ with the DNA plasmid described above by varying both the hydrophile:phosphate ratios and the alkali metal cations.

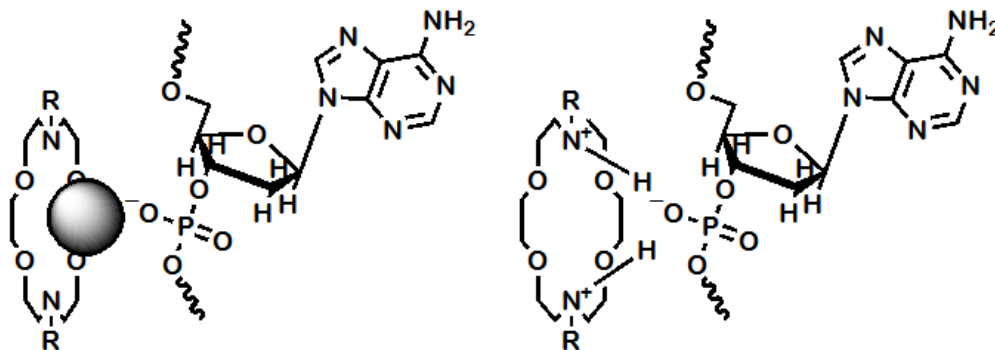


Figure 3.3. Left: A tripartite sandwich complex in which both crown and phosphate anion bind Na⁺. Right: Alternate complexation mode in which protonated crown serves as an H-bond donor for phosphate anion. The anion could also be closer to the positive charge than represented schematically.

We first obtained the required cation-DNA salt by precipitation from aqueous ethanol in the presence of NaCl, LiCl, or KCl. It seemed possible that the tris ammonium cation in the gel running buffer would exchange with the alkali metal cation so a metal cation-borate system was used.³² Borate buffers were prepared by dissolving the appropriate alkali metal hydroxide in pure water and then adjusting the pH with boric acid followed by sterile filtering. The final buffer pH was 8.2.

Either benzyl C₈ or benzyl C₁₄ hydrophile was mixed with DNA in concentration ratios (hydrophile:DNA phosphate) ranging from 0.1 to 17 equivalents. Identical results were obtained whether the gel was run in lithium, sodium, or potassium borate buffer. In each case, the DNA remained in the well at ratios as high as 5 equivalents of benzyl C₁₄ hydrophile or 17 equivalents of benzyl C₈ hydrophile. We concluded that there was no differential alkali metal cation participation in the hydrophile-DNA binding.

An alternate hypothesis was that the nitrogen atoms within the diazacrown ethers were protonated in the running buffer and the resulting ammonium cations interact with the DNA phosphate residues. This hypothesis was addressed experimentally by varying buffer solution pH. At lower pH values, the macrocyclic nitrogen atoms protonate to form a diammonium salt as shown at the right Figure 3.3. A *bis*(cation) is unlikely to bind a third cation, but it may interact with an anion by hydrogen bonding or by simple charge-charge stabilization. To the extent that cations are solvent separated from the DNA phosphates, the diprotonated macrocycle can form the type of diammonium phosphate complex shown.

The protonated diazacrown hypothesis was tested by mixing varying equivalents of benzyl C₈ or benzyl C₁₄ hydrophile with DNA, then running tris-acetate buffered gels at pH values of 7.4, 8.5, and 9.4 (Figure 3.4). We expect no appreciable change in the protonation state of DNA phosphates over this range, as the pK_A of the phosphate residues is ~0-2. Greater DNA retention in the wells at lower equivalents of benzyl C₈ hydrophile was observed as pH decreased. The results were similar, but less pronounced, for benzyl C₁₄ hydrophile. The pH dependence confirms the interaction of protonated hydrophiles with DNA. These results suggest a pH-dependent release mechanism that might be used to protect DNA from acid hydrolysis.

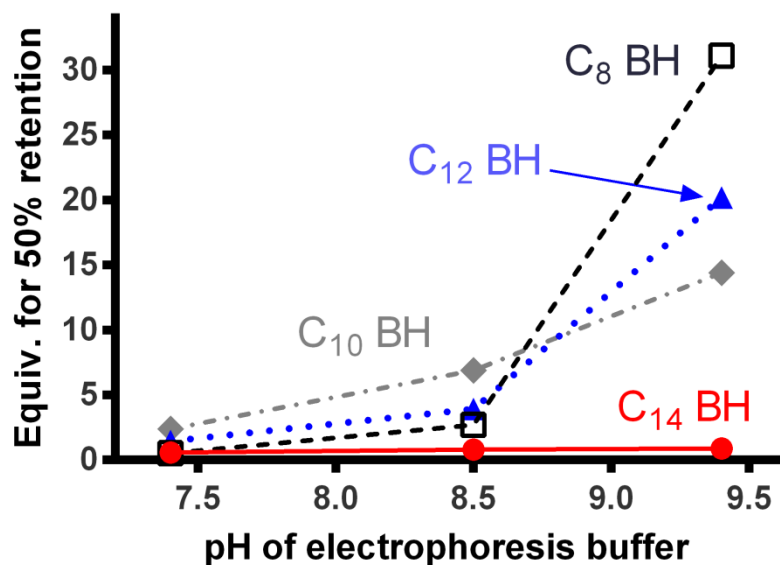


Figure 3.4: Graph showing the number of equivalents of benzyl hydraphiles having the indicated spacer chain lengths required for 50% retention of 10 kb plasmid DNA in the agarose gel wells. BH represents benzyl hydraphile and C_n indicates the spacer chain length.

The dependence on pH and chain length implied that both electrostatic and hydrophobic interactions drive complex formation. In order to further probe the forces that comprise the hydraphile-DNA interaction, a variety of compounds were tested for their ability to prevent complex formation. The anionic amphiphiles sodium dodecyl sulfate (SDS) and sodium dodecanoate are surfactants and they could form complexes with protonated hydraphiles in preference to DNA. They could also compete in binding DNA with hydraphiles that have formed sodium complexes. Crown-cation complexes are typically weak in water but increase in strength in lower dielectric media such as the nonpolar environment of a lipid membrane. The anionic surfactants, the hydraphiles, or assemblies formed from either or both could therefore inhibit aggregation.

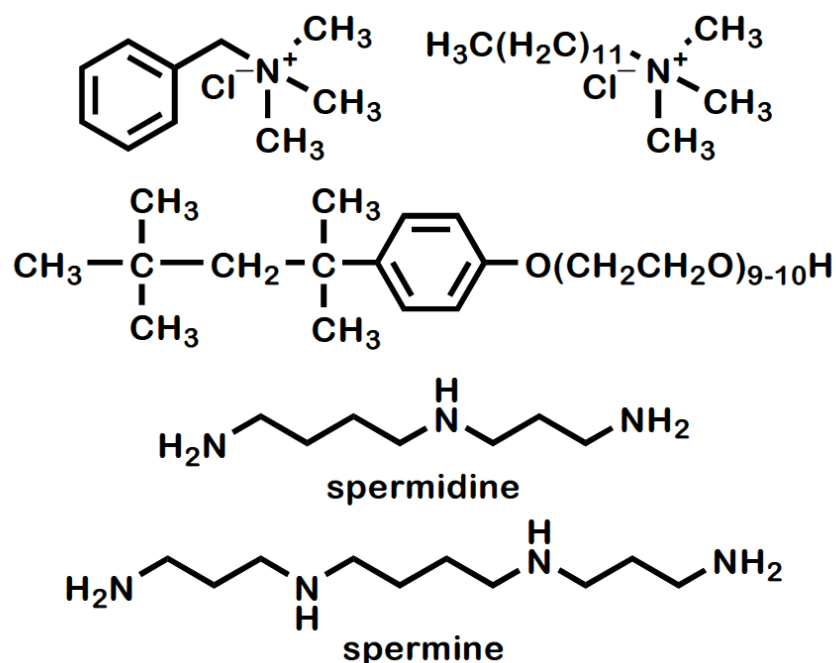


Figure 3.5. Structures of benzyltrimethylammonium chloride (upper left), dodecyltrimethylammonium chloride (upper right), Triton X-100 (center) and the polyamines spermine and spermidine.

It was speculated that the cationic amphiphiles benzyltrimethylammonium chloride and dodecyltrimethylammonium chloride and the nonionic amphiphile Triton X-100 would compete for phosphate ion pairs or would solvate the hydrophile and prevent complexation (Figure 3.5). The known DNA binding polyamines spermine and spermidine (used as hydrochloride salts) were also tested. The prevention agents were added to DNA before the addition of hydrophile. Benzyl C₁₄ hydrophile was used at 1 equivalent and the prevention agents were tested at 1 equivalent and 25 equivalents both in the presence and absence of hydrophile. No prevention of hydrophile-DNA complex formation was observed at 1 equivalent; the DNA remained in the well. However at 25 equivalents sodium dodecyl sulfate was successful in preventing complex formation and the DNA migrated normally. The ratio of 25 equivalents corresponds to a concentration of ~750 μ M, over an order of magnitude below the critical micelle concentration of SDS.³³ Spermine tetrahydrochloride also reduced complex formation, but the control experiment conducted in the absence of hydrophile showed an increase in the open circular band. The nicked plasmid likely resulted from acid catalyzed single-strand hydrolysis. The results of the prevention experiment are shown in Figure 3.6, left panel.

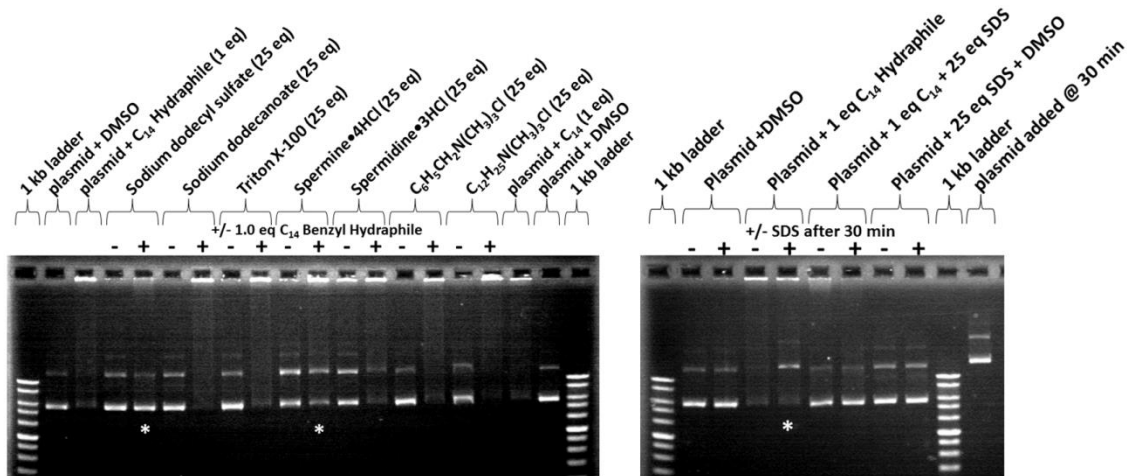


Figure 3.6. Left: Prevention experiment. DNA and the indicated prevention agent were mixed with (+) or without (-) 1.0 equivalent of benzyl C₁₄ hydraphile. Normal DNA migration was observed with sodium dodecyl sulfate (SDS). Partial DNA migration was observed with spermine. Right: Disruption experiment. 10 kb plasmid DNA and hydraphile were run for 30 minutes then SDS was added to the well and the gel was run an additional 1 hour. Partial liberation of the hydraphile•DNA complex was observed.

Sodium dodecyl sulfate prevented DNA-hydraphile formation, but it was unknown if this detergent could disrupt the complex after formation. A disruption experiment was conducted in which DNA and benzyl C₁₄ hydraphile were allowed to react and then the gel was run for 30 minutes. Because the hydraphile-DNA complex was known to remain in the well, adding a reagent that disrupts the complex should release DNA, which can then migrate normally. SDS was added to the well (25 eq) and plasmid DNA was placed in another well as a control. After an additional hour of electrophoresis, the gel was stained and the image showed that some DNA was released upon addition of SDS. Therefore while 25 eq SDS can prevent the formation the hydraphile-DNA complex, the same amount is insufficient to fully release the DNA once the complex is formed. This may be due either to complex stability or to the inability of the surfactant to access (penetrate) the complex, or both.

Agarose gel electrophoresis was also used to evaluate the effect, if any, of lariat ethers (LEs) on plasmid DNA. The dependence on alkyl chain length was investigated using lariat ethers having *n*-alkyl chains ranging in length from C₄ to C₁₈ (even numbers). Each experiment was conducted at lariat ether concentrations of 17 and 50 equivalents. Figure 3.7 shows that when the lariat side arms were C₄, C₆, or C₈, DNA migrated normally at both concentrations. Lariat ethers having C₁₀-C₁₈ side

chains retained DNA in the well at 50 equivalents, while only C₁₂ and C₁₄ LEs fully inhibited migration at 17 equivalents. At the lower concentration, C₁₀, C₁₆, and C₁₈ but not C₁₂ or C₁₄ lariat ethers showed streaking, suggesting there is both a lower limit and upper limit on chain length for optimum complex formation. It is unclear why there appears to be a mid-range discontinuity. Lariat ether amides, whose alkyl chains connect to the diazacrown through amide bonds were also tested. The side arms were equivalent in length to the saturated compounds. None showed any activity in the gel experiments (data not shown). This result supports the need for amine protonation in complex formation.

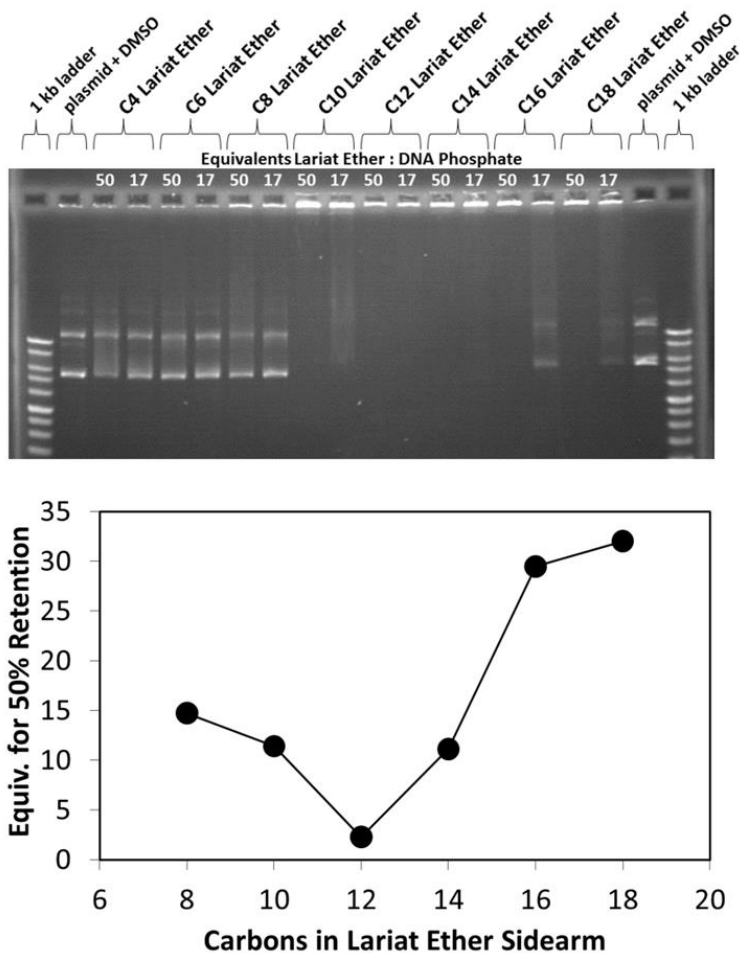


Figure 3.7. Top: Gel retardation assay for 17 or 50 equivalents of lariat ethers of varying side chain lengths with 10 kb plasmid DNA. Bottom: Graph showing the number of equivalents of lariat ether of varying chain length required for 50% plasmid DNA retention.

Condensation of DNA by cationic lipids is known to generate lyotropic liquid crystalline phases. Lamellar or inverted columnar hexagonal assemblies are the

predominant morphologies that are observed.³⁴ The lamellar phase consists of hydrated DNA layers alternating with cationic lipid bilayers.³⁵ In the columnar hexagonal phase, the DNA helix comprises the axis and cationic lipid head groups contact the DNA. The lipid tails interdigitate between the hexagonally packed columns to exclude water. We have previously reported the solid state structure of a sodium iodide complex of the C₁₂ lariat ether determined by X-ray diffraction.³⁰ The lariat ether is organized in a bilayer structure with interdigitated alkyl chains. This provides evidence that these compounds are capable of forming assemblies similar to those formed by DNA and cationic lipids. Models of lamellar and columnar hexagonal phases were generated from C₁₂ lariat ether (CSD: HUTGUY) and B-form DNA (PDB: 1BNA) structures (Figure 3.8). The ability to efficiently complex DNA may rely on the interdigitation of the alkyl chains. The shortest C₄ and C₆ chains offer little hydrophobic surface area for bilayer formation. The longest C₁₆ and C₁₈ chains may possess too much conformational flexibility to efficiently pack or they may preferentially form assemblies excluding DNA through rapid aggregation.

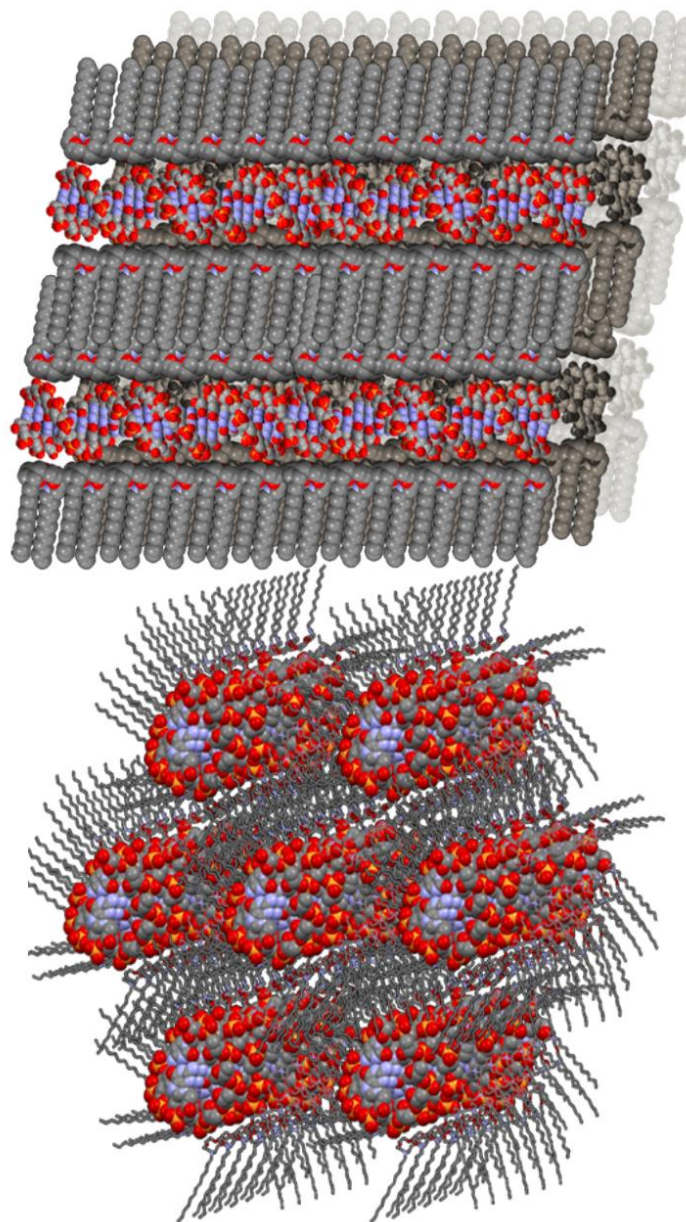


Figure 3.8. Proposed models of lamellar (top) and inverted columnar hexagonal (bottom) assemblies of DNA with C₁₂ lariat ether.

3.2.3. Electron microscopy of a benzyl C₁₄ hydrophile•DNA complex.

An electron microscopy study was performed in order to probe the morphology of the benzyl hydrophile•DNA complex. Benzyl C₁₄ hydrophile and plasmid DNA were mixed, the complex was diluted with dH₂O, and adsorbed to a formvar-coated lacey carbon copper grid. Uranyl acetate was used as the counter-stain. Figure 3.9 shows a representative image. Semi-spherical particles were observed by a transmission electron microscopy; the particles appeared to reside predominantly at the edges of the lacey carbon support. The particles showed a similar morphology and diameters

of ~100-150 nm. The density of the particles appeared to be constant. These results suggest that the particles are aggregates of hydrophile and DNA rather than having a vesicular structure.

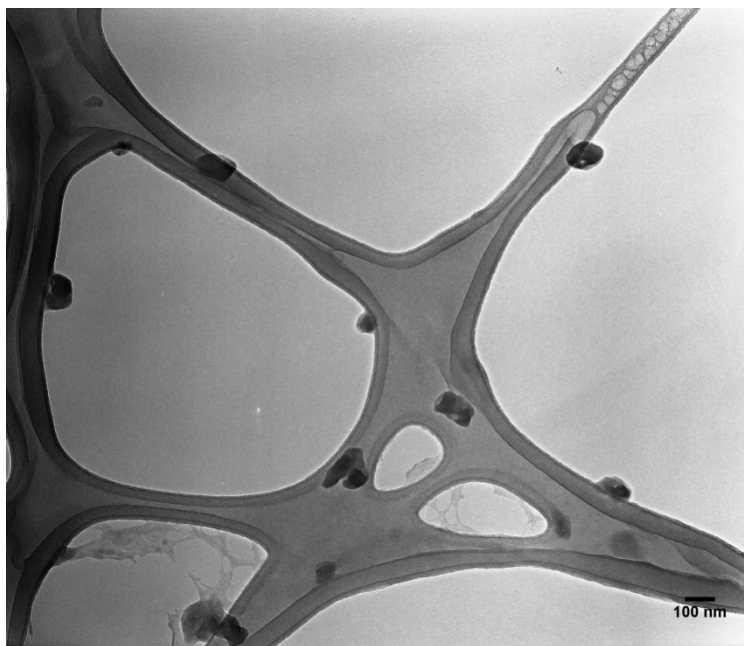


Figure 3.9. Transmission electron micrograph of benzyl C₁₄ hydrophile•plasmid DNA particles. The particles are semispherical in morphology, ~100-150 nm diameter, and reside at the edges of the web-like lacey carbon support.

3.3. Conclusion.

The use of gel electrophoresis has permitted an evaluation of lariat ether and hydrophile binding of DNA. This work shows that the complexation of plasmid DNA by benzyl hydrophiles and lariat ethers is dependent on both the protonation state and the hydrophobic character of the amphiphiles. Large aggregates form as shown by electron microscopy, which revealed spherical particles of fairly uniform size (~1,000-1,500 Å) and density. The complex could be deaggregated as shown by disruption experiments using the anionic surfactant sodium dodecyl sulfate. An additional electrophoretic mobility study demonstrated that the same surfactant can inhibit complex formation as can the presence of competing polyamines such as spermine. Further studies are underway to characterize the dynamics of complex formation with an eye toward the transport of genetic material into viable cells.

3.4. Experimental.

3.4.1. Compounds used. Sodium dodecyl sulfate, sodium dodecanoate, Triton X-100, benzyltrimethylammonium chloride, dodecyltrimethylammonium chloride, spermine, and spermidine were purchased from Sigma-Aldrich and used as received.

The C₄-C₁₈ lariat ethers were prepared as previously reported (³⁶). Benzyl C₈-C₁₄ hydrophile compounds were prepared as previously reported (²⁴).

3.4.2. Plasmid DNA. pKLMF-FX (10 kb) was obtained from New England Biosciences and amplified in JM109 *E. coli* (Promega cat. #2005). The plasmid was extracted using a Zyppy™ Plasmid Maxiprep Kit (cat. #D4027) and then further purified by ethanol precipitation in the presence of NaCl, LiCl, or KCl and dissolved in 18.2 MΩ water. The sodium DNA salt was used in nearly every case.

3.4.3. Agarose gel electrophoresis. Gel retardation assays were carried out in 0.5% agarose gels and run in various buffers. Gels were run at 105 ± 4 V for 2.5 h in borate buffers and 1.5 h in tris buffers unless noted otherwise. In each experimental sample 20 ng/μL aqueous plasmid DNA (no buffer) was mixed with an equal volume of the compound of interest in DMSO and incubated for 15 min at room temperature before being transferred to the well. These samples did not receive loading dye. Each gel included 1 kb DNA ladder (Promega) controls that included loading dye. Gels were stained with 2 μg/mL ethidium bromide for 15 m and destained in running buffer without dye for 5 m before visualization on a UV transilluminator.

3.4.4. Transmission electron microscopy (TEM). Amphiphile•DNA complexes were prepared as described for agarose gel electrophoresis and then diluted 10-fold with pure water. A 10 μL sample was applied to lacey formvar/carbon 300 mesh copper TEM grids (Ted Pella, Inc.) for 60 seconds and the grid was washed with 18.2 MΩ H₂O (30 s), stained with 2 % uranyl acetate (30 s), and washed twice with H₂O (15 s each). The above solutions were applied at a volume of 10 μL, wicked away between each application, and the grid was finally dried with a gentle N₂ stream. Specimens were examined on a JEOL JEM-2000 FX transmission electron microscope operated at 300 keV.

3.5. References.

- 1 Micklos, D.A.; Freyer, G.A.; Crotty, D.A. *DNA Science*; 2 ed.; Cold Spring Harbor Laboratory Press: Cold Spring Harbor, NY, 2003.
- 2 Yelle, J.; Dion, M.; Hamelin, C. Efficient transfection of mammalian cells with viral DNA in optimal culture conditions. *J. Virol. Methods* **1983**, *7*, 321-326.
- 3 (a) Zabner, J.; Fasbender, A.J.; Moninger, T.; Poellinger, K.A.; Welsh, M.J. Cellular and molecular barriers to gene transfer by a cationic lipid. *J. Biol. Chem.* **1995**, *270*, 18997-19007. (b) Dalby, B.; Cates, S.; Harris, A.; Ohki, E. C.; Tilkins, M.L.; Price, P.J.; Ciccarone, V.C. Advanced transfection with

- Lipofectamine 2000 reagent: primary neurons, siRNA, and high-throughput applications. *Methods* **2004**, *33*, 95-103.
- 4 Karasev, A.V.; Foulke, S.; Wellens, C.; Rich, A.; Shon, K.J.; Zwierzynski, I.; Hone, D.; Koprowski, H.; Reitz, M. Plant based HIV-1 vaccine candidate: Tat protein produced in spinach. *Vaccine* **2005**, *23*, 1875-1880.
- 5 Felgner, P.L.; Gadek, T.R.; Holm, M.; Roman, R.; Chan, H.W.; Wenz, M.; Northrop, J.P.; Ringold, G.M.; Danielsen, M. Lipofection: a highly efficient, lipid-mediated DNA-transfection procedure. *Proc. Natl. Acad. Sci. U S A* **1987**, *84*, 7413-7417.
- 6 Inoue, Y., Gokel, G.W., Eds.; *Cation Binding by Macrocycles*; Marcel Dekker: New York, 1990.
- 7 Xie, Q.; Gokel, G.W.; Hernandez, J. C.; Echegoyen, L. Efficient Sodium Cation Transport Across Liposome Membranes Using Synthetic Carriers. *J. Am. Chem. Soc.* **1994**, *116*, 690-696.
- 8 (a) Pajewski, R.; Ferdani, R.; Schlesinger, P.H.; Gokel, G.W. Chloride complexation by heptapeptides: influence of C- and N-terminal sidechains and counterion. *Chem. Commun.* **2004**, 160-161. (b) You, L.; Ferdani, R.; Gokel, G.W. Chloride Ion Efflux from Liposomes is Controlled by Sidechains in a Channel-forming Heptapeptide. *Chem. Commun.* **2006**, 603-605.
- 9 (a) Gokel, G.W.; Dishong, D.M.; Diamond, C.J. Lariat Ethers. Synthesis and Cation Binding Properties of Macrocyclic Polyethers Possessing Axially Disposed Secondary Donor Groups. *J. C. S. Chem. Commun.* **1980**, 1053-1054. (b) Leevy, W.M.; Weber, M.E.; Gokel, M.R.; Hughes-Strange, G.B.; Daranciang, D.D.; Ferdani, R.; Gokel, G.W. Correlation of bilayer membrane cation transport and biological activity in alkyl-substituted lariat ethers. *Org. Biomol. Chem.* **2005**, *3*, 1647-1652.
- 10 Gokel, G.W. Hydraphiles: Design, Synthesis, and Analysis of a Family of Synthetic, Cation-Conducting Channels; *Chem. Commun.* **2000**, 1-9.
- 11 Sewbalas, A.; Islam, R.U.; van Otterlo, W.A.L.; de Koning, C.B.; Singh, M.; Arbuthnot, P.; Ariatti, M. Enhancement of transfection activity in HEK293 cells by lipoplexes containing cholesteryl nitrogen-pivoted aza-crown ethers, *Med. Chem. Res.* **2013**, *22*, 2561-2569.
- 12 Gokel, G.W.; Hernandez, J.C.; Viscariello, A.M.; Arnold, K.A.; Campana, C.F.; Echegoyen, L.; Fronczek, F.R.; Gandour, R.D.; Morgan, C.R.; Trafton, J.E.; Minganti, C.; Eiband, D.; Schultz, R.A.; Tamminen, M. Steroidal Lariat Ethers: A New Class of Macrocycles and the Crystal Structure of *N*-(Cholesteryloxycarbonyl)aza-15-crown-5, *J. Org. Chem.* **1987**, *52*, 2963-2968.
- 13 Echegoyen, L.E.; Hernandez, J.C.; Kaifer, A.; Gokel, G.W.; Echegoyen, L. Aggregation of Steroidal Lariat Ethers: The First Example of Nonionic

- Liposomes (Niosomes) formed from Neutral Crown Ether Compounds, *Chem. Commun.* **1988**, 1988, 836-837.
- 14 Meisel, J.W.; Gokel, G.W. A Simplified Direct Lipid Mixing Lipoplex Preparation: Comparison of Liposomal-, Dimethyl Sulfoxide-, and Ethanol-Based Methods. *Scientific Reports*, **2016**, In Press.
- 15 (a) Murillo, O.; Watanabe, S.; Nakano, A.; Gokel, G.W. Synthetic models for transmembrane channels: Structural variations that alter cation flux. *J. Am. Chem. Soc.* **1995**, *117*, 7665-7679. (b) Gokel, G.W.; Murillo, O. Synthetic organic chemical models for transmembrane channels. *Acc. Chem. Res.* **1996**, *29*, 425-432.
- 16 (a) Gokel, G.W.; Barbour, L.J.; Ferdani, R.; Hu, J. Lariat ether receptor systems show experimental evidence for alkali metal cation- π interactions. *Acc. Chem. Res.* **2002**, *35*, 878-886. (b) Elliott, E.K.; Hu, J.; Gokel, G.W. The Fluorescence Properties of Free and Cation-complexed Lariat Ethers having Sidearms Terminated by a Benzene Ring. *Supramol. Chem.* **2007**, *19*, 175-183.
- 17 Muñoz, S.; Mallén, J.V.; Nakano, A.; Chen, Z.; Echegoyen, L.; Gay, I.; Gokel, G.W. Lariat ether bola-amphiphiles: formation of crown ether based bola-amphisomes. *Chem. Commun.* **1992**, 520-522.
- 18 Gokel, G.W.; Trafton, J.E., Cation Binding by Lariat Ethers. In *Cation Binding by Macrocycles*; Gokel, G. W.; Inoue, Y., Eds. Marcel Dekker, Inc.: New York, 1990; pp. 253-310.
- 19 Gokel, G.W.; Echegoyen, L., Lariat Ethers in Membranes and as Membranes. In *Advances in Bio-organic Frontiers*; Dugas, H., Ed. Springer Verlag: Berlin, 1990; pp. 116-141.
- 20 Weber, M.E.; Schlesinger, P.H.; Gokel, G.W. Dynamic Assessment of Bilayer Thickness by Varying Phospholipid and Hydraphile Synthetic Channel Chain Lengths. *J. Am. Chem. Soc.* **2005**, *126*, 636-642.
- 21 Shabany, H.; Murray, C.L.; Gloeckner, C.A.; Grayson, M.A.; Gross, M.L.; Gokel, G.W. Evidence for multiple alkali metal cation complexation in membrane-spanning ion transporters. *Chem. Commun.* **2000**, 2375-2376.
- 22 UniProt: The Universal Protein Resource.
<http://www.uniprot.org/taxonomy/568094>. (accessed March 31, 2016).
- 23 Gokel, G.W. Lariat Ethers: From Simple Sidearms to Supramolecular System; *Chem. Soc. Rev.* **1992**, *21*, 39-47.
- 24 Curvey, N.S.; Luderer, S.E.; Walker, J.K.; Gokel, G.W. Improved Syntheses of Benzyl Hydraphile Synthetic Cation-conducting Channels. *Synthesis* **2014**, *46*, 2771-2779.

- 25 Arnold, K.A.; Hernandez, J.C.; Li, C.; Mallen, J.V.; Nakano, A.; Schall, O.F.; Trafton, J.E.; Tsesarskaja, M.; White, B.D.; Gokel, G.W. Analysis of sodium, potassium, calcium, and ammonium cation binding selectivity in one- and two-armed nitrogen-pivot lariat ethers. *Supramol. Chem.* **1995**, *5*, 45-60.
- 26 Hernandez, J.C.; Trafton, J.E.; Gokel, G.W. A Direct Comparison of Extraction and Homogeneous Binding Constants as Predictors of Efficacy in Alkali Metal Cation Transport. *Tetrahedron Lett.* **1991**, 6269-6272.
- 27 Murray, C.L.; Gokel, G.W. Cation flux dependence on carbon chain length in tris(macrocycle) channels as assessed by dynamic ²³Na NMR studies in phospholipid bilayers, *Chem. Commun.* **1998**, 2477-2478.
- 28 LePecq, J.B.; Paoletti, C., A fluorescent complex between ethidium bromide and nucleic acids. Physical-chemical characterization, *J. Mol. Biol.* **1967**, *27*, 87-106.
- 29 Gokel, G.W. *Crown Ethers and Cryptands*; The Royal Society of Chemistry: London, England, 1991; Vol. 3.
- 30 De Wall, S.L.; Barbour, L.J.; Gokel, G.W. Solid state bilayer formation from a dialkyl-substituted lariat ether that forms stable vesicles in aqueous suspension. *J. Phys. Org. Chem.* **2001**, *14*, 383-391.
- 31 Martin, R. *Gel Electrophoresis: Nucleic Acids*; Bios Scientific Publishers: Oxford, 1996, 175 pp.
- 32 Zhang, J.; Wang, F.; Wang, T. A simple and effective SuperBuffer for DNA agarose electrophoresis, *Gene* **2011**, *487*, 72-74.
- 33 Evans, H.C. Alkyl sulfates. I. Critical micelle concentrations of the sodium salts. *J. Chem. Soc.* **1956**, 579-586.
- 34 Safinya, C. Structures of lipid-DNA complexes: supramolecular assembly and gene delivery. *Curr. Opin. Struct. Biol.* **2001**, *11*, 440-448.
- 35 Rädler, J.O., Koltover, I., Salditt, T.; Safinya, C.R. Structure of DNA-cationic liposome complexes: DNA intercalation in multilamellar membranes in distinct interhelical packing regimes. *Science* **1997**, *275*, 810-814.
- 36 Gatto, V.J.; Arnold, K.A.; Viscariello, A.M.; Miller, S.R.; Morgan, C.R.; Gokel, G.W. Synthesis and binding properties of bibracchial lariat ethers (BiBLEs): survey of synthetic methods and cation selectivities; *J. Org. Chem.* **1986**, *51*, 5373-5384.

Chapter 4

De Novo Design, Synthesis, and Biophysical Characterization of Bis(aminoamides) that Bind and Condense Plasmid DNA

4.1. Introduction.

Since the report by Crabtree and his collaborators¹ that relatively simple tris-arene compounds such as isophthalic acid dianilide can bind chloride and bromide ions, a vast literature has emerged in the area of anion receptors.² Sessler, Anslyn, and their coworkers reported hundreds of compounds limited to binding phosphorylated molecules.³ Two monographs have recently dealt with the enormous interest in anion complexation.^{4,5}

The initial interest in halides in the Gokel laboratory was their transport through bilayers. A family of synthetic anion transporters (SATs)⁶ was developed that selectively transported Cl⁻ through both liposomal⁷ and vital cellular membranes.⁸ Computational studies by Burkhardt, Skelton, and Fried⁹ confirmed the dimer¹⁰ nature of the functional channel. Detailed NMR studies showed that two of the seven amino acid amide NH residues were key as H-bond donors to chloride in solution.¹¹ This piqued interest in assessing whether relatively simple peptides could function as Cl⁻ complexing agents. Indeed, the SATs having Gly₃-Pro-Gly₃ peptide sequences were competitive with the Crabtree tris-arenes in binding strength,¹² although the nature of the counteraction clearly played a role as well.¹³

Since the binding of the heptapeptide SATs and the Crabtree tris-arenes was similar in strength, previous colleagues in the Gokel laboratory attempted unsuccessfully to develop Cl⁻-selective channels based on that module. Instead, it was found that appropriately-substituted tris-arenes could form pores that showed the open-close behavior characteristic of channels.¹⁴ It was observed in a spectroscopic study designed primarily to assess halide ion complexation by dipicolinamides and isophthalamides that binding of H₂PO₄⁻ was visible to the eye.¹⁵ The success with peptides and phosphates suggested that amino acid derivatives mimicking some features of the Crabtree tris-arenes might bind the phosphates of DNA. The notion was that complexation between anion-selective binders might surround and condense DNA. This is an important prerequisite for both transformation of bacteria or transfection of higher cells.

Lessons from the burgeoning field of anion supramolecular chemistry provided a framework for the investigation of novel structures capable of binding and condensing DNA. Previous work elaborated in Chapter 2 of this thesis showed that known liposomal-based transfection reagents could be brought to interact with DNA

and transfect cells without forming the liposome intermediate. The new procedure provided the means to test chemicals that do not readily form liposomes and that may not be water soluble. This method was utilized to characterize the interaction of diaza-18-crown-6-based amphiphiles with DNA, reported in Chapter 3. A 2002 report by Bloomfield and coworkers showed that protonated simple primary amines with normal alkyl chains can bind and condense DNA.¹⁶ This served as the inspiration for the work described in this chapter: a determination of the minimal structural features required for DNA binding and condensation and the development of a new class of DNA binding small molecules. The primary goal of this work was to address whether a more diverse range of chemical structures, outside the canonical cationic lipids and cationic polymers, are suitable for more efficient and less toxic *in vitro* transfection. Better transfection reagents for cultured cells may then progress to *in vivo* applications and ultimately gene therapy in humans to treat disease.

4.2. Results and Discussion.

4.2.1. DNA binding and condensation by simple amines measured by agarose gel electrophoresis. Preliminary to the design of novel DNA-condensing molecules, several DNA binding studies were undertaken with the goal of identifying the minimal structural characteristics required for DNA binding. Primary and secondary linear-chained amines were tested as were α,ω -diamino-*n*-alkanes and phenylenediamines (Figure 4.1). All compounds were tested as the hydrochloride or dihydrochloride salts. Our model plasmid was pKLMF-FX (9.988 kb, New England Biolabs) and was purified as the sodium salt by ethanol precipitation. While oligonucleotides have seen increasingly widespread use in biological research and as a therapeutic strategy,¹⁷ the binding and transport of oligonucleotides is beyond the scope of these studies.

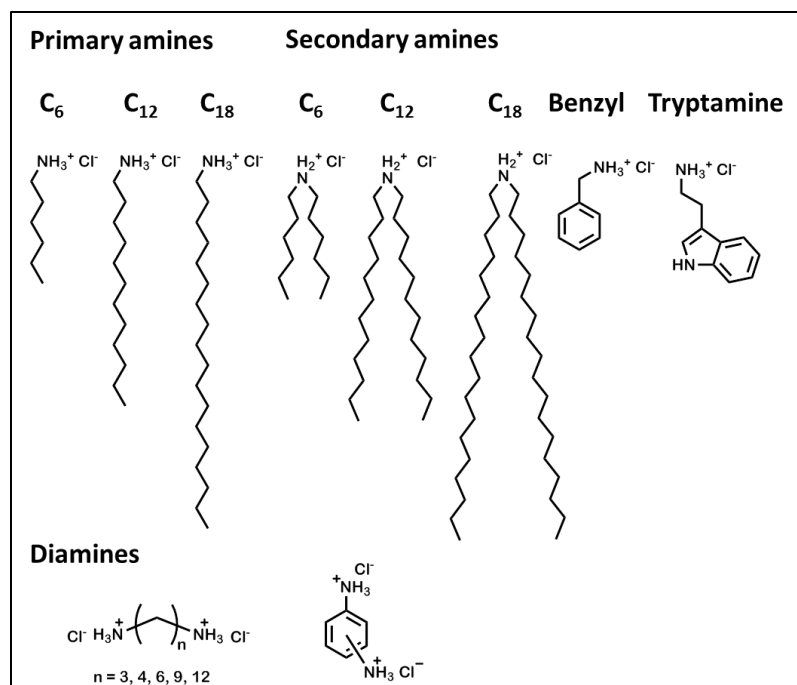


Figure 4.1. Simple amines tested for DNA binding and condensation.

The simple amines were tested by using agarose gel electrophoresis. Amines of varying chain lengths were screened at two concentrations: 50 and 17 molar equivalents of molecule to DNA phosphate. Based on findings described in Chapter 1 electrophoretic studies, it was observed that the cationic lipid DOTAP condensed DNA and fully retained it in the well at 1-2 equivalents. Because we are screening for DNA interaction, we chose 50 equivalents as the maximum amount of compound where DNA retention on the gel can be considered a specific interaction with DNA rather than non-specific aggregation. The results can be seen in Figure 4.2. The shortest C₆ *n*-alkyl primary amine did not retain DNA to any appreciable extent. The intermediate length C₁₂ chain retained some DNA, but streaking was observed at 50 equivalents. The longest C₁₈ chain fully retained DNA at both concentrations. That these simple compounds could bind and condense DNA suggests minimally two structural requirements for DNA condensation: a positively charged group that confers affinity to the negatively charged DNA phosphates, and a self-associative moiety to drive reagent-reagent interactions. In this case the self-association is through the exclusion of solvent from the hydrophobic tails. The dependence on chain length demonstrates that there is a certain degree of self-association necessary to form the condensed DNA-reagent particle. This may manifest in the thermodynamic contribution of entropy by the release of solvent from the hydrophobic surface. However, it may also be related to the geometry of how the reagent packs with DNA to form an organized particle. To the extent that either of

these is true, we are unable to form any specific conclusions from electrophoretic experiments alone.

Secondary amines possessing two *n*-alkyl chains of identical length showed a similar trend in electrophoretic DNA retention. As was the case with single-chained primary amines, the shortest C₆-chained secondary amines were also unsuccessful at retaining DNA in the well. However, some streaking of the DNA was observed, which indicates that an interaction between the reagent and the DNA did occur. Unlike the primary C₁₂ amines, the secondary C₁₂ amine did retain DNA in the well. The increase in DNA interaction is likely due to the increase in hydrophobic surface area of the twin chains compared to the single chained primary amine, and therefore the entropic contribution to DNA condensation was increased. We could also say that the self-association of the twin chains is higher than amines of the same length less one chain. Once again, we cannot eliminate the contribution of the geometry of the reagent. The twin-chained analog is more conical with a wider hydrophobic area compared to the more cylindrical primary amine.

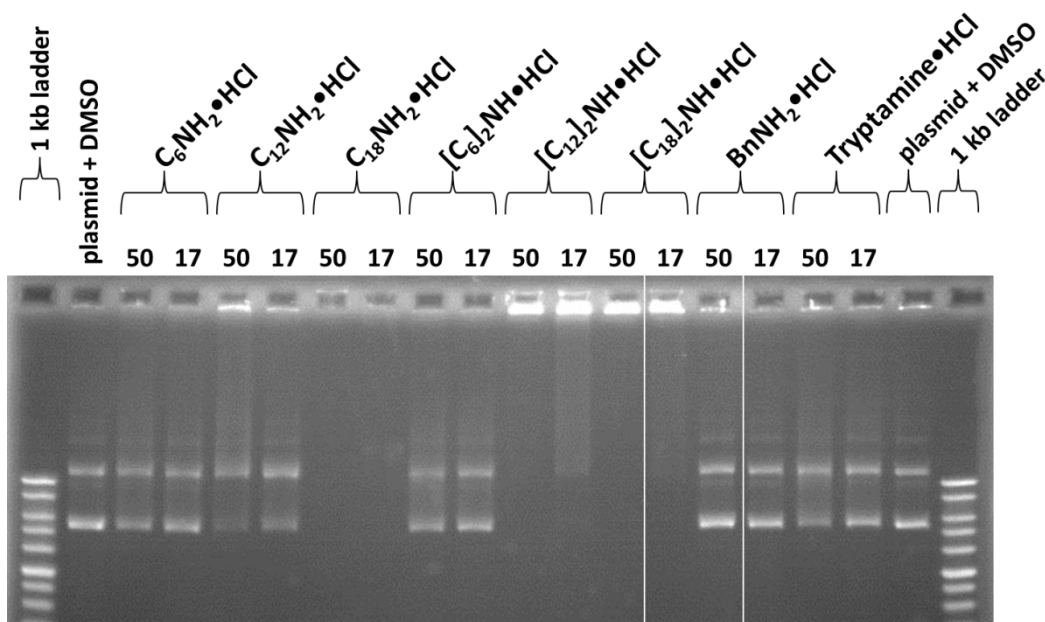


Figure 4.2. Agarose gel electrophoresis of primary and secondary amines with 10 kb plasmid DNA. The breaks in the gel arose from the accidental inversion of two samples during loading; the results are from a single gel, the lanes were switched back to their intended positions for clarity.

We identified two requirements for small molecule reagents that bind and condense DNA: positive charge and self-association. The self-associative nature of aliphatic

carbon chains can be increased or decreased by changing the number of carbons in the chain. With this information in hand, we wondered whether other structural motifs were sufficiently self-associative to condense DNA. Our first consideration was inspired by the base pairs in DNA. DNA uses planar aromatic heterocycles—the nitrogenous bases adenine, thymine, guanine, and cytosine—to promote the assembly of the two helical strands. This is driven by hydrogen bonding, pi-pi stacking, and the exclusion of water from hydrophobic surfaces. All of these forces are individually weak, but collectively strong. Therefore, we tested aromatic structures that contained amino groups that could be protonated. The two structures on the right of Figure 4.2 are the hydrochloride salts of benzylamine and tryptamine. These compounds did not strongly interact with DNA, however, tryptamine did show streaking at 50 equivalents, suggesting that it has some interaction with DNA and that perhaps the indole functional group is more efficient at self-association than the phenyl group.

Aromatic diamines were tested for their interaction with plasmid DNA. Phenylenediamines with the amino groups *ortho*, *meta*, or *para* were tested as the dihydrochloride salts. The results are shown on the left of Figure 4.3. While the DNA was not retained in the well, the migration of the DNA has changed. For each compound a slower-moving band appears. We had previously shown (Chapter 1) using a DNA-nicking enzyme that the slower-moving band represents an open-circular form of the DNA. This is typically caused by enzymatic or chemical hydrolysis of the phosphate backbone in one strand of the DNA. In the case of the phenylenediamine dihydrochlorides the DNA nicking is caused by acid catalyzed hydrolysis. The pK_1 and pK_2 respectively for the diprotonated phenylenediamines are *ortho* = 0.80, 4.57; *meta* = 2.50, 5.11; *para* = 2.97, 6.31.¹⁸ Clearly these are quite acidic compounds. From these results we can conclude that protonated arylamines are unsuitable as DNA binding agents on their own because they are not sufficiently charged at a pH compatible with DNA stability.

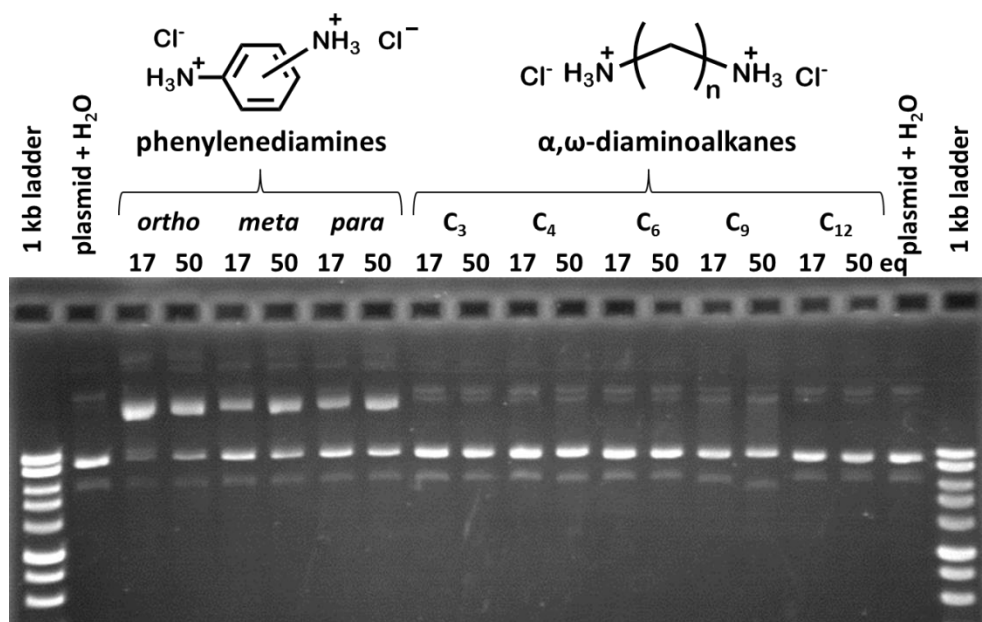


Figure 4.3. Agarose gel electrophoresis of aryl and alkyl diamines with 10 kb plasmid DNA.

In addition to primary and secondary *n*-alkyl amines, we tested α,ω -diaminoalkanes. While the former examples are typical amphiphiles with a polar head group and hydrophobic tail, the latter is an example of a simple bolaamphiphile. Bolaamphiphiles consist of two polar headgroups separated by a hydrophobic connector.¹⁹ The name originates from the South American throwing weapon—the *bola*—that consists of two weights on opposing ends of a rope. The length $(CH_2)_n$ of the carbon chain tested included $n = 3, 4, 6, 9,$ and 12 . All of the compounds were soluble in water and none of them showed an interaction with DNA. Furthermore, none of these compounds showed DNA nicking or hydrolysis. This confirms that the diaminoalkanes, with a higher pK_a than the phenylenediamines, do not increase the acidity of the DNA-reagent solution and do not hydrolyze the phosphate backbone.

In summary, several classes of simple amines were tested for binding and condensation of DNA by agarose gel electrophoresis. All amines were tested in their protonated state as hydrochloride salts. Monoamines of sufficient *n*-alkyl carbon chain length were capable of retarding the migration of DNA in electrophoresis. Twin-chained amines were better than single-chained amines of the same chain length. Amines with aromatic groups (benzylamine and tryptamine) did not interact significantly with DNA. Aromatic diamines did not interact with DNA, but did give up their protons in solution to result in acid-catalyzed phosphate backbone hydrolysis. Aliphatic diamines with up to 12 carbons were unsuccessful at

condensing DNA but did not catalyze DNA strand hydrolysis. The results from this study emphasize the importance of charge and reagent self-association in DNA binding and condensation. The amphiphilic linear amines can be considered simple approximations of the cationic lipids already known to bind, condense, and transfect cells with plasmid DNA.

4.2.2. Structure-based design of novel DNA binding agents using molecular modeling.

With a general plan for developing DNA binding small molecules, a structural analysis of the DNA helix was performed. This was done primarily using molecular modelling software (Mercury, CCDC) and a crystal structure of B-form DNA (PDB: 1BNA²⁰), which is one of the dominant forms of DNA alone and in lipoplexes.²¹ Figure 4.4 shows the canonical antiparallel DNA double helix. Highlighted in green are the distances between phosphates across the major groove (16.112 Å), minor groove (9.133 Å) and between neighboring phosphates on the same strand (6.340 Å). These values represent precise distances measured in the crystal. Of course, solution-phase DNA is expected to be much more flexible. The average of the major and minor groove interphosphate distances is 12.6 Å, roughly twice the distance between adjacent phosphates on the backbone. We aimed to incorporate these distances into our DNA binding molecules.

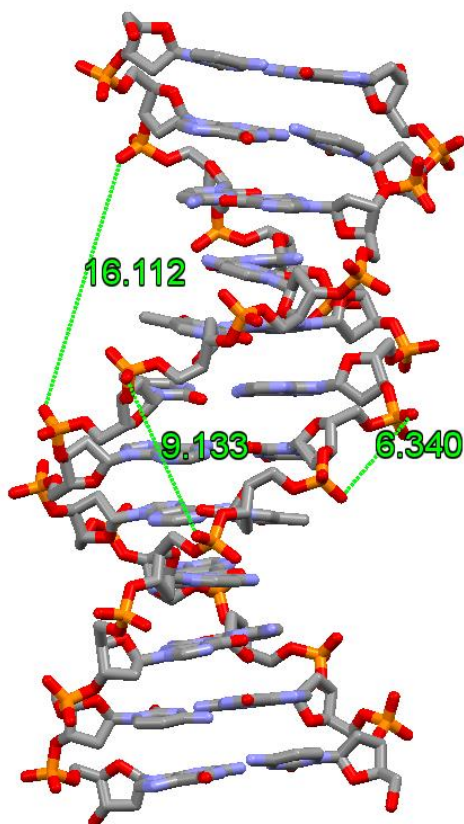


Figure 4.4. Crystal structure of a 12 base pair B-form DNA double helix (PDB: 1BNA). Interphosphate distances for the major groove (16.112 Å), minor groove (9.133 Å) and neighboring intrastrand phosphates (6.340 Å) are shown.

The DNA-binding and transfection literature is replete with many examples of cationic lipid and lipid-like molecules. In the previous section we demonstrated that only a positively charged head group and a hydrophobic chain is necessary to efficiently bind and condense DNA. Therefore, we sought to identify different modes of DNA binding and condensation. We surmised that a doubly charged molecule of appropriate positive charge spacing could bridge inter- or intrastrand phosphates. Therefore, we proposed a general structure of N^+ —spacer— N^+ . While the phenylenediamine molecules did not bind DNA, we chose to use these as the spacer for four main reasons: 1) they are inexpensive and commercially available, 2) they are rigid compared to aliphatic spacers, 3) they are aromatic and hydrophobic, so self-association may occur by stacking and solvent exclusion mechanisms, and 4) *ortho*, *meta*, and *para* spacers can be used to vary the spacer length and charged group orientation.

With a spacer in mind, we then had to choose an appropriate cationic group. Amino acids were the immediate choice for a number of reasons. Amino acids are commercially available, with a wide variety of chemical functionalities, and with a vast history of protecting group²² and synthetic²³ strategies. We envisioned connecting the carboxy terminus of the amino acid to the phenylene diamine by amide bond formation. This would require a protected amino terminus to prevent polymerization. We would then deprotect the amino terminus to form the free amine, which can be protonated to form a positively charged ammonium group. The formation of an amide was desirable because they are generally stable under physiological conditions and they offer additional hydrogen bond donor (N-H) and acceptor (C=O) moieties. In order to understand the expected orientation of the aminoamide structure, a CCDC Crystal Structure Database survey of molecules containing the $\text{-NHC(O)CH}_2\text{NH}_3^+$ group was performed. Over 150 structures were identified and every structure had the same three-dimensional orientation: the amide was always the *trans* isomer (nearly always the case for secondary amides) and the ammonium group was always *syn*-periplanar to the carbonyl oxygen despite its ability to freely rotate (see Figure 4.5).

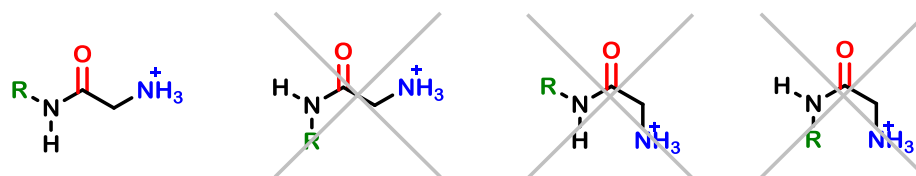


Figure 4.5. Possible conformations of protonated aminoamides. All of the 158 matching structures in the CCDC CSD survey were *syn*-amino, *trans*-amides (far left).

We quickly realized that even if our design was limited to symmetrical structures using the 20 common L-amino acids and the three regioisomers of phenylenediamine, the 60 possible compounds (not including protected intermediates) was a daunting synthetic challenge. So we decided to first narrow our linker to a single isomer of phenylenediamine.

First, the *ortho*, *meta*, and *para bis*(glycylamido)benzene structures were built using CPK models (Harvard Apparatus) and the $\text{N}^+—\text{N}^+$ spacing was compared to a 4 base pair DNA double helix. While this may seem rather crude, the models are designed with the appropriate Van der Waals distances, bond lengths, and bond angles. Manual manipulation of the three isomers against the DNA model suggested that the *meta* isomer may be the most favorable. Perhaps the most useful observation with the models was the *ortho* structure is likely to form a cyclic hydrogen bond

(NH \cdots O=C) between the amides. This eliminates the symmetry of the structure and more notably, reduces the N $^+$ —N $^+$ spacing.

Second, the protonated *ortho*-, *meta*-, and *para*-bis(glycylamido)benzene structures were modeled and minimized using molecular mechanics simulations (MM2, ChemBio3D Ultra 12.0) and N $^+$ —N $^+$ spacing was compared. The major conformers are shown in Figure 4.6. Symmetric orientations of the *meta* isomer with amide protons *syn,syn* relative to the phenyl H2 (top left) and *anti,anti* (top right) show N $^+$ —N $^+$ spacings (measured from proton to proton) of 13.1 Å and 11.8 Å, respectively. These distances are slightly above or below the average interstrand DNA phosphate spacing of 12.6 Å. The hydrogen bonded *ortho* isomer is shown in the bottom left of the Figure and has a shorter spacing of 9.2 Å. The *para* isomer is represented in the bottom right and has a longer spacing of 14.3 Å. These results seem to favor adoption of the *meta* isomer for preliminary investigations.

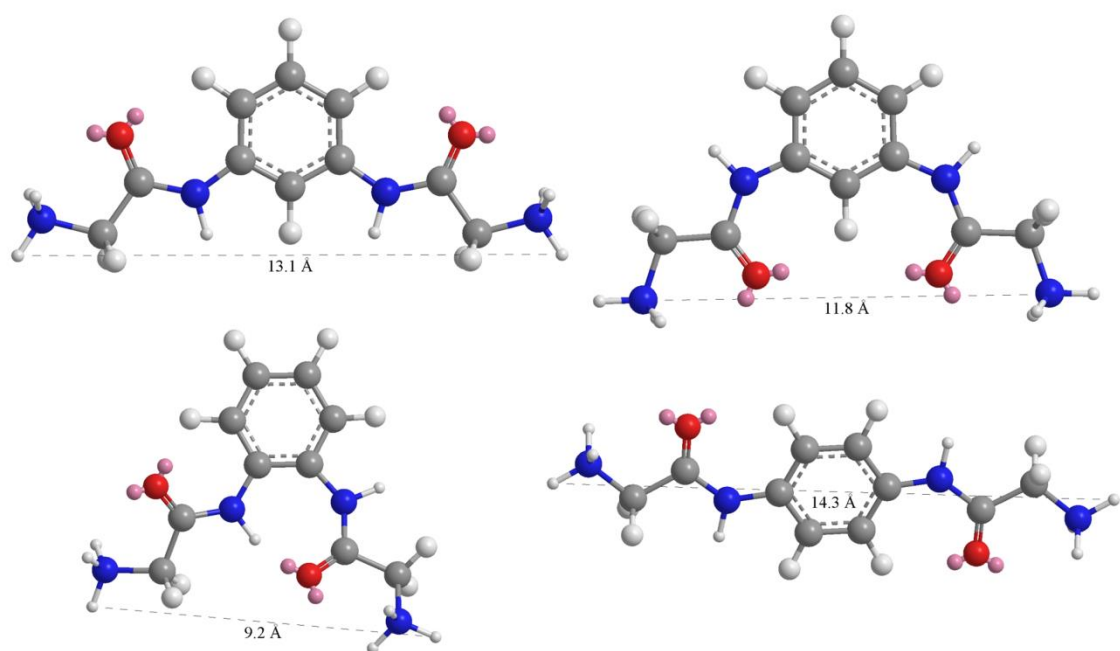


Figure 4.6. Minimized structures of *ortho*, *meta*, and *para*-bis(glycylamido)benzene isomers and measurements of the ammonium proton separation distance.

Finally, a survey of the CCDC Crystal Structure Database for *ortho*-, *meta*-, and *para*-bis(amido)benzene compounds was performed to identify the orientation and packing of amide bonds within these structures. The structures identified did not contain cationic residues. Most *ortho* isomers adopted the cyclic hydrogen bonded conformation shown in Figure 4.6 (bottom left). Most *para* isomers were also found

in the orientation shown in the Figure (bottom right) and formed hydrogen bonded planar sheets. The *meta* isomers were found in a variety of conformations, with the amides both as *syn,syn* and *anti,anti* (Figure 4.6, top left and right, respectively). The *syn,anti* conformation was also observed. The hydrogen bonding motifs also showed greater variation than the *para* isomers. Four examples of *meta-bis*(amido)benzene structures are shown in Figure 4.7. It should be noted that all of these structures are *bis*(benzamido)benzenes, which may contribute to different stacking than may be observed with *bis*(aminoamide)benzene. Intermolecular hydrogen bonding was observed between co-planar molecules (CSD: ATIQOJ) and between molecules in adjacent planes (CSD: ATIQID, VUXVIU). Non-traditional hydrogen bonding was also observed as aryl CH \cdots O=C motifs (CSD: HITWEN) in *anti,anti* conformations. Our hope was that the various modes of supramolecular interactions observed would allow for additional contributions to the self-associative characteristic necessary for these compounds to condense DNA. In summary, manual molecular modeling, molecular mechanics simulations, and CCDC Crystal Structure Database survey results all suggested that the *meta*-phenylenediamine spacer ought to be chosen as our preliminary focus.

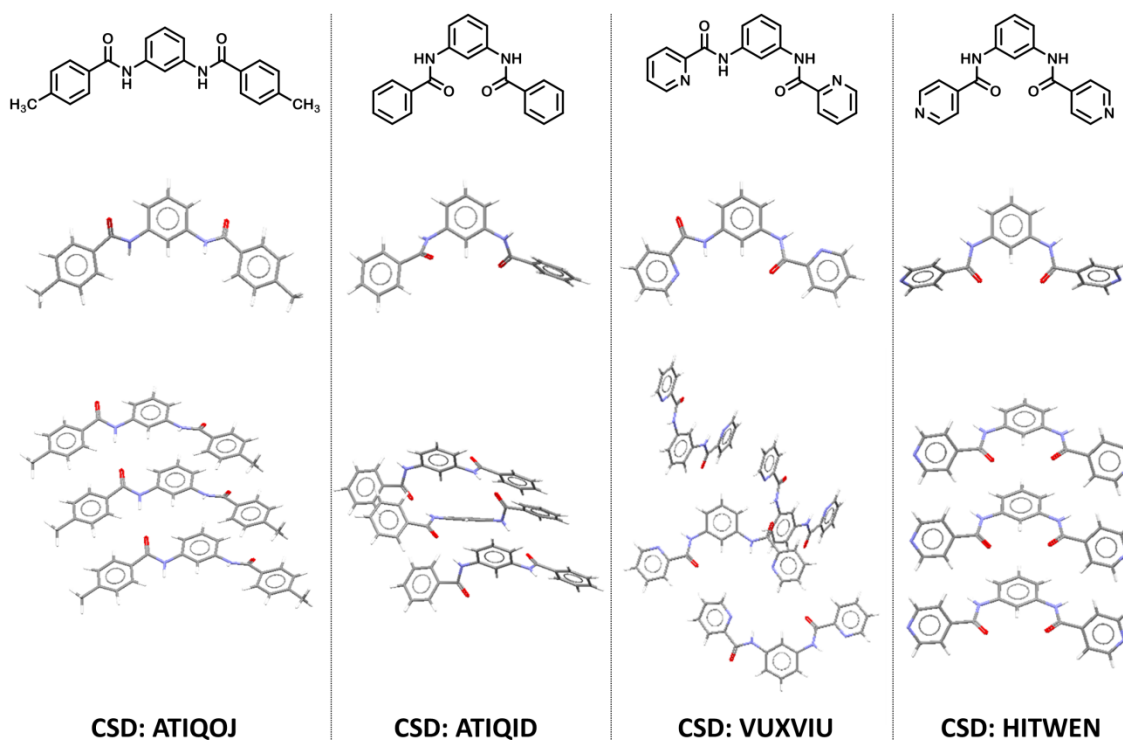


Figure 4.7. Results of a CCDC CSD structural search for *meta-bis*(amido)benzene structures. *Syn,syn* (far left) *anti,anti* (middle left and far right) and *syn,anti* (middle right) rotamers were observed with varying hydrogen bonding and stacking motifs.

Structural studies pointed to *meta*-phenylenediamine as the most suitable spacer for preliminary investigations. We then selected amino acids with different side chains to use in the synthesis of a small library of symmetrical receptors.

4.2.3. Synthesis of bis(aminoamide)benzene DNA binding and condensing reagents.

Amino acid side chains can be organized into 5 categories: polar negatively charged, polar positively charged, polar neutral, hydrophobic aromatic, and hydrophobic aliphatic. The 20 genetically encoded amino acids are shown in Figure 4.8.

Our initial strategy was to choose and prepare compounds using at least one amino acid from each group. We chose not to prepare any structures with negatively charged side chains, as this would result in an overall neutral molecule that is unlikely to interact with DNA. *Bis*(aminoamides) of *m*-phenylenediamine were prepared using glycine, alanine, serine, threonine, proline, lysine, tryptophan, leucine, phenylalanine, and tyrosine. In most cases the α -amino group was protected by *tertiary*-butyl carbamate (Boc) groups.

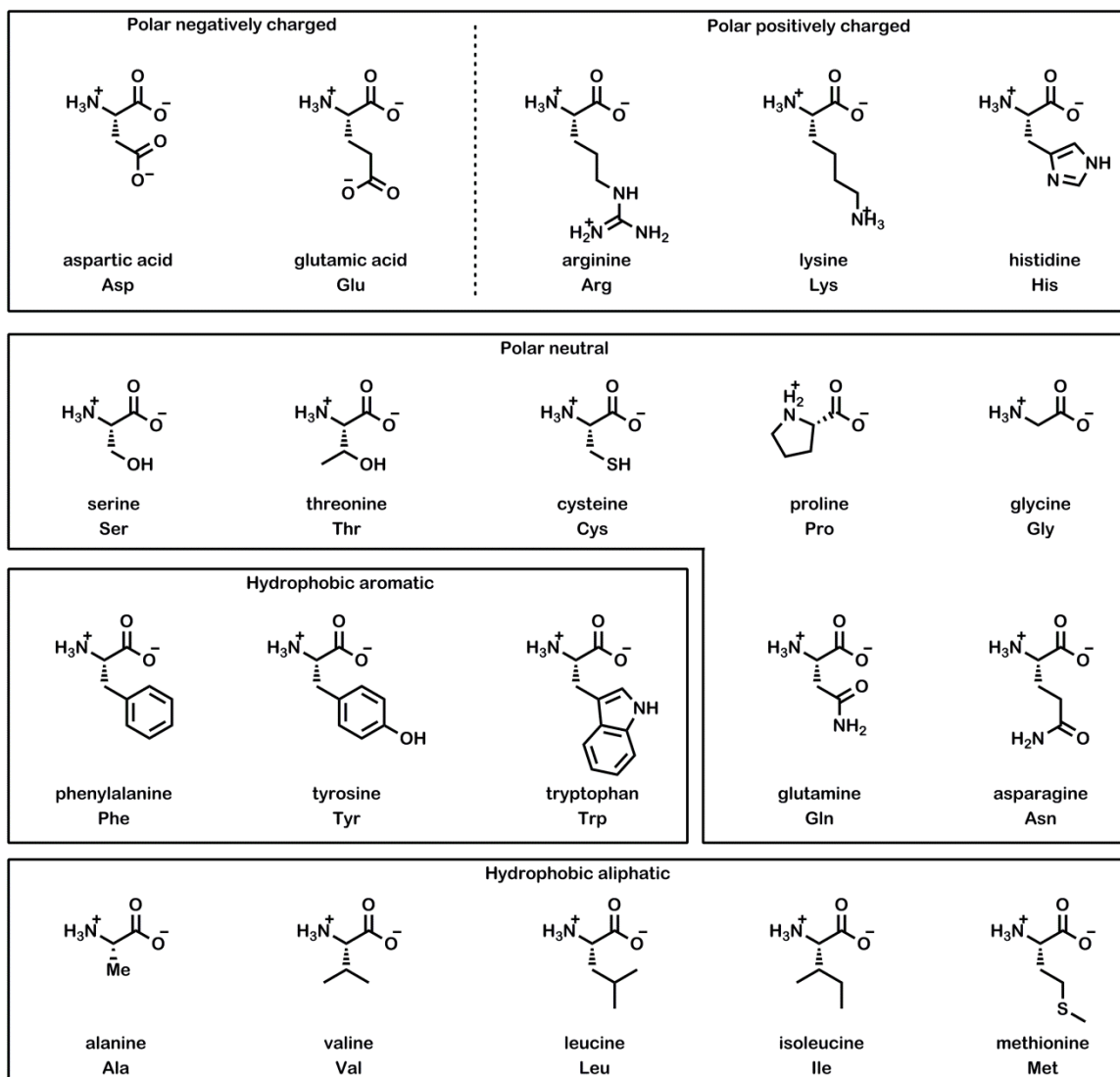


Figure 4.8. The twenty genetically encoded amino acids at physiological pH.

The Boc-protected amino acids were coupled to the diamine using *N,N,N',N'*-tetramethyl-*O*-(1*H*-benzotriazol-1-yl)uronium hexafluorophosphate (HBTU) and diisopropylethylamine in DMF. After workup and isolation of the desired Boc-protected *bis*(aminoamido)benzene product, deprotection was carried out using either HCl or trifluoroacetic acid. Certain amino acid side chains required additional protecting groups as indicated in the experimental section. The various protection and deprotection reactions are described therein. The compounds prepared for the study are presented in Table 1. Regioisomers *ortho*-, *meta*-, and *para*-*bis*(glycylamido)benzene, compounds **11**, **12**, and **13** respectively, were prepared for comparison to **1**.

Compound	Amino Acid	R =	Anion (A ⁻)
1	Gly	-H	Cl ⁻
2	L-Ala	-CH ₃	Cl ⁻
3	L-Ser	-CH ₂ OH	Cl ⁻
4	L-Thr	-CH(OH)CH ₃	CF ₃ COO ⁻
5	L-Pro	-CH(CH ₂) ₃ NH*	CF ₃ COO ⁻
6	L-Lys	-(CH ₂) ₄ NH ₂	2 CF ₃ COO ⁻
7	L-Trp	-CH ₂ -1 <i>H</i> -indol-3-yl	Cl ⁻
8	L-Leu	-CH ₂ CH(CH ₃) ₂	Cl ⁻
9	L-Phe	-CH ₂ Ph	Cl ⁻
10	L-Tyr	-CH ₂ Ph-4-OH	Cl ⁻
11	Gly (<i>ortho</i>)	H	CF ₃ COO ⁻
12	Gly (<i>meta</i>)	H	CF ₃ COO ⁻
13	Gly (<i>para</i>)	H	CF ₃ COO ⁻

Table 4.1. Chemical structures of synthesized compounds **1-13**.

*Proline contains a cyclic side chain.

A shorthand nomenclature was developed in order to facilitate the identification of different structures. For example, compound **1** is abbreviated mPh-(Gly-HCl)₂ and compound **6** is abbreviated mPh-(L-Lys-2TFA)₂.

4.2.4. Solid state structures. Three solid state structures were obtained for compounds **11** and **13** with different anions. The compounds were crystallized from different solvent compositions in the presence of different anions (see Experimental Section). The structures illustrate different conformational possibilities for this simplest of the compounds synthesized. In all three structures, the *bis*(glycylamido)benzene compound is essentially planar irrespective of its conformation or interaction with other molecules or with ions. Panel A of Figure 4.9 shows two molecules of **11**, which are present as the bromide salt. The two molecules, both in the *anti,anti*-conformation are separated by a molecule of methanol (solvent). An investigation of the packing showed that one of the ammonium groups forms hydrogen bonds with the amide oxygen lone pairs of the adjacent molecule. The other ammonium interacts with the bromide anion.

Panel B shows **11** in the diamide *anti,syn* conformation. The counter anion in this case is trifluoroacetate, two of which are proximate to **11**. In addition, a molecule

each of water and of acetonitrile are present in the crystal. In addition to ammonium-trifluoroacetate interactions, $\text{CH}_2\text{NH}_3\cdots\text{O}=\text{C}$ hydrogen bonds similar to the structure in Panel A are observed. Panel C shows a crystal structure of **13** in the *anti,anti* conformation with a H_2PO_4^- anion and a molecule of water present in the crystal. It is interesting that in each crystal structure the ammonium interacts with both the amide oxygen and with the anion.

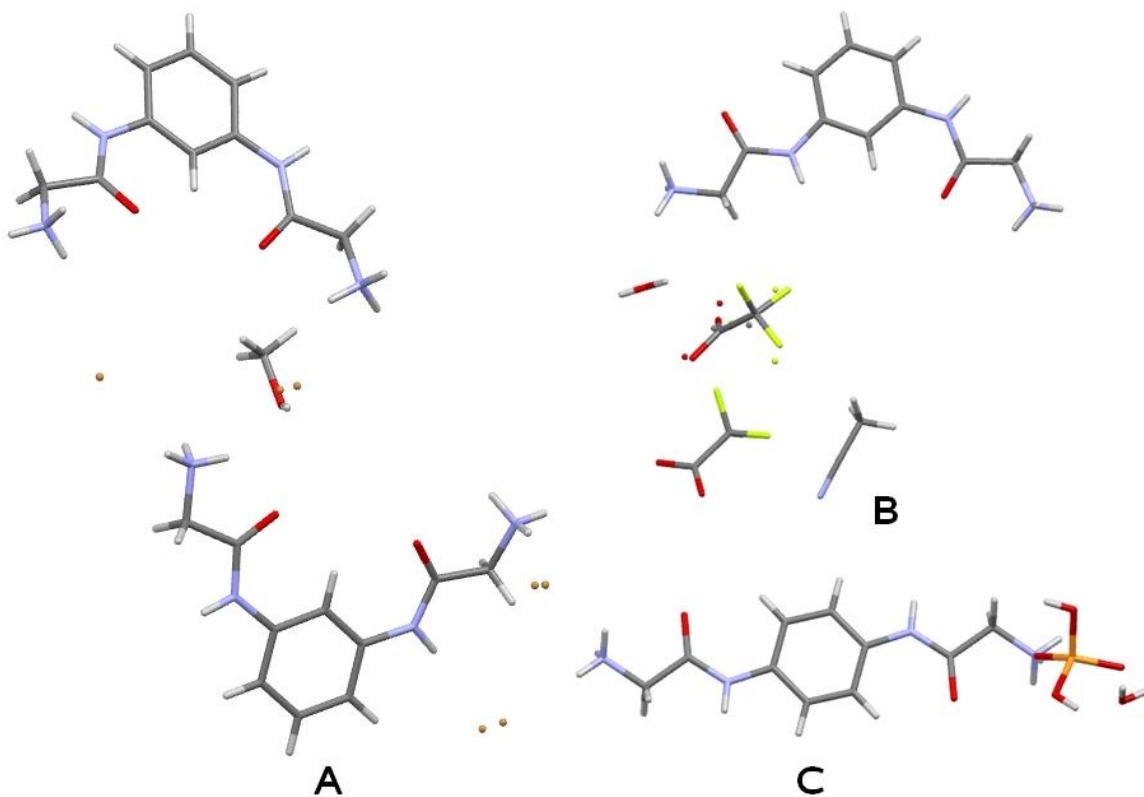


Figure 4.9. Solid state structures of **9** crystallized from different solvent systems and in the presence of different anions.

In each of these conformations, either amide NH bonds or ammonium cations (and NH bonds) are available to interact with DNA phosphates. In A, the distance between the distal ammonium proton atoms is 10 Å. In B, there are two potential interactions. The first is the ammonium to ammonium distance of 12 Å. The second is the *syn* NH and the more distant ammonium cation. This distance is 7 Å. In conformation C, the ammonium-ammonium distance is 14 Å and the ammonium to amide NH is 9 Å. These values are slightly lower than those predicted above (Figure 4.6).

4.2.5. Assessment of bis(aminoamide)-DNA binding by gel electrophoresis. Our key interest in the present study was to determine if these compounds could interact with DNA. If they bound to one or preferably two phosphates, they could screen the

charge. Self-association of the compound through hydrogen bonding or stacking could, in turn, lead to condensation and potentially to a vehicle for transfection. As a screening method, we again used agarose gel electrophoresis. In this experiment, 20 ng/ μL (60.6 μM DNA phosphates) 10 kb DNA plasmid (pKLMF-FX, New England Biolabs) is mixed with a specified amount of **1-13** in an equal volume of DMSO and pipetted into a well on the gel plate. A current is applied and the degree of DNA migration from the well is determined. To the extent the DNA charge is masked or compensated, migration will be minimized or prevented. A typical gel is shown in Figure 4.10 for compound **2** and the data obtained from the electrophoresis analysis is presented in Table 2. DNA-binding ability is assessed in two ways: 1) visual observation of the minimum concentration (expressed as equivalents) to retain DNA in the well (effective concentration of retention, EC_{ret}), and 2) densitometric analysis of the gel image by using ImageJ software (available from NIH) to determine the concentration (expressed as equivalents) at which DNA was 50% retained in the well (effective concentration for 50% retention, EC_{50}).²⁴ Serial dilutions are employed in the screening method starting from 50 equivalents and progressing with a dilution factor of $\frac{1}{2}$. Therefore, the resolution for an EC_{ret} of x is typically $+2x/-0.5x$. The value for EC_{50} is extracted quantitatively from the binding curve generated by ImageJ analysis and therefore represents a more precise value. While up to 800 equivalents of compound to DNA phosphate was tested in the gel shown in Figure 4.10, we considered anything over 50 equivalents as very weak DNA binding agents and therefore inactive.

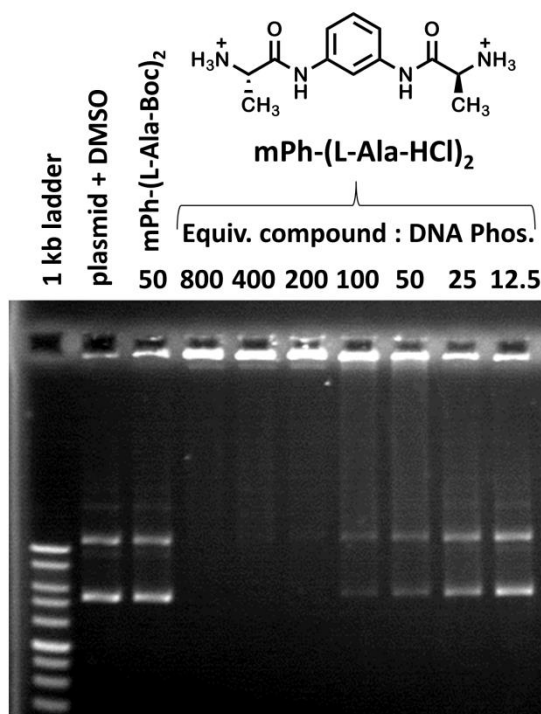


Figure 4.10. Agarose gel electrophoresis of 2 mPh-(L-Ala-HCl)₂.

The electrophoresis data presented in Table 4.2 demonstrate that certain *bis*(aminoamides) are capable of binding and condensing DNA. First, the role of the counter-anion deserves comment. The hydrochloride salt of the *bis*(glycylamido) compound **1** was found to weakly interact with DNA, retaining 50% of the DNA in the well at 37 molar equivalents of compound to DNA phosphate. However, the trifluoroacetate salt did not retain DNA under the same conditions. This may suggest that the compounds are better receptors for oxoanions than spherical halide ions. This may mean that they also have higher affinity for phosphate oxoanions. Initially, we suspected that the counter-anion would be solvent separated under the mixing conditions and therefore TFA and HCl were used interchangeably. Further work is underway to assess the role of the counter-anion and we have attempted to be cautious in our comparisons of different side-chained compounds when the counter-anions differ.

The simple *bis*(glycine) compound **1** showed minor DNA interaction. The *bis*(alanine) compound **2** has a methyl group on the amino acid α -carbon rather than a hydrogen. This prevented any additional interaction compared to **1**. However, appending a hydroxyl to the methyl group increased DNA binding to an EC₅₀ value of 24 equivalents. We then explored the limitations of the hydrogen bond donor hydroxyl group by appending a methyl group to the β -carbon. This was achieved with the synthesis of the *bis*(threonine) analog **4**. The additional methyl group inhibited DNA binding altogether. In an abundance of caution, we note that **4** is the trifluoroacetate salt, and the effect of the counter-anion is still being investigated. The *bis*(proline) compound is interesting in that the side chain is fused to the α -amino group. This does not preclude rotation about the carbonyl carbon— α -carbon bond. A CCDC CSD survey of protonated prolinamides shows that the ammonium—carbonyl relationship is, like protonated glycinamides, *syn*-perplanar. The *bis*(proline) compound **5** did not show DNA binding. A *bis*(lysine) compound **6** was prepared as well. This analog contains two additional positive charges and therefore ought to have greater affinity for the polyanionic DNA backbone. Compound **6** had moderately strong DNA binding and condensation activity, retaining 50% of DNA with 9.6 equivalents of the tetrakis(trifluoroacetate) salt. Compound **7**, the *bis*(tryptophan) analog, was the most active of all compounds in this study, requiring only 4.1 equivalents to fully retain DNA. The TFA salt analog (not shown in the table) bound DNA with an EC_{ret} = 12.5 and EC₅₀ = 7.2 equivalents. The difference caused by the counter-anion is appreciable. After obtaining these results, an effort was made to prepare only the hydrochloride salts.

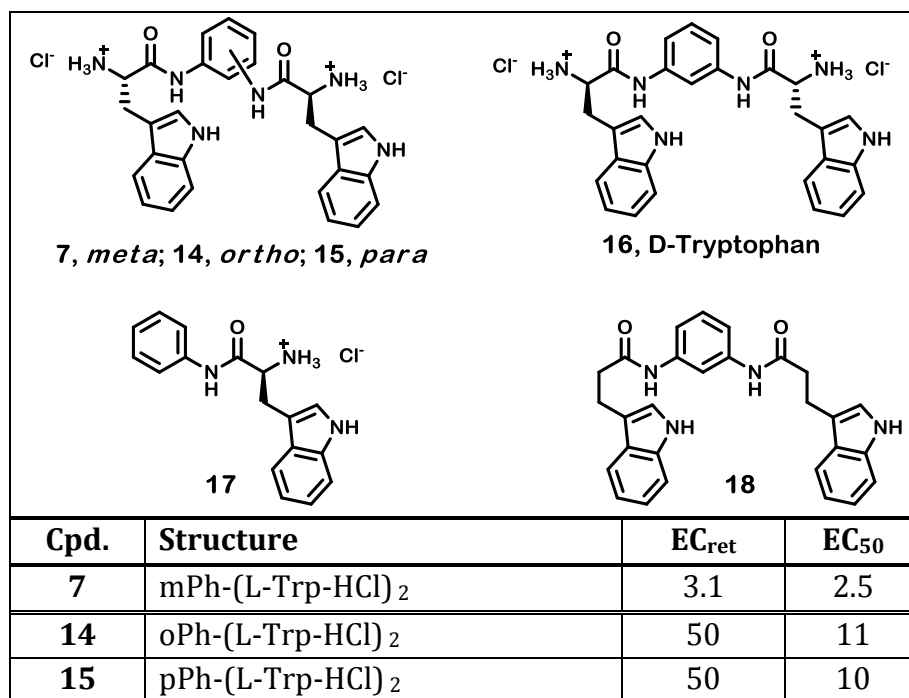
Cpd.	Structure	EC _{ret}	EC ₅₀
1	mPh-(Gly-HCl) ₂	>50	37
2	mPh-(L-Ala-HCl) ₂	>50	>50
3	mPh-(L-Ser-HCl) ₂	50	24
4	mPh-(L-Thr-TFA) ₂	>50	>50
5	mPh-(L-Pro-TFA) ₂	>50	>50
6	mPh-(L-Lys-2TFA) ₂	25	9.6
7	mPh-(L-Trp-HCl) ₂	3.1	2.5
8	mPh-(L-Leu-HCl) ₂	>50	>50
9	mPh-(L-Phe-HCl) ₂	>50	>50
10	mPh-(L-Tyr-HCl) ₂	>50	>50 ^a
11	oPh-(Gly-TFA) ₂	>50	>50
12	mPh-(Gly-TFA) ₂	>50	>50
13	pPh-(Gly-TFA) ₂	>50	>50

Table 4.2. Summary of agarose gel electrophoresis results for the interaction of compounds **1-13** with 10 kb plasmid DNA. ^aMinor streaking resulting in ~20% DNA retention was observed for **10** at 50 equivalents.

The indole side chain in the strong DNA binding compound **7** is hydrophobic, aromatic, contains a N-H hydrogen bond donor, and can also participate in cation- π and π - π stacking interactions. In order to examine the extent to which any of these characteristics influence DNA binding, compounds **8-10** were prepared. The *bis*(leucine) compound **8** contains a hydrophobic side chain that is known to self-associate in DNA-binding proteins in the canonical *leucine zipper*.²⁵ If hydrophobicity was the primary self-associative characteristic driving strong DNA binding with **7**, then we would expect the same from **8**. However, no DNA binding was observed at 50 equivalents of **8**. The role of a hydrophobic and aromatic side chain was probed with *bis*(phenylalanine) **9**. This compound was also inactive up to 50 equivalents. Finally, the role of a hydrophobic and aromatic side chain that also contains a hydrogen-bond donor was tested. It should be noted, however, that the location and directionality of the H-bond donor differs in tyrosine and tryptophan. The *bis*(tyrosine) compound **10** did not retain DNA at concentrations as high as 50 equivalents. However, minor streaking resulting in approximately 20% retention was observed at 50 equivalents. This suggests that the phenolic-OH hydrogen bond donor improved DNA interaction compared to **9** but not to a great extent. A similar increase in DNA affinity was observed in *bis*(alanine) and *bis*(serine) compounds **2** and **3** with the additional hydrogen bond donor -OH group in the latter structure.

Together, these results suggest that the indole side chain of **7** results in strong DNA binding for a reason other than simply being hydrophobic, aromatic, and containing an extra H-bond donor.

A structural study of different characteristics of *bis*(tryptophan) **7** was undertaken to identify the requisite components for strong DNA interactions. Compounds **14** and **15** are the *ortho* and *para* isomers of **7**. While these compounds did interact with DNA, the retention was significantly lower than the *meta* regioisomer. This confirms that the modelling studies elaborated in Section 4.2.2 were informative. The role of stereochemistry was probed with **16**, an enantiomer of **7** prepared with D-tryptophan rather than the naturally occurring isomer L-trp. The DNA binding was essentially unchanged. This suggests that the chirality of the molecule does not influence how it packs with the right-handed DNA double helix. Finally, mono-tryptophan compound **18** and the uncharged deaminated compound **19** were synthesized and tested for DNA interaction. Compound **18** showed very weak interaction with DNA, however some streaking was observed at 50 equivalents. Compound **19** is prepared by condensation of indole-3-propionic acid (IPA) and *meta*-phenylenediamine. Absent the charged ammonium groups, **19** has low solubility in water and is observed to precipitate in the well. However, this precipitation does not affect the mobility of the DNA. This result emphasizes the necessity that the compound is both self-associative *and* has affinity for DNA, the latter of which is typically achieved through cationic ammonium groups.



16	mPh-(D-Trp-HCl) ₂	3.1	2.2
17	Ph-(L-Trp-HCl)	>50	>50 ^a
18	mPh-(CH ₂ CH ₂ -1 <i>H</i> -indol-3-yl) ₂	>50 ^b	>50 ^b

Table 4.3. Structures and summary of agarose gel electrophoresis results for the interaction of compounds **14-18** with 10 kb plasmid DNA. ^aMinor streaking resulting in ~20% DNA retention was observed for **17** at 50 equivalents.

The tryptophan compounds are intriguing for reasons in addition to the impressive DNA binding results. Tryptophan occurs in proteins with the lowest frequency of the 20 genetically coded amino acids.²⁶ Tryptophan is not found in the ubiquitous eukaryotic DNA-binding histone proteins.^{27,28} However a sequence of regularly spaced tryptophan residues is conserved in the myb DNA-binding proteins.^{29,30} The evolutionary persistence of the unusually high amount of tryptophan along with mutagenesis experiments³¹ demonstrates their importance to the DNA-binding ability of these proteins. The chemical environment of the tryptophans were shown to change upon DNA binding³². Interestingly, the tryptophans are flanked by positively charged amino acids, which are critical to the DNA binding function.³³ More recent crystallographic evidence shows that the tryptophans stabilize a helix-turn-helix motif that organizes cationic lysine and arginine residues toward the DNA.³⁴ Some tryptophan residues in the structure were shown to interact directly with the DNA major groove. A trp residue was also identified as crucial to the DNA binding mode in another well-known transcription cofactor, PC4.³⁵ In the 2015 report it was shown by crystallography that a trp to tyr mutation altered the DNA binding mode from a two-nucleotide to a single-nucleotide interaction. Interestingly, the tryptophan in these structures is in proximity to cationic residues, as was found in the myb family of DNA-binding proteins. A similar motif of tryptophan residues adjacent to positively charged amino acids has been employed in oligonucleotide-transfecting synthetic peptides.^{36,37} Tryptophan may also be capable of intercalating and stacking with DNA bases³⁸, and at least one structural example of this occurs in a natural protein.³⁹

Just as important as the evidence of tryptophan's role in DNA-binding is the well-established observation that tryptophan is found near the polar-nonpolar interface of membrane-spanning proteins.^{40,41} NMR spectroscopic measurements suggest that this preference does not simply arise from the amphipathic nature of the indole side chain, rather more specific interactions of the aromatic π system including cation- π forces may also play a role.⁴² A 2002 report from the Gokel laboratory published in the *Journal of the American Chemical Society* demonstrated the versatility of the indole ring as a π -donor.⁴³ Crown ethers with pendant indole groups were co-

crystallized with sodium and potassium salts. Both the benzo and pyrrolo rings were found to form cation- π interactions. Another contribution to the tryptophan canon was made by the Gokel lab. Indole groups alkylated at the nitrogen or at the 3-position were found to form vesicles in water when the aliphatic chain was of sufficient length.^{44,45} This discovery was relevant because the indole side chain of tryptophan was considered by most to be too hydrophobic to serve as a headgroup in a bilayer. When considered as a viable headgroup, the indolyl N-H was thought to be critical, yet the N-alkylated indoles surprisingly form stable vesicles.

Before undertaking biophysical characterization of the *bis*(tryptophan)-DNA complex, we considered the toxicity and mutagenicity of the linker molecules. The cell possesses amidases that are capable of hydrolyzing amide bonds. Hydrolysis of the amino acids from the linker would result in the presence of phenylenediamine within the cell. A survey of toxicity studies found that 1,3-phenylenediamine is moderately toxic with an LD₅₀ = 325 mg/kg in rat, and 290 mg/kg in mouse when administered by intraperitoneal injection.⁴⁶ Other phenylenediamine isomers had similar toxicity. While these values do not represent an extraordinarily high risk of toxicity, we explored the use of other linkers. In 1,3-phenylenediamine the amino groups are separated by 3 carbons. However, altering the linker to 1,3-diaminopropane would not alleviate toxicity concerns: LD₅₀ = 177 mg/kg in rabbits by dermal application and LD₅₀ = 308 mg/kg in rats by oral administration.⁴⁷ In contrast, 1,4-diaminobutane (cadaverine) is considerably less toxic with LD₅₀ = 2000 mg/kg in rats administered orally.⁴⁸ We therefore examined *bis*(aminoamide)s with aliphatic linkers.

The DNA-binding ability of *bis*(tryptophan) compounds containing saturated hydrocarbon linkers was tested. The effect of chain length was investigated by preparing compounds **19-22**, containing aliphatic spacers of 3, 4, 6, or 10 methylenes. Their DNA interaction was assessed by gel electrophoresis. The gel image obtained by the standard process of staining with ethidium bromide and imaging by UV-transillumination is shown in Figure 4.11. The structures of **19-22** and the results are summarized in Table 3, along with the DNA-binding results for compound **7**, which bears a *meta*-phenylenediamine spacer.

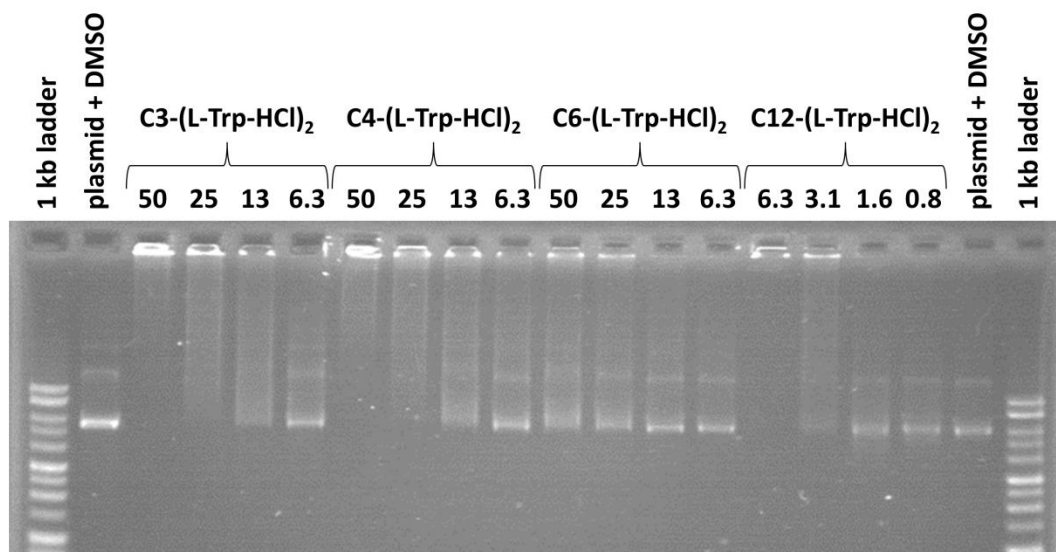


Figure 4.11. Agarose gel electrophoresis image of *bis*(tryptophan) compounds with C₃ (**19**), C₄ (**20**), C₆ (**21**), and C₁₂ (**22**) methylene spacers.

The C₃ and C₄ linked *bis*(trp) compounds **19** and **20** were moderate DNA-condensation agents with similar EC₅₀ values of about 40 equivalents. It is surprising that the longer-chained **21** was a worse DNA-binding molecule despite the potential for greater intermolecular hydrophobic interactions between C₆ chains by the exclusion of water molecules. The longest chain tested was C₁₂ (compound **22**), which showed dramatically stronger DNA-binding. The EC₅₀ of 4.4 equivalents for **22** is on the order of the strong interactions observed with *meta*-phenylenediamine-linked **7**. The observation of moderate binding for shorter chains, poor binding for medium-length chains, and strong binding for longer chains suggest the existence of two modes of binding. *Bis*(tryptophan) compounds with aromatic or short aliphatic linkers may cause DNA condensation by interactions of proximate indole side chains. The *meta*-phenylene linker organizes the side chains into an optimal geometry for binding compared to *ortho* and *para* linkers. The short aliphatic linkers can access the preferred conformation, but lack the rigidity and additional stacking interactions conferred by the phenylene linkers. The C₆ chain of **21** is bulkier than the C₃ and C₄ chains and therefore inhibits the preferred formation accessible to **7**, **20**, and **21**. The C₆ linker is more hydrophobic than the shorter chains, but not to a degree sufficient to drive efficient condensation observed with the longest C₁₂ linker of **22**. C₁₂-(L-Trp-HCl)₂, compound **22**, may be considered a bolaamphiphile. The tryptophan residues must play an important role in the DNA binding and condensation, as the linker itself did not show DNA condensation (see Figure 4.3 above).

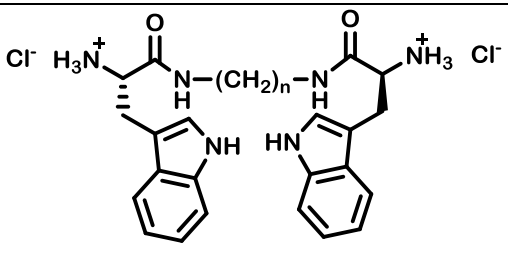
			
19, n = 3; 20, n = 4; 21, n = 6; 22, n = 12			
Cpd.	Structure	EC _{ret}	EC ₅₀
7	mPh-(L-Trp-HCl) ₂	3.1	2.5
19	C ₃ -(L-Trp-HCl) ₂	50	38
20	C ₄ -(L-Trp-HCl) ₂	50	37
21	C ₆ -(L-Trp-HCl) ₂	>50	>50
22	C ₁₂ -(L-Trp-HCl) ₂	6.25	4.4

Table 4.4. Structures and summary of agarose gel electrophoresis results for the interaction of compounds **19-22** with 10 kb plasmid DNA.

4.2.6. *The effect of pH on the DNA-binding of a bis(tryptophan) and a bis(lysine) compound.* An important component of our hypothesis for the DNA-binding and for the condensation mechanism of *bis*(aminoamide) compounds is the association of the cationic protonated α -amino group with the negatively charged DNA phosphates. The pK_a of a typical amino group in an amino acid is around 9-10. In order to assay the role of protonation, agarose gel electrophoresis studies were performed under buffer conditions of pH 7.2 and pH 8.8. The compounds tested were a trifluoroacetate analog of **20** (**23**, C₄-(L-Trp-TFA)₂) and a *bis*(lysine) compound (**24**, C₄-(L-Lys-2TFA)₂). The resulting concentration-retention profiles are shown in Figure 4.12.

Both **23**, *bis*(trp) and **24**, *bis*(lys) compounds are moderately strong DNA binding agents. The concentration-retention profile for the bivalent *bis*(tryptophan) compound is largely unchanged as pH is increased from 7.2 to 8.8. However, the tetravalent *bis*(lysine) compound is considerably affected by the increase in pH. It takes nearly four times as much **24** to retain DNA at pH 8.8 compared to pH 7.2. This suggests that protonation plays a much greater role in the mechanism of DNA condensation by **24** compared to compound **23**. We hypothesize that the mechanism of DNA condensation for **24** involves binding the DNA and neutralizing its charge resulting in aggregation. While the protonated nitrogens are likely to play a large role in the condensation of DNA by **23**, the compound also bears the indole

side chains. The data in Figure 4.12 suggest that the tryptophan residues play a large role in the self-association and resultant condensation of the DNA-complex.

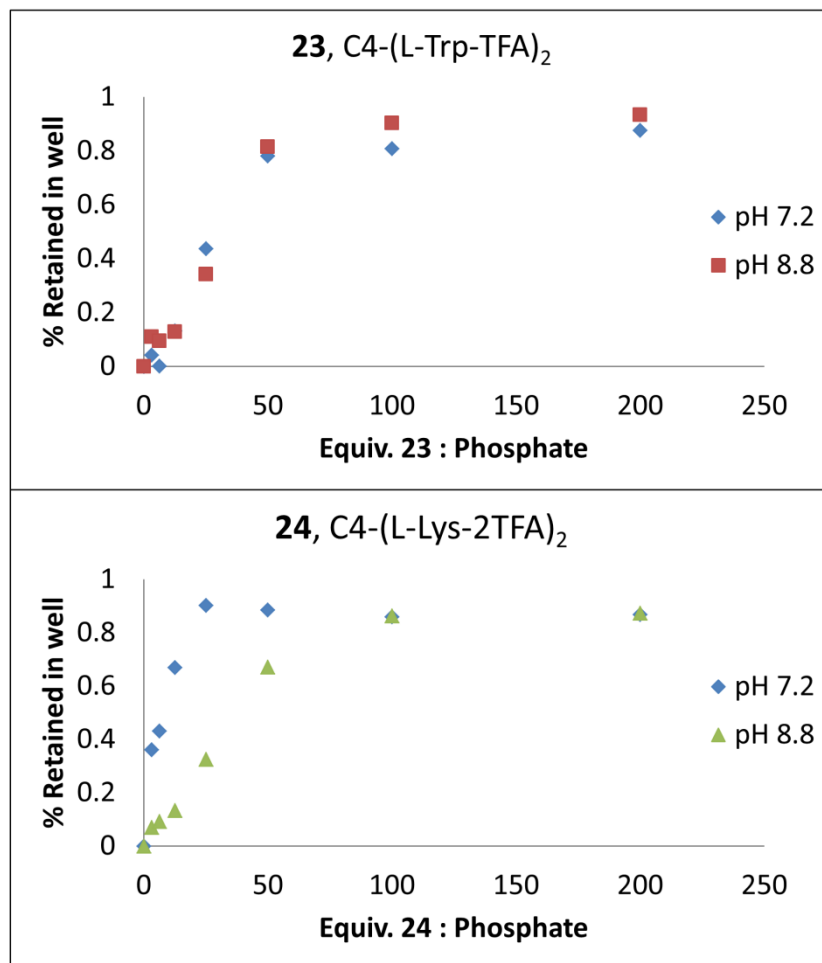


Figure 4.12. Concentration-retention profile for a tetramethylene linked *bis*(tryptophan) (top) and *bis*(lysine) (bottom) compounds tested at pH 7.2 and pH 8.8.

4.2.7. Electron microscopy of the plasmid DNA complexes of a *bis*(tryptophan) and a *bis*(lysine) compound. Electron microscopy studies were undertaken to characterize the presumed complexes of **23**, C₄-(L-Trp-2TFA)₂ and **24**, C₄-(L-Lys-2TFA)₂ with plasmid DNA. Transmission electron microscopy (TEM) was used to assess the size and morphology of the particles. The compounds were mixed with plasmid DNA and then adsorbed to formvar-coated lacey carbon copper grids. The grids were then counterstained with uranyl acetate observed at 81,000X magnification. Representative micrographs are shown in Figures 4.13 and 4.14.

The *bis*(lysine) compound **24** with plasmid DNA formed spherical aggregates ranging from 50-150 nm in diameter (Figure 4.14). The particles did not have especially distinct borders, suggesting that their densities may vary at the particle surface, however the interior of the particle was regular in density. The complexes formed from *bis*(tryptophan) compound **23** were spherical and generally regular in size with a diameter of 150-250 nm (Figure 4.13). Unlike the particles formed from **24**, the tryptophan-derived particles varied in density throughout the structure. The spheres were observed to contain fibrils of denser material. These can be seen in the magnified insets of Figure 4.13. The width of the fibers is 4-5 nm, and they appear coiled and toroidal. This is consistent with supercoiled plasmid DNA in both size and morphology. These particles were examined in greater detail by scanning electron microscopy (SEM).

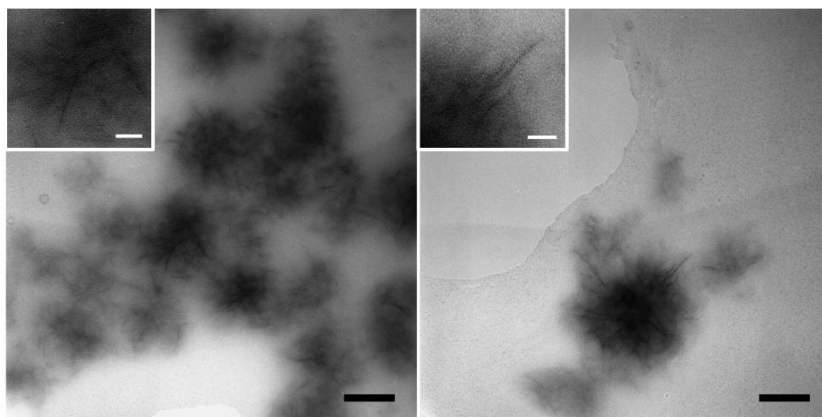


Figure 4.13. Transmission electron micrographs of complexes of **23**, C_4 -(L-Trp-2TFA) $_2$ with 10 kb plasmid DNA counterstained with uranyl acetate. Black scale bars represent 100 nm, white scale bars represent 25 nm.

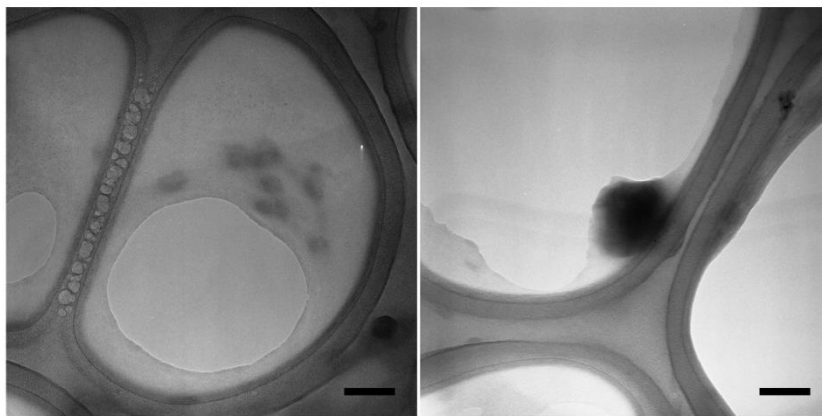


Figure 4.14. Transmission electron micrographs of complexes of **24**, C_4 -(L-Lys-2TFA) $_2$ with 10 kb plasmid DNA counterstained with uranyl acetate. Scale bars represent 100 nm.

The TEM grid from which the images in Figure 4.13 originated was sputter-coated with elemental gold and then observed by scanning electron microscopy. SEM is advantageous because of the greater depth of field obtained in the images than those from TEM. These images have three-dimensionality that makes it easier to examine certain structures in detail. Representative images from the SEM study are shown in Figure 4.15.

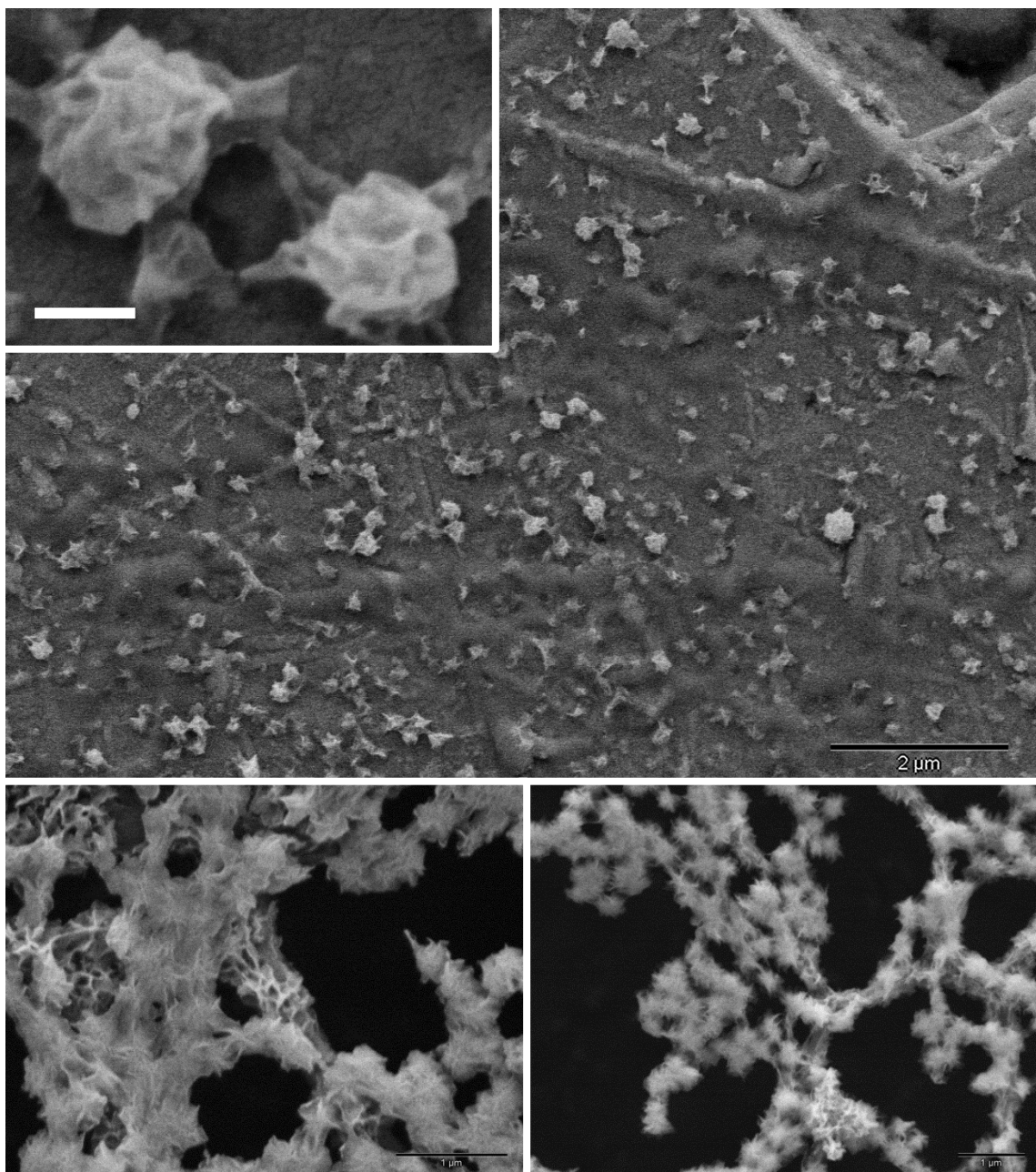


Figure 4.15. Scanning electron micrographs of the of complexes of **23**, $C_4-(L-Trp-2TFA)_2$ with 10 kb plasmid DNA after gold sputter-

coating. The top image and inset show particles on the surface of the copper grid. The bottom images show particles on the lacey carbon support. The white scale bar (top left inset) represents 200 nm. The scale bars in the bottom images represent 1 μm .

The micrographs in Figure 4.15 show particles of the same size as the particles observed in the TEM study. The structures are spherical with a surface that consists of curvilinear articulations. In some cases these articulations appear as appendages protruding from the structure. It is likely that these features are the same ones observed as fibrils in Figure 4.13. The fibrils are thicker than those observed by TEM. We attribute the thickness to a coating of the *bis*(tryptophan) compound. The *bis*(trp) aggregates are less dense than the DNA and therefore do not add to the appearance of the thickness of fibrils in TEM. The layer of gold from sputter-coating is likely too thin to create such a drastic increase in fibril thickness by itself. Together, these electron micrographs suggest that the compounds are binding DNA, presumably by charge interactions and cooperative exclusion of water, to form regularly sized nanoparticles. These nanoparticles may be too large or not sufficiently charged to migrate through an agarose gel.

4.2.8. Circular Dichroism of a bis(lysine) compound with plasmid DNA. The influence of *bis*(aminoamide) binding on the helical structure of the plasmid DNA is unknown. Circular dichroism spectroscopy (CD) was used in order to determine if the helicity of DNA is influenced by binding and condensation with the *bis*(lysine) compound **24**. CD measures the differential absorption of circularly polarized light by chiral molecules or supramolecular systems. DNA typically exists in a right-handed helix (B-form) that has a characteristic CD absorption spectrum. Because CD is based on absorption phenomena, the spectrum is observed only over the range where the chromophore absorbs light. For DNA, this occurs with maximal intensity at 260 nm. Compound **24**, $\text{C}_4\text{-(L-Lys-2TFA)}_2$, was chosen because it was shown to bind and condense DNA by agarose gel electrophoresis, the particles were characterized by TEM, and most importantly because it does not have any aromatic functional groups that overlap the characteristic DNA absorption signal centered at 260 nm. The results of a titration of plasmid DNA with **24** are shown in Figure 4.16. The addition of the *bis*(lysine) compound increases the intensity of the major absorption bands observed at 245 nm (negative ellipticity) and at 275 nm (positive ellipticity). Furthermore, a bathochromic shift of about 15-20 nm is observed for both absorption bands. This demonstrates that the *bis*(lysine) compound is interacting intimately with the plasmid DNA and induces a conformational change in its helical structure. While the binding mode for **24** may differ from other *bis*(aminoamide)

compounds, it may be inferred that those compounds could also bind and influence the DNA structure.

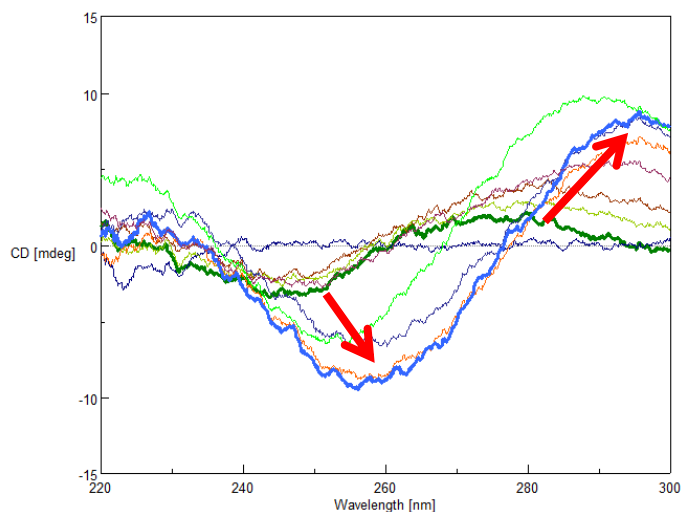


Figure 4.16. The circular dichroism spectrum for the titration of plasmid DNA with **24**, C_4 -(L-Lys-2TFA)₂, from 0 equivalents **24** (bold green) to 10 equivalents **24** (bold blue). Addition of the *bis*(lysine) compound increased the ellipticity and induced a bathochromic shift in the DNA absorption bands to a negative maximum at 260 nm and positive maximum at 295 nm.

4.2.9. Preliminary screening of bis(lysine) and bis(tryptophan) compounds for the transfection of human embryonic kidney (HEK-293) cells. A preliminary transfection experiment was conducted following the synthesis and structural and biophysical studies on *bis*(aminoamide)-DNA binding. Complexes of compounds **23** and **24** with plasmid DNA encoding a green fluorescent protein (EGFP) were tested by themselves and together with the cationic transfection lipid DOTAP (see Chapter 1) for transfection ability in HEK-293 cells. Only a limited concentration range was tested. No compounds showed transfection on their own and no observable enhancement of transfection with DOTAP was observed. Presently, no other compound described in this chapter has been tested as a transfection agent.

4.3. Conclusion.

The method described in Chapter 1 for the facile formation of a DNA-lipid complex was employed to examine the DNA-binding properties of simple alkyl and aryl amines and diamines. Two features were identified that promoted DNA-binding and condensation by small molecules: 1) DNA affinity by positively charged ammonium groups and 2) self-association of the DNA-binding agents through hydrophobic effects or other intermolecular forces. These concepts were applied in the design of

novel DNA-binding agents consisting of amino acids linked through their carboxy-termini to a phenylenediamine spacer. The interaction of the synthesized *bis*(aminoamides) with DNA was assessed by agarose gel electrophoresis. In agreement with the initial design, the *meta*-phenylenediamine spacer provided the most effective geometry for DNA condensation. The amino acids lysine and tryptophan were identified as the most active in DNA-binding studies. A series of structurally related *bis*(tryptophan) compounds was prepared. Plasmid DNA complexes of *bis*(tryptophan) and *bis*(lysine) compounds linked by diaminobutane were characterized by electron microscopy. The resulting particles were on the order of 150 nm in diameter and fibrillary features exemplifying plasmid DNA were identified in the structure. The *bis*(lysine) compound was observed to influence the helicity of DNA by circular dichroism spectroscopy. Preliminary transfection experiments did not result in increased efficiencies in human embryonic kidney cells. Nevertheless, a novel strategy for developing non-lipidic small molecule DNA-binding and condensation agents was elucidated.

4.4. Experimental.

4.4.1. Synthesis and characterization. The *tert*-butyl carbamate-protected (Boc-protected) amino acids were coupled to the diamine using a uronium-based coupling reagent HBTU in DMF with diisopropylethylamine. After workup and isolation of the desired Boc-protected *bis*(aminoamide) product, deprotection was carried out using acid (HCl or trifluoroacetic acid) in methylene chloride. Certain amino acid side chains required additional protecting groups. Their deprotection reactions are described below.

Serine. The *bis*(serine) compound used the benzyl carbamate (Cbz) nitrogen protecting group and the side chain hydroxyl was protected as the *tert*-butyl ether. The Cbz group was removed first by catalytic hydrogenation and the *t*-butyl group was removed by neat trifluoroacetic acid. The trifluoroacetate anion was exchanged for chloride using dowex 1 chloride exchange resin.

Threonine. The *bis*(threonine) compound used the Boc nitrogen protecting group and the side chain hydroxyl was protected as the benzyl ether. The benzyl group was removed first by catalytic hydrogenation and the Boc group was then removed by trifluoroacetic acid in methylene chloride/methanol.

Lysine. The *bis*(lysine) compounds used the Boc nitrogen protecting group on the α -nitrogen and the side chain amine was protected with Cbz. The Cbz group was removed first by catalytic hydrogenation and the Boc group was removed by

trifluoroacetic acid in chloroform/methanol to give the tetrakis(trifluoroacetate) salt.

General procedure A: coupling with HBTU. The *tert*-butyl carbamate-protected (Boc-protected) amino acids and HBTU (2.1 equivalents) were dissolved in 10 mL anhydrous DMF with diisopropylethylamine (4.0 equivalents for the neutral diamines; 6.0 equivalents for diaminedihydrochlorides). The reaction was stirred overnight at room temperature under an argon atmosphere. The mixture was taken up in 75 mL ethyl acetate and washed with 1 M NaHSO₄ (2 x 75 mL), 5% NaHCO₃ (3 x 50 mL), and brine. The organic layer was dried by filtration through a MgSO₄/celite plug and the solvent removed *in vacuo*. The Boc-protected *bis*(amino acid) was used without further purification or was crystallized/precipitated from CH₂Cl₂/hexane.

General procedure B: Boc deprotection with HCl/dioxane. The Boc-protected *bis*(aminoamide) deprotection was carried out by using 10 equivalents of HCl in dioxane/methanol and the product was obtained by precipitation and trituration with cold methylene chloride.

General procedure C: Boc deprotection with TFA. The Boc-protected *bis*(aminoamide) deprotection was carried out by using 10 or more equivalents of trifluoroacetic acid in methylene chloride or used neat. The product was obtained by removal of the solvent and TFA *in vacuo*. The product was used without further purification or recrystallized from methanol/chloroform/hexane.

General procedure D: Cbz deprotection. The Cbz-protected amine was dissolved in absolute EtOH to which 0.1 molar equivalents of 10% Pd/C was added. The mixture was shook on a Parr shaker at 60 psi for 4h then filtered through celite and the solvent was removed *in vacuo*.

General procedure E: ROtBu deprotection with TFA. See general procedure C.

General procedure F: ROBn deprotection. See general procedure D.

Di-*tert*-butyl ((1,3-phenylenebis(azanediyl))bis(2-oxoethane-2,1-diyl))dicarbamate (1a) was prepared according to general procedure A using 1,3-phenylenediamine (150 mg, 1.39 mmol) and Boc-Gly-OH. White powder (0.33 g, 57% yield), mp 95°C (dec.). ¹H-NMR (300 MHz, CDCl₃): δ 1.44 (s, 18H, (CH₃)₃), 3.90 (d, 4H, αCH₂), 5.86 (m, 2H, Boc-NH), 7.12 (t, *J* = 7.2 Hz, 1H, phenyl H5), 7.23 (d, *J* = 7.2 Hz, 2H, phenyl H4, H6), 7.64 (s, 1H, phenyl H2), 8.92 (s, 2H, PhNHCO-). ¹³C-NMR

(75 MHz, CDCl₃): δ 28.27, 44.90, 80.28, 111.72, 116.02, 129.27, 138.00, 156.60, 168.52. HRMS (FAB⁺): calcd for (C₂₀H₃₀N₄O₆) 422.2165, found 422.2163.

2,2'-(1,3-phenylenebis(azanediy))bis(2-oxoethanaminium) chloride (1) was prepared according to general procedure B using **1a** (309 mg, 0.731 mmol). White powder (0.20 g, 94% yield), mp 310 °C (dec.). ¹H-NMR (300 MHz, D₂O): δ 3.88 (s, 4H, α CH₂), 7.14 (d, *J* = 8.1 Hz, 2H, phenyl H4, H6), 7.32 (t, *J* = 8.1 Hz, 1H, phenyl H5), 7.68 (s, 1H, phenyl H2). ¹³C-NMR (75 MHz, D₂O): δ 40.92, 113.72, 117.97, 129.92, 136.99, 165.49. HRMS (FAB⁺): calcd for (C₁₀H₁₄N₄O₂Na) 245.1015, found 245.1014.

Di-tert-butyl ((2S,2'S)-(1,3-phenylenebis(azanediy))bis(1-oxopropane-2,1-diyl))dicarbamate (2a) was prepared according to general procedure A using 1,3-phenylenediamine (0.100 mg, 0.92 mmol) and Boc-L-Ala-OH. White powder (0.35 g, 84% yield), mp 159-161 °C. ¹H-NMR (300 MHz, CDCl₃): δ 1.42 (d, *J* = 7.0 Hz, 6H, β CH₃), 1.47 (s, 18H, (CH₃)₃), 4.37 (m, 2H, α CH), 5.31 (m, 2H, Boc-NH), 7.10 (m, 1H, phenyl H5), 7.19 (m, 2H, phenyl H4, H6), 7.60 (s, 1H, phenyl H2), 8.65 (s, 2H, PhNHCO-). ¹³C-NMR (75 MHz, CDCl₃): δ 17.98, 28.35, 50.81, 80.46, 111.28, 115.50, 129.16, 138.22, 156.13, 171.39, 188.71.

((2S,2'S)-1,1'-(1,3-phenylenebis(azanediy))bis(1-oxopropan-2-aminium) chloride (2) was prepared according to general procedure B using **2a** (105 mg, 0.23 mmol). White powder (0.07 g, 93% yield), mp 195 °C (dec.). ¹H-NMR (300 MHz, CD₃OD): δ 1.60 (d, *J* = 7.0 Hz, 6H, β CH₃), 4.08 (q, *J* = 7.0 Hz, 2H, α CH), 7.22-7.39 (m, 3H, phenyl H4, H5, H6), 8.05 (m, 1H, phenyl H2). ¹³C-NMR (75 MHz, CD₃OD): δ 17.89, 51.06, 112.94, 117.34, 130.50, 139.86, 169.48.

Dibenzyl ((2S,2'S)-(1,3-phenylenebis(azanediy))bis(3-(tert-butoxy)-1-oxopropane-2,1-diyl))dicarbamate (3a) was prepared according to general procedure A using 1,3-phenylenediamine (0.100 mg, 0.92 mmol) and Cbz-L-Ser-(OtBu)-OH. White powder (0.61 g, 99% yield), mp 81-83 °C. ¹H-NMR (300 MHz, CDCl₃): δ 1.23 (s, 18H, OC(CH₃)₃), 3.50 (ABX, 2H, β CH₂), 3.88 (ABX, 2H, β CH₂), 4.44 (ABX, 2H, α CH), 5.16 (s, 4H, OCH₂Ph), 6.02 (m, 2H, Boc-NH), 7.20-7.37 (m, 13H, Cbz, phenyl H4-6), 7.86 (s, 1H, phenyl H2), 8.86 (s, 2H, PhNHCO-). ¹³C-NMR (75 MHz, CDCl₃): δ 27.51, 54.94, 61.86, 67.27, 74.78, 111.23, 115.50, 128.26, 128.34, 128.65, 129.81, 136.13, 138.26, 156.19, 168.56.

((2S,2'S)-1,1'-(1,3-phenylenebis(azanediy))bis(3-hydroxy-1-oxopropan-2-aminium) 2,2,2-trifluoroacetate (3) was prepared by Cbz deprotection from **3a** (360 mg, 0.54 mmol) according to general procedure D (0.16 g, 75% yield) followed by t-butyl ether deprotection by general procedure E. White powder (0.16 g, 77%

yield). ¹H-NMR (300 MHz, CD₃OD): δ 3.92-4.11 (m, 4H, βCH₃), 4.22 (m, 2H, αCH), 7.28-7.42 (m, 3H, phenyl H4, H5, H6), 8.09 (m, 1H, phenyl H2).

Di-tert-butyl ((2S,2'S,3R,3'R)-(1,3-phenylenebis(azanediy))bis(3-(benzyloxy)-1-oxobutane-2,1-diyl))dicarbamate (4a) was prepared according to general procedure A using 1,3-phenylenediamine (150 mg, 1.39 mmol) and Boc-L-Thr-(OBn)-OH. White powder (0.90 g, 94% yield). ¹H-NMR (300 MHz, CDCl₃): δ 1.21 (d, *J* = 6.4 Hz, 6H, γCH₃), 1.44 (s, 18H, (CH₃)₃), 4.15 (m, 2H, βCH), 4.44-4.61 (m, 6H, αCH, OCH₂Ph), 5.83 (d, *J* = 6.8 Hz, 2H, Boc-NH), 7.05-7.31 (m, 13H, OBn, phenyl H4-6), 7.74 (s, 1H, phenyl H2), 8.80 (br, 2H, PhNHCO-). ¹³C-NMR (75 MHz, CDCl₃): δ 15.35, 27.84, 58.16, 70.89, 74.43, 79.58, 111.07, 115.36, 127.28, 127.83, 127.98, 128.78, 137.39, 137.69, 155.63, 168.18.

((2S,2'S,3R,3'R)-1,1'-(1,3-phenylenebis(azanediy))bis(3-hydroxy-1-oxobutan-2-aminium) 2,2,2-trifluoroacetate (4) was prepared by benzyl deprotection from **4a** (0.9 g, 1.30 mmol) according to general procedure F (0.66 g, 99% yield) followed by Boc deprotection by general procedure C. Off-white solid (0.36 g, 93% yield), mp 85 °C (dec.). ¹H-NMR (300 MHz, CD₃OD): δ 1.33 (d, *J* = 6.4 Hz, 6H, γCH₃), 3.81 (d, *J* = 6.2 Hz, 2H, αCH), 4.14 (m, 2H, βCH), 7.20-7.40 (m, 3H, phenyl H4-6), 8.07 (s, 1H, phenyl H2). ¹³C-NMR (75 MHz, CD₃OD): δ 20.38, 60.99, 67.58, 113.04, 117.50, 130.52, 139.65, 167.03.

((2S,2'S)-di-tert-butyl 2,2'-((1,3-phenylenebis(azanediy))bis(carbonyl))bis(pyrrolidine-1-carboxylate)(5a) was prepared according to general procedure A using 1,3-phenylenediamine (0.150 mg, 1.39 mmol) and Boc-L-Pro-OH. White powder (0.57 g, 81% yield), mp 121 °C (dec.). ¹H-NMR (300 MHz, CDCl₃): δ 1.49 (s, 18H, (CH₃)₃), 1.85-2.55 (m, 8H, βCH₂, γCH₂), 3.31-3.67 (m, 4H, δCH₂), 4.30-4.48 (m, 2H, αCH), 7.06-7.52 (m, 3H, phenyl H4-6), 7.62 (br, 1H, phenyl H2), 9.34 (br, 2H, PhNHCO-). ¹³C-NMR (75 MHz, CDCl₃): δ 24.58, 28.47, 47.28, 60.71, 80.83, 110.91, 115.37, 129.23, 138.71, 156.32, 170.35.

((2S,2'S)-2,2'-((1,3-phenylenebis(azanediy))bis(carbonyl))bis(pyrrolidin-1-ium) 2,2,2-trifluoroacetate (5) was prepared according to general procedure C using **5a** (400 mg, 0.80 mmol). White powder (0.39 g, 91% yield), mp 80 °C (dec.). ¹H-NMR (300 MHz, DMSO-*d*₆): δ 1.87-2.04 (m, 6H, γCH₂, βCH), 2.32-2.43 (m, 2H, βCH), 3.30 (m, 4H, δCH₂), 4.41 (m, 2H, αCH), 7.35 (m, 3H, phenyl H4-6), 8.07 (s, 1H, phenyl H2), 8.79 (br, 2H, NH₂⁺), 9.90 (br, 2H, NH₂⁺), 10.77 (s, 2H, PhNHCO-). ¹³C-NMR (75 MHz, DMSO-*d*₆): δ 23.52, 29.65, 45.69, 59.63, 110.69, 115.16, 129.35, 138.59, 158.65, 166.93.

Di-tert-butyl ((2S,2'S)-(1,3-phenylenebis(azanediyl))bis(6-benzylcarboxamido-1-oxohexane-2,1-diyl))dicarbamate (6a) was prepared according to general procedure A using 1,3-phenylenediamine (150 mg, 1.39 mmol) and Boc-L-Lys-(NεCbz)-OH. Yellow solid (1.10 g, 95% yield). ¹H-NMR (300 MHz, CDCl₃): δ 1.33-1.55 (m, 26H, (CH₃)₃, γCH₂, δCH₂), 1.58-1.86 (m, 4H, βCH₂), 3.13 (m, 4H, εCH₂), 4.29 (m, 2H, αCH₂), 5.06 (s, 4H, CH₂Ph), 5.59 (br, 2H Cbz-NH), 5.92 (br, 2H, Boc-NH), 7.06 (m, 1H, phenyl H5), 7.23 (m, 12H, Cbz-ArH, phenyl H4, H6), 7.99 (s, 1H, phenyl H2), 9.18 (br, 2H PhNHCO-).

(5S,5'S)-6,6'-(1,3-phenylenebis(azanediyl))bis(6-oxohexane-1,5-diaminium) 2,2,2-trifluoroacetate (6) was prepared according to general procedure D using **6a** (1.10 g, 1.32 mmol). Cbz deprotected product **6b** (0.60 g, 81% yield) was used without further purification. Boc deprotection by general procedure C using **6b** (600 mg, 1.06 mmol) afforded yellow solid (0.76 g, 87% yield). ¹H-NMR (300 MHz, CD₃OD): δ 1.58 (m, 4H, γCH₂), 1.75 (m, 4H, δCH₂), 2.01 (m, 4H, βCH₂), 2.98 (t, *J* = 7.6 Hz, 4H, εCH₂), 4.09 (t, *J* = 6.4 Hz, 2H, αCH), 7.28-7.40 (m, 3H, phenyl H4-6), 8.08 (s, 1H, phenyl H2). ¹³C-NMR (75 MHz, CD₃OD): δ 23.05, 28.20, 32.29, 40.35, 54.96, 113.26, 117.62, 130.54, 139.70, 162.95, 163.49, 168.67.

Di-tert-butyl ((2S,2'S)-(1,3-phenylenebis(azanediyl))bis(3-(1H-indol-3-yl)-1-oxopropane-2,1-diyl))dicarbamate (7a) was prepared according to general procedure A using 1,3-phenylenediamine (150 mg, 1.39 mmol) and Boc-L-Trp-OH. White powder (0.80 g, 85% yield), mp 148 °C (dec.). ¹H-NMR (300 MHz, DMSO-*d*₆): δ 1.34 (s, 18H, 2(CH₃)₃) 2.95-3.14 (ABX, 4H, 2CH₂β), 4.39 (ABX, 2H, 2CHα), 6.90-7.12 (m, 6H, indole H5, indole H6, ArNH), 7.15-7.40 (m, 7H, indole H2, phenylene H4), phenylene H5, indole H7), 7.68 (d, *J* = 7.7 Hz, 2H, indole H4), 7.99 (s, 1H, phenylene H2). ¹³C-NMR (75 MHz, DMSO-*d*₆): δ 28.07, 30.59, 55.67, 77.94, 109.85, 111.15, 114.34, 118.07, 118.54, 120.76, 123.71, 127.15, 131.24, 135.89, 139.16, 155.19, 171.11. HRMS (FAB⁺): calcd for (C₃₈H₄₄N₆O₆Na) 703.3220, found 703.3224.

(2S,2'S)-1,1'-(1,3-phenylenebis(azanediyl))bis(3-(1H-indol-3-yl)-1-oxopropan-2-aminium) chloride (7) was prepared according to general procedure B using **7a** (313 mg, 0.46 mmol). White powder (0.24 g, 94% yield), mp 223 °C (dec.). ¹H-NMR (300 MHz, CD₃OD): δ 3.33-3.53 (ABX, 4H, 2CH₂β), 4.26 (ABX, 2H, 2CHα), 7.01 (t, *J* = 7.4 Hz, 2H, indole H5), 7.12 (t, *J* = 7.0 Hz, 2H, indole H6), 7.22 (s, 2H, indole H2), 7.26 (m, 2H, phenylene H4), 7.27 (m, 1H, phenylene H5), 7.38 (d, *J* = 8.1 Hz, 2H, indole H7), 7.67 (d, *J* = 7.9 Hz, 2H, indole H4), 7.93 (s, 2H, phenylene H2). ¹³C-NMR (75 MHz, CD₃OD): δ 29.01, 55.68, 107.84, 112.61, 113.28, 117.54, 119.29, 120.35, 122.93, 125.73, 128.35, 130.32, 138.32, 139.60, 168.52. HRMS (FAB⁺): calcd for (C₂₈H₂₉N₆O₂⁺) 481.2347, found 481.2356.

((2S,2'S)-(1,3-phenylenebis(azanediy))bis(4-methyl-1-oxopentane-2,1-diyl))dicarbamate (8a) was prepared according to general procedure A using 1,3-phenylenediamine (0.150 mg, 1.39 mmol) and Boc-L-Leu-OH. White powder (0.66 g, 89% yield). ¹H-NMR (300 MHz, CDCl₃): δ 0.94 (dd, *J* = 6.9, 6.7 Hz, 12H, CH(CH₃)₂), 1.47 (s, 18H, (CH₃)₃), 1.55-1.85 (m, 6H, βCH₂, γCH), 4.48 (m, 2H, αCH), 5.73 (m, 2H, Boc-NH), 6.85 (m, 1H, phenyl H5), 7.04 (m, 2H, phenyl H4, H6), 7.74 (s, 1H, phenyl H2), 9.30 (s, 2H, PhNHCO-). ¹³C-NMR (75 MHz, CDCl₃): δ 21.42, 23.07, 24.61, 28.34, 41.15, 53.80, 80.02, 111.34, 115.03, 128.52, 156.42, 171.73.

(2S,2'S)-1,1'-(1,3-phenylenebis(azanediy))bis(4-methyl-1-oxopentan-2-aminium) chloride (8) was prepared according to general procedure B using **8a** (500 mg, 0.935 mmol). White powder (0.35 g, 91% yield). ¹H-NMR (300 MHz, CD₃OD): δ 1.04 (d, *J* = 5.8 Hz, 12H, CH(CH₃)₂), 1.71-1.85 (m, 6H, βCH₂, γCH), 4.06 (t, *J* = 7.0 Hz, 2H, αCH), 7.29-7.34 (m, 1H, phenyl H5), 7.39-7.42 (m, 2H, phenyl H4, H6), 8.08 (t, *J* = 1.9 Hz, 1H, phenyl H2). ¹³C-NMR (75 MHz, CD₃OD): δ 22.14, 23.28, 25.57, 41.77, 53.76, 113.11, 117.49, 130.49, 138.32, 139.73, 169.15.

Di-tert-butyl ((2S,2'S)-(1,3-phenylenebis(azanediy))bis(1-oxo-3-phenylpropane-2,1-diyl))dicarbamate (9a) was prepared according to general procedure A using 1,3-phenylenediamine (0.150 mg, 1.39 mmol) and Boc-L-Phe-OH. White powder (0.80 g, 96% yield). ¹H-NMR (300 MHz, CDCl₃): δ 1.37 (s, 18H, (CH₃)₃), 2.90-3.20 (m, 4H, βCH₂), 4.73 (m, 2H, αCH), 5.74 (br, 2H, Boc-NH), 6.92 (m, 1H, phenyl H5), 7.04 (m, 2H, phenyl H4, H6), 7.20 (m, 10H, C₆H₅), 7.61 (s, 1H, phenyl H2), 8.98 (br, 2H, PhNHCO-). ¹³C-NMR (75 MHz, CDCl₃): δ 28.22, 38.57, 56.41, 80.14, 111.73, 115.63, 126.63, 128.39, 128.77, 129.17, 136.62, 137.90, 156.14, 170.43.

(2S,2'S)-1,1'-(1,3-phenylenebis(azanediy))bis(1-oxo-3-phenylpropan-2-aminium) chloride (9) was prepared according to general procedure B using **9a** (550 mg, 0.913 mmol). White powder (0.40 g, 93% yield). ¹H-NMR (300 MHz, CD₃OD): δ 3.14-3.34 (m, 4H, βCH₂), 4.26 (t, *J* = 7.3 Hz, 2H, αCH), 7.26-7.35 (m, 13H, phenyl H4-6, C₆H₅), 7.90 (t, *J* = 1.7 Hz, 1H, phenyl H2). ¹³C-NMR (75 MHz, CD₃OD): δ 38.76, 56.41, 113.14, 117.53, 128.88, 130.11, 130.33, 130.64, 135.53, 139.42, 167.93.

Di-tert-butyl ((2S,2'S)-(1,3-phenylenebis(azanediy))bis(3-(4-benzyloxy)phenyl)-1-oxopropane-2,1-diyl))dicarbamate (10a) was prepared according to general procedure A using 1,3-phenylenediamine (0.150 mg, 1.39 mmol) and Boc-L-Tyr-(OBn)-OH. White powder (1.10 g, 97% yield). ¹H-NMR (300 MHz, CDCl₃): δ 1.38 (s, 18H, (CH₃)₃), 2.83-3.17 (m, 4H, βCH₂), 4.70 (m, 2H, αCH), 4.94

(s, 4H, CH₂Ph), 5.74 (br, 2H, Boc-NH), 6.84 (d, *J* = 8.4 Hz, 4H, phenolic H₂, H₆), 6.91 (m, 1H, phenyl H₅), 7.04 (m, 2H, phenyl H₄, H₆), 7.12 (d, *J* = 8.4 Hz, 4H, phenolic H₃, H₅), 7.20-7.37 (m, 10H, C₆H₅), 7.67 (s, 1H, phenyl H₂), 9.06 (br, 2H, PhNHCO-). ¹³C-NMR (75 MHz, CDCl₃): δ 28.22, 37.69, 56.47, 69.72, 80.12, 111.61, 114.69, 115.52, 127.29, 127.72, 128.36, 128.76, 128.84, 130.20, 136.85, 137.93, 156.18, 157.53, 170.51.

Di-tert-butyl ((2*S*,2'*S*)-(1,3-phenylenebis(azanediyl))bis(3-(4-hydroxyphenyl)-1-oxopropane-2,1-diyl))dicarbamate (10b) was prepared according to general procedure F using **10a** (1.00 g, 1.23 mmol). White solid (0.77 g, 99% yield). ¹H-NMR (300 MHz, 2:1 CD₃OD/CDCl₃): δ 1.39 (s, 18H, (CH₃)₃), 2.82-3.11 (m, 4H, βCH₂), 4.43 (m, 2H, αCH), 6.75 (d, *J* = 6.4 Hz, 4H, phenolic H₂, H₆), 7.05 (d, *J* = 6.5 Hz, 4H, phenolic H₃, H₅), 7.14-7.35 (m, 3H, phenyl H₄-H₆), 7.69 (s, 1H, phenyl H₂), 9.64 (br, 2H, PhNHCO-). ¹³C-NMR (75 MHz, CDCl₃): δ 28.68, 38.71, 57.66, 80.64, 113.29, 116.05, 117.30, 128.37, 129.77, 131.11, 139.07, 156.59, 157.03, 172.31.

((2*S*,2'*S*)-1,1'-(1,3-phenylenebis(azanediyl))bis(3-(4-hydroxyphenyl)-1-oxopropan-2-aminium) chloride (10) was prepared according to general procedure B using **10b** (770 mg, 1.21 mmol). Off-white solid (0.61 g, 99% yield). ¹H-NMR (300 MHz, CD₃OD): δ 3.15-3.34 (m, 4H, βCH₂), 3.70 (s, 2H, ArOH), 4.39 (m, 2H, αCH), 6.76 (m, 4H, phenolic H₂, H₆), 7.09-7.33 (m, 7H, phenyl H₄-6, phenolic H₃, H₅), 8.09 (s, 1H, phenyl H₂), 8.39 (br, 2H, PhNHCO-). ¹³C-NMR (75 MHz, CD₃OD): δ 37.90, 56.78, 113.56, 116.93, 117.79, 126.13, 130.41, 132.04, 139.34, 158.03, 168.36.

Di-tert-butyl ((1,2-phenylenebis(azanediyl))bis(2-oxoethane-2,1-diyl))dicarbamate (11a) was prepared according to general procedure A using 1,2-phenylenediamine (0.100 mg, 0.92 mmol) and Boc-Gly-OH. White powder (0.30 g, 77% yield). ¹H-NMR (300 MHz, CDCl₃): δ 1.43 (s, 18H, (CH₃)₃), 3.82 (s, 4H, αCH₂), 5.87 (s, 2H, Boc-NH), 7.07 (m, 2H, phenyl H₄, H₅), 7.28 (m, 2H, phenyl H₃, H₆), 8.73 (s, 2H, PhNHCO-). ¹³C-NMR (75 MHz, CDCl₃): δ 28.37, 44.50, 80.23, 125.51, 126.49, 130.31, 156.44, 169.41.

2,2'-(1,2-phenylenebis(azanediyl))bis(2-oxoethanaminium) 2,2,2-trifluoroacetate (11) was prepared according to general procedure C using **11a** (260 mg, 0.62 mmol). White powder (0.27 g, 99% yield), mp 163-166 °C. ¹H-NMR (300 MHz, DMSO-*d*₆): δ 3.36 (s, 4H, αCH₂), 7.24 (dd, *J* = 6.0, 3.6, 2H, phenyl H₄, H₅), 7.61 (dd, *J* = 5.8, 3.6, 2H, phenyl H₃, H₆), 8.23 (br, 6H, NH₃⁺), 9.87 (br, 2H, PhNHCO-). ¹³C-NMR (75 MHz, DMSO-*d*₆): δ 40.03, 114.90, 124.75, 125.53, 129.69, 158.69, 165.29.

2,2'-(1,3-phenylenebis(azanediyl))bis(2-oxoethanaminium) trifluoroacetate (12) was prepared according to general procedure C using **1a**. The product was spectroscopically identical to **1**.

Di-tert-butyl ((1,4-phenylenebis(azanediyl))bis(2-oxoethane-2,1-diyl))dicarbamate (13a) was prepared according to general procedure A using 1,4-phenylenediamine (0.150 g, 1.39 mmol) and Boc-Gly-OH. White powder (0.27 g, 46% yield). ¹H-NMR (300 MHz, DMSO-*d*₆): δ 1.42 (s, 18H, (CH₃)₃), 3.73 (d, *J* = 6.0 Hz, 4H, αCH₂), 7.07 (t, *J* = 5.9 Hz, 2H, Boc-NH), 7.54 (s, 4H, phenyl H2-3, H4-5), 10.02 (s, 2H, PhNHCO-). ¹³C-NMR (75 MHz, DMSO-*d*₆): δ 28.23, 43.71, 78.01, 119.42, 134.39, 156.51, 167.93.

2,2'-(1,4-phenylenebis(azanediyl))bis(2-oxoethanaminium) 2,2,2-trifluoroacetate (13) was prepared according to general procedure C using **13a** (210 mg, 0.50 mmol). White powder (0.11 g, 51% yield) mp 234 °C (dec.). ¹H-NMR (300 MHz, DMSO-*d*₆): δ 3.78 (s, 4H, αCH₂), 7.59 (s, 4H, phenyl H3-6), 8.23 (br, 6H, NH₃⁺), 10.67 (br, 2H, PhNHCO-). ¹³C-NMR (75 MHz, DMSO-*d*₆): δ 40.87, 119.69, 134.15, 160.90, 164.51.

Di-tert-butyl ((2S,2'S)-(1,2-phenylenebis(azanediyl))bis(3-(1H-indol-3-yl)-1-oxopropane-2,1-diyl))dicarbamate (14a) was prepared according to general procedure A using 1,2-phenylenediamine (150 mg, 1.39 mmol) and Boc-L-Trp-OH. White powder (0.76 g, 80% yield), mp 129 °C (dec.). Two hydrogen bonded conformations were observed spectroscopically, peaks for the major conformer are reported herein. ¹H-NMR (300 MHz, CDCl₃): δ 1.50 (s, 9H, (CH₃)₃), 3.05-3.33 (ABX, 2H, βCH₂), 4.21 (ABX, 1H, αCH), 5.40 (d, *J* = 7.3 Hz, 1H, Boc-NH), 6.55-7.62 (m, 7H, ArH, ArNH), 8.98 (s, 1H, indole NH). ¹³C-NMR (75 MHz, CDCl₃): δ 28.48, 28.84, 56.01, 80.53, 110.14, 111.55, 118.99, 119.65, 122.19, 123.45, 124.68, 126.10, 127.37, 129.33, 136.16, 155.71, 171.35. HRMS (FAB⁺): calcd for (C₃₈H₄₄N₆O₆Na) 703.3220, found 703.3218.

(2S,2'S)-1,1'-(1,2-phenylenebis(azanediyl))bis(3-(1H-indol-3-yl)-1-oxopropan-2-aminium) chloride (14) was prepared according to the general procedure B using **5a** (600 mg, 0.88 mmol). White powder (0.21 g, 43% yield), mp 201 °C (dec.). Two hydrogen bonded conformations were observed spectroscopically, peaks for the major conformer are reported herein. ¹H-NMR (300 MHz, CD₃OD): δ 3.35-3.65 (ABX, 2H, βCH₂), 4.58 (t, *J* = 6.9 Hz, 1H, αCH), 7.00-7.73 (m, 7H, ArH, ArNH). ¹³C-NMR (75 MHz, CD₃OD): δ 28.79, 55.74, 107.93, 112.56,

119.58, 120.36, 122.92, 125.81, 126.35, 127.36, 128.48, 130.99, 138.27, 169.44.
HRMS (FAB⁺): calcd for (C₂₈H₂₉N₆O₂⁺) 481.2347, found 481.2359.

Di-tert-butyl ((2S,2'S)-(1,4-phenylenebis(azanediy))bis(3-(1H-indol-3-yl)-1-oxopropane-2,1-diyl))dicarbamate (15a) was prepared according to general procedure A using 1,4-phenylenediamine (150 mg, 1.39 mmol) and Boc-L-Trp-OH. White powder (0.84 g, 89% yield), mp 167 °C (dec.). ¹H-NMR (300 MHz, CD₃OD): δ 1.41 (s, 9H, (CH₃)₃), 3.19-3.36 (ABX, 2H, βCH₂), 4.47 (ABX, 1H, αCH), 6.98-7.12 (m, 3H, indole H5, indole H6, indole H2), 7.27-7.42 (m, 3H, indole H7, phenylene CH), 7.61 (d, *J* = 7.7 Hz, 1H, indole H4), 7.78 (s, 1H, indole NH). ¹³C-NMR (75 MHz, CD₃OD): δ 28.50, 29.26, 56.66, 80.52, 110.06, 111.90, 118.97, 119.50, 121.52, 122.07, 124.15, 128.14, 134.88, 137.26, 156.85, 172.14. HRMS (FAB⁺): calcd for (C₃₈H₄₄N₆O₆Na) 703.3220, found 703.3210.

(2S,2'S)-1,1'-(1,4-phenylenebis(azanediy))bis(3-(1H-indol-3-yl)-1-oxopropan-2-aminium) chloride (15) was prepared according to general procedure B using **15a** (475 mg, 0.70 mmol). White powder (0.36 g, 93% yield), mp 237 °C (dec.). ¹H-NMR (300 MHz, CD₃OD): δ 3.34-3.54 (ABX, 2H, βCH₂), 4.27 (ABX, 1H, αCH), 6.97-7.14 (m, 2 H, indole H5, indole H6), 7.24 (s, 1H, indole H7), 7.38 (d, *J* = 8.1 Hz, 1H, indole H7), 7.67 (d, *J* = 7.9 Hz, 1H, indole H4). ¹³C-NMR (75 MHz, CDCl₃): δ 28.93, 55.69, 107.90, 112.57, 119.33, 120.29, 121.88, 122.87, 125.72, 128.38, 135.61, 138.26, 168.33. HRMS (FAB⁺): calcd for (C₂₈H₂₈N₆O₂Na) 503.2171, found 503.2166.

Di-tert-butyl ((2R,2'R)-(1,3-phenylenebis(azanediy))bis(3-(1H-indol-3-yl)-1-oxopropane-2,1-diyl))dicarbamate (16a) was prepared according to general procedure A using 1,3-phenylenediamine (200 mg, 1.85 mmol) and Boc-D-Trp-OH. White powder (1.05 g, 84% yield), mp 141 °C (dec.). ¹H-NMR (300 MHz, CDCl₃): δ 1.38 (s, 18H, 2(CH₃)₃) 3.10-3.45 (ABX, 4H, 2CH₂β), 4.62 (ABX, 2H, 2CHα), 6.90-7.23 (m, 6H, indole H5, indole H6, ArNH), 7.29-7.40 (m, 7H, indole H2, phenylene H4), phenylene H5, indole H7), 7.66 (d, *J* = 7.0 Hz, 2H, indole H4), 8.21 (s, 1H, phenylene H2). ¹³C-NMR (75 MHz, CDCl₃): δ 28.35, 28.98, 56.04, 80.49, 109.66, 111.63, 112.74, 116.83, 118.67, 119.35, 121.90, 123.79, 127.64, 129.34, 136.64, 138.14, 156.25, 171.58. HRMS (FAB⁺): calcd for (C₃₈H₄₄N₆O₆Na) 703.3220, found 703.3219.

(2R,2'R)-1,1'-(1,3-phenylenebis(azanediy))bis(3-(1H-indol-3-yl)-1-oxopropan-2-aminium) chloride (16) was prepared according to general procedure B using **16a** (440 mg, 0.65 mmol). Off-white powder (0.23 g, 64% yield), mp 242 °C (dec.). ¹H-NMR (300 MHz, CD₃OD): δ 3.33-3.53 (ABX, 4H, 2CH₂β), 3.65 (s, 6H, 2NH₃), 4.26 (ABX, 2H, 2CHα), 7.01 (t, *J* = 7.4 Hz, 2H, indole H5), 7.12 (t, *J* = 7.0 Hz,

2H, indole H6), 7.22 (s, 2H, indole H2), 7.26 (m, 2H, phenylene H4), 7.27 (m, 1H, phenylene H5), 7.38 (d, $J = 8.1$ Hz, 2H, indole H7), 7.67 (d, $J = 7.9$ Hz, 2H, indole H4), 7.93 (s, 2H, phenylene H2). $^{13}\text{C-NMR}$ (75 MHz, CD_3OD): δ 28.96, 55.67, 107.84, 112.58, 113.31, 117.55, 119.33, 120.32, 122.89, 125.76, 128.37, 130.28, 138.27, 139.56, 168.52. HRMS (FAB⁺): calcd for ($\text{C}_{28}\text{H}_{29}\text{N}_6\text{O}_2^+$) 481.2347, found 481.2350.

(S)-tert-butyl (3-(1H-indol-3-yl)-1-oxo-1-(phenylamino)propan-2-yl)carbamate (17a) was prepared according to general procedure A using aniline (200 mg, 2.15 mmol) and Boc-L-Trp-OH. White powder (0.65 g, 80% yield). Compound previously reported⁴⁹ and matched spectroscopically where available.

(S)-3-(1H-indol-3-yl)-1-oxo-1-(phenylamino)propan-2-aminium chloride (17) was prepared according to general procedure B using **17a** (350 mg, 0.92 mmol). White powder (0.17 g, 57% yield). Compound previously reported⁵⁰ and matched spectroscopically where available.

N,N'-(1,3-phenylene)bis(3-(1H-indol-3-yl)propanamide) (18) was prepared according to general procedure A using 1,3-phenylenediamine (70 mg, 0.65 mmol) and indole-3-propionic acid. White powder (0.23 g, 78% yield), mp 154-156 °C. $^1\text{H-NMR}$ (300 MHz, CD_3OD): δ 2.76 (t, $J = 7.6$ Hz, 4H, $2\text{COCH}_2\text{CH}_2\text{-indole}$), 3.18 (t, 7.6 Hz, 4H, $2\text{COCH}_2\text{CH}_2\text{-indole}$), 7.04-7.39 (m, 9H, indole H5, indole H6, indole H2, phenylene H4, phenylene H6), 7.37 (d, $J = 7.9$ Hz, 2H, indole H7), 7.60-7.66 (m, 3H, indole H4, phenylene H5). $^{13}\text{C-NMR}$ (75 MHz, CD_3OD): δ 21.81, 38.37, 111.71, 114.33, 116.43, 117.53, 118.72, 119.06, 121.83, 122.40, 127.52, 137.04, 139.11, 173.38. HRMS (FAB⁺): calcd for ($\text{C}_{28}\text{H}_{26}\text{N}_4\text{O}_2\text{Na}$) 473.1954, found 473.1945.

Di-tert-butyl ((2S,2'S)-(propane-1,3-diylbis(azanediy))bis(3-(1H-indol-3-yl)-1-oxopropane-2,1-diyl)dicarbamate (19a) was prepared according to general procedure A using 1,3-diaminopropane dihydrochloride (200 mg, 1.36 mmol) and Boc-L-Trp-OH. White powder (0.51 g, 58% yield). Compound previously reported⁵¹ and matched spectroscopically where available.

(2S,2'S)-1,1'-(propane-1,3-diylbis(azanediy))bis(3-(1H-indol-3-yl)-1-oxopropan-2-aminium) chloride (19) was prepared according to general procedure B using **19a** (380 mg, 0.59 mmol). White powder (0.30 g, 98% yield), mp 234°C (dec.). $^1\text{H-NMR}$ (300 MHz, CD_3OD): δ 1.40 (m, 2H, $-\text{CH}_2\text{CH}_2\text{NH}-$), 2.98 (m, 4H, $-\text{CH}_2\text{CH}_2\text{NH}-$), 3.22-3.65 (m, 4H, $\text{CH}_2\beta$), 4.13 (ABX, 2H, $\text{CH}\alpha$), 6.99-7.18 (m, 4H, indole H5, indole H6), 7.25 (s, 2H, indole H2), 7.39 (d, $J = 6.4$ Hz, 2H, indole H7), 7.69 (d, $J = 4.7$ Hz, 2H, indole H4), 8.30 (br, CONH). $^{13}\text{C-NMR}$ (75 MHz, CD_3OD): δ 28.78, 29.39,

37.76, 55.27, 108.03, 112.62, 119.34, 120.22, 122.80, 125.71, 128.29, 138.02, 170.05. HRMS (FAB⁺): calcd for (C₂₅H₃₁N₆O₂⁺) 447.2503, found 447.2503.

Di-tert-butyl ((2S,2'S)-(butane-1,4-diylbis(azanediyl))bis(3-(1H-indol-3-yl)-1-oxopropane-2,1-diyl))dicarbamate (20a) was prepared according to general procedure A using 1,4-diaminobutane dihydrochloride (210 mg, 1.30 mmol) and Boc-L-Trp-OH. White powder (0.79 g, 92% yield). Compound previously reported⁵¹ and matched spectroscopically where available.

(S)-1-((4-((R)-2-ammonio-3-(1H-indol-3-yl)propanamido)butyl)amino)-3-(1H-indol-3-yl)-1-oxopropan-2-aminium chloride (20) was prepared according to general procedure B using **20a** (650 mg, 0.98 mmol). White powder (0.51 g, 97% yield), mp 204 °C (dec.). ¹H-NMR (300 MHz, CD₃OD): δ 1.18 (m, 2H, -CH₂CH₂NH-), 3.05 (m, 2H, -CH₂CH₂NH-), 3.22-3.41 (ABX, 2H, CH₂β), 4.09 (ABX, 1H, CHα), 7.05-7.17 (m, 2H, indole H5, indole H6), 7.23 (s, 2H, indole H2), 7.40 (d, *J* = 7.9 Hz, 1H, indole H7), 7.66 (d, *J* = 7.9 Hz, 2H, indole H4), 8.25 (br, 1H, CONH). ¹³C-NMR (75 MHz, CD₃OD): δ 27.24, 29.06, 40.28, 55.40, 68.27, 108.29, 112.73, 119.38, 120.37, 123.00, 125.68, 128.51, 138.34, 170.13. HRMS (FAB⁺): calcd for (C₂₆H₃₃N₆O₂⁺) 461.2660, found 461.2668.

Di-tert-butyl ((2S,2'S)-(hexane-1,6-diylbis(azanediyl))bis(3-(1H-indol-3-yl)-1-oxopropane-2,1-diyl))dicarbamate (21a) was prepared according to general procedure A using 1,6-diaminohexane dihydrochloride (250 mg, 1.32 mmol) and Boc-L-Trp-OH. White powder (0.90 g, 99% yield). Compound previously reported⁵¹ and matched spectroscopically where available.

(2S,2'S)-1,1'-(hexane-1,6-diylbis(azanediyl))bis(3-(1H-indol-3-yl)-1-oxopropan-2-aminium) chloride (21) was prepared according to general procedure B using **21a** (650 mg, 0.94 mmol). White powder (0.33 g, 62% yield), mp 193 °C (dec.). ¹H-NMR (300 MHz, CD₃OD): δ 1.05 (m, 2H, aliphatic CH₂), 1.26 (m, 2H, aliphatic CH₂) 2.97-3.39 (m, 4H, -CH₂CH₂NH-, CH₂β), 4.06 (ABX, 2H, CHα), 7.02-7.15 (m, 2H, indole H5, indole H6), 7.20 (s, 1H, indole H2), 7.37 (d, *J* = 8.1 Hz, 1H, indole H7), 7.63 (d, *J* = 7.5 Hz, 2H, indole H4), 8.19 (br, CONH). ¹³C-NMR (75 MHz, CD₃OD): δ 27.38, 28.98, 29.85, 40.61, 55.29, 108.19, 112.64, 119.22, 120.27, 122.91, 125.52, 128.40, 138.26, 169.95. HRMS (FAB⁺): calcd for (C₂₈H₃₇N₆O₂⁺) 489.2973, found 489.2972.

Di-tert-butyl ((2R,2'S)-(dodecane-1,12-diylbis(azanediyl))bis(3-(1H-indol-3-yl)-1-oxopropane-2,1-diyl))dicarbamate (22a) was prepared according to general procedure A using 1,12-diaminododecane (250 mg, 1.25 mmol) and Boc-L-

Trp-OH. Off-white powder (0.93 g, 96% yield), mp 86 °C (dec.). ¹H-NMR (300 MHz, CDCl₃): δ 1.08-1.34 (m, 22H, aliphatic CH₂), 1.41 (s, 18H, C(CH₃)₃), 2.99-3.32 (m, 8H, -CH₂CH₂NH-, CH₂β), 4.42 (ABX, 2H, CHα), 5.36 (br, 2H, Boc-NH), 6.03 (br, 2H, CONH), 6.95 (s, 2H, indole H2) 7.03-7.16 (m, 4H, indole H5, indole H6), 7.32 (d, *J* = 7.9 Hz, 2H, indole H7), 7.60 (d, *J* = 7.7 Hz, 2H, indole H4). ¹³C-NMR (75 MHz, CDCl₃): δ 26.52, 28.16, 28.54, 28.99, 29.22, 29.28, 31.43, 39.38, 55.22, 65.72, 79.83, 110.12, 111.23, 118.60, 119.27, 121.81, 123.22, 127.26, 136.19, 155.44, 171.68. HRMS (FAB⁺): calcd for (C₄₄H₆₄N₆O₆Na) 785.4785, found 785.4792.

(S)-1-((12-((R)-2-ammonio-3-(1H-indol-3-yl)propanamido)dodecyl)amino)-3-(1H-indol-3-yl)-1-oxopropan-2-aminium chloride (22) was prepared according to general procedure B using **22a** (715 mg, 0.92 mmol). White powder (0.56 g, 93% yield), mp 158 °C (dec.). ¹H-NMR (300 MHz, CD₃OD): δ 1.08-1.34 (m, 22H, aliphatic CH₂), 2.99-3.38 (m, 8H, -CH₂CH₂NH-, CH₂β), 4.04 (ABX, 2H, CHα), 7.02-7.15 (m, 4H, indole H5, indole H6), 7.20 (s, 2H, indole H2), 7.37 (d, *J* = 7.9 Hz, 2H, indole H7), 7.62 (d, *J* = 7.9 Hz, 2H, indole H4). ¹³C-NMR (75 MHz, CD₃OD): δ 27.92, 28.98, 30.01, 30.43, 30.69, 30.77, 40.77, 55.29, 108.18, 112.62, 119.20, 120.24, 122.88, 125.51, 128.40, 138.25, 169.90. HRMS (FAB⁺): calcd for (C₃₄H₄₉N₆O₂⁺) 573.3912, found 573.3929.

(S)-1-((4-((R)-2-ammonio-3-(1H-indol-3-yl)propanamido)butyl)amino)-3-(1H-indol-3-yl)-1-oxopropan-2-aminium trifluoroacetate (23) was prepared according to general procedure C using **20a**. The product was spectroscopically identical to **20**.

1,4-bis(N_α-Boc-N_ε-Cbz-L-lysylamido)butane (24a) was prepared according to general procedure A using 1,4-diaminobutane dihydrochloride (200 mg, 1.24 mmol) and N_α-Boc-N_ε-Cbz-L-Lys-OH. Off-white solid (0.95 g, 94% yield). ¹H-NMR (300 MHz, CDCl₃): δ 1.28-1.71 (m, 34H, (CH₃)₃, βCH₂, γCH₂, δCH₂, linker CH₂CH₂NHCO), 3.04-3.29 (m, 4H, εCH₂, linker CH₂NHCO), 4.17 (m, 2H, αCH₂), 5.06 (s, 4H, CH₂Ph), 5.57 (br, 2H Cbz-NH), 5.82 (br, 2H, Boc-NH), 7.30 (m, 12H, Cbz-ArH, linker CH₂NHCO). ¹³C-NMR (75 MHz, CDCl₃): δ 22.38, 26.02, 28.04, 28.99, 32.17, 38.62, 40.30, 54.04, 66.09, 79.33, 127.66, 128.10, 136.38, 155.77, 156.33, 172.58.

1,4-bis(lysylamido)butane tetrakis(trifluoroacetate) (24) was prepared in a two-step procedure. The Cbz-deprotected compound **24b** was prepared according to general procedure D from **24a** (840 mg, 1.03 mmol). White solid (0.52 g, 93% yield). Compound **24** was prepared according to general procedure C from **24b** (0.22 g, 0.40 mmol). Off-white glassy solid (0.16 g, 50% yield). ¹H-NMR (300 MHz, CD₃OD): δ 1.44-1.69 (m, 8H, γCH₂, linker CH₂CH₂NHCO), 1.81 (m, 4H, δCH₂), 1.97 (m,

4H, β CH₂), 3.04 (m, 4H, linker CH₂NHCO), 3.33 (m, 4H, ϵ CH₂), 4.02 (m, 2H, α CH₂), 8.01(br, 6H, ϵ NH₃⁺), 8.41 (br, 6H, α NH₃⁺), 8.64 (br, 2H, linker CH₂NHCO). ¹³C-NMR (75 MHz, CD₃OD): δ 22.98, 27.45, 27.89, 32.02, 40.19, 40.46, 54.22, 169.92.

4.4.2. Agarose Gel Electrophoresis.

Agarose powder was obtained from Sigma Aldrich. Purified water with 18.2 M Ω resistivity (Milli-Q) was used in all cases. Gels were cast by heating a 0.5% w/v solution of agarose in 40 mM tris-acetate buffer (pH 7.2) until fully dissolved, then cast by cooling the solution to room temperature in an Owl B2 horizontal electrophoresis chamber with a centrally placed 20-well comb. The gel was submerged under 40 mM tris-acetate (pH 7.2) running buffer, samples were added to the wells, and the gel was run 90 minutes at 105 \pm 3 volts. Gels were stained in 2.5 μ g/mL ethidium bromide for 15 minutes at 37 $^{\circ}$ C, 50 rpm, and destained in Milli-Q water for 5 minutes at 37 $^{\circ}$ C, 50 rpm. Ethidium bromide-stained DNA was visualized using a UV trans-illuminator.

Gel images were analyzed by densitometry using ImageJ software.²⁴ Lane profile plots were generated and integrated (data not shown). Using manual baselines, the control plasmid was set as 100% DNA migration. The inverse of the DNA migration in experimental wells relative to control DNA migration gave a measure of percent DNA retention. Results presented are the average of three gels.

4.4.3. Electron Microscopy.

Transmission Electron Microscopy. A 10 μ L sample was applied to lacey formvar/carbon 300 mesh copper TEM grids (Ted Pella, Inc.) for 60 seconds and the grid was washed with 18.2 M Ω H₂O (30 s), stained with 2 % uranyl acetate (30 s), and washed twice with H₂O (15 s each). The above solutions were applied at a volume of 10 μ L, wicked away between each application, and the grid was finally dried with a gentle N₂ stream. Specimens were examined on a JEOL JEM-2000 FX transmission electron microscope operated at 300 keV.

Scanning Electron Microscopy. The copper grids treated with samples for TEM were sputter-coated with elemental gold and imaged on a JEOL JSM-6320F field emission scanning electron microscope.

4.4.4. Circular Dichroism.

Samples were prepared according to agarose gel mixing procedures (Section 4.4.2) with the substitution of water for DMSO. Samples were placed in a 1 mm path length microsampling disc and examined on a JASCO 1500 circular dichroism spectropolarimeter.

4.5. References.

- 1 (a) Kavallieratos, K.; de Gala, S. R.; Austin, D. J.; Crabtree, R. H., Readily Available Non-preorganized Neutral Acyclic Halide Receptor with an Unusual Nonplanar Binding Conformation. *J. Am. Chem. Soc.* **1997**, *119*, 2325-2326. (b) Kavallieratos, K.; Bertao, C. M.; Crabtree, R. H., Hydrogen Bonding in Anion Recognition: A Family of Versatile, Nonpreorganized Neutral and Acyclic Receptors. *J. Org. Chem.* **1999**, *64*, 1675-1683.
- 2 (a) Kubik, S., Amino acid containing anion receptors. *Chem. Soc. Rev.* **2009**, *38*, 585-605. (b) Steed, J. W., Coordination and organometallic compounds as anion receptors and sensors. *Chem. Soc. Rev.* **2009**, *38*, 506-519. (c) Ballester, P., Anion binding in covalent and self-assembled molecular capsules. *Chem. Soc. Rev.* **2010**, *39*, 3810-3830. (d) Brotherhood, P. R.; Davis, A. P., Steroid-based anion receptors and transporters. *Chem. Soc. Rev.* **2010**, *39*, 3633-47. (e) Galbraith, E.; James, T. D., Boron based anion receptors as sensors. *Chem. Soc. Rev.* **2010**, *39*, 3831-3842. (f) Gross, D. E.; Yoon, D. W.; Lynch, V. M.; Lee, C. H.; Sessler, J. L., Anion binding behavior of heterocycle-strapped calix[4]pyrroles. *J. Incl. Phenom. Macrocycl. Chem.* **2010**, *66*, 81-85. (g) Hancock, L. M.; Gilday, L. C.; Carvalho, S.; Costa, P. J.; Felix, V.; Serpell, C. J.; Kilah, N. L.; Beer, P. D., Rotaxanes capable of recognising chloride in aqueous media. *Chemistry* **2010**, *16*, 13082-94. (h) Juwarker, H.; Jeong, K.-S., Anion-controlled foldamers. *Chem. Soc. Rev.* **2010**, *39*, 3664-3674. (i) Li, A.-F.; Wang, J.-H.; Wang, F.; Jiang, Y.-B., Anion complexation and sensing using modified urea and thiourea-based receptors. *Chem. Soc. Rev.* **2010**, *39*, 3729-3745. (j) McConnell, A. J.; Serpell, C. J.; Thompson, A. L.; Allan, D. R.; Beer, P. D., Calix[4]arene-based rotaxane host systems for anion recognition. *Chemistry* **2010**, *16*, 1256-1264. (k) Mercer, D. J.; Loeb, S. J., Metal-based anion receptors: an application of second-sphere coordination. *Chem. Soc. Rev.* **2010**, *39*, 3612-3620. (l) Gale, P. A.; Busschaert, N.; Haynes, C. J.; Karagiannidis, L. E.; Kirby, I. L., Anion receptor chemistry: highlights from 2011 and 2012. *Chem. Soc. Rev.* **2014**, *43*, 205-241.
- 3 Hargrove, A. E.; Nieto, S.; Zhang, T.; Sessler, J. L.; Anslyn, E. V., Artificial receptors for the recognition of phosphorylated molecules. *Chem. Rev.* **2011**, *111*, 6603-6782.
- 4 Sessler, J. L.; Gale, P.; Cho, W.-S., *Anion Receptor Chemistry*. Royal Society of Chemistry: Cambridge, 413 pp., 2006; 413 pp.
- 5 Bowman-James, K.; Bianchi, A.; García-Espana, E., *Anion Coordination Chemistry*. ed.; Wiley VCH: New York, 574 pp.; 2012, 574 pp.
- 6 (a) Schlesinger, P. H.; Ferdani, R.; Liu, J.; Pajewska, J.; Pajewski, R.; Saito, M.; Shabany, H.; Gokel, G. W., SCMTR: a chloride-selective, membrane-anchored peptide channel that exhibits voltage gating. *J. Am. Chem. Soc.* **2002**, *124*, 1848-1849.
- 7 (a) Ferdani, R.; Pajewski, R.; Djedovic, N.; Pajewska, J.; Schlesinger, P. H.; Gokel, G. W., Anion Transport in Liposomes is Altered by Changes in the Anchor Chains and the Fourth Amino Acid of Heptapeptide Ion Channels.

- New J. Chem.* **2005**, *29*, 673-680. (b) Ferdani, R.; Li, R.; Pajewski, R.; Pajewska, J.; Winter, R. K.; Gokel, G. W., Transport of chloride and carboxyfluorescein through phospholipid vesicle membranes by heptapeptide amphiphiles. *Org. Biomol. Chem.* **2007**, *5*, 2423-2432.
- 8 Pajewski, R.; Garcia-Medina, R.; Brody, S. L.; Leevy, W. M.; Schlesinger, P. H.; Gokel, G. W., A synthetic, chloride-selective channel that alters chloride transport in epithelial cells. *Chem. Commun.* **2006**, 329-331.
- 9 Burkhardt, J. B.; Skelton, A. A.; Fried, J. R., The water-channel forming ability of heptapeptide-based anion channels: insights from molecular dynamics simulations. *Soft Matter* **2013**, *9*, 4444-4454.
- 10 Pajewski, R.; Ferdani, R.; Pajewska, J.; Djedovic, N.; Schlesinger, P. H.; Gokel, G. W., Evidence for dimer formation by an amphiphilic heptapeptide that mediates chloride and carboxyfluorescein release from liposomes. *Org. Biomol. Chem.* **2005**, *3*, 619-625.
- 11 Cook, G. A.; Pajewski, R.; Aburi, M.; Smith, P. E.; Prakash, O.; Tomich, J. M.; Gokel, G. W., NMR structure and dynamic studies of an anion-binding, channel-forming heptapeptide. *J. Am. Chem. Soc.* **2006**, *128*, 1633-1638.
- 12 Pajewski, R.; Ferdani, R.; Pajewska, J.; Li, R.; Gokel, G. W., Cation Dependence of Chloride Ion Complexation by Open-Chained Receptor Molecules in Chloroform Solution. *J. Am. Chem. Soc.* **2005**, *126*, 18281-18295.
- 13 Pajewski, R.; Ferdani, R.; Schlesinger, P. H.; Gokel, G. W., Chloride complexation by heptapeptides: influence of C- and N-terminal sidechains and counterion. *Chem. Commun.* **2004**, 160-161.
- 14 Yamnitz, C. R.; Negin, S.; Carasel, I. A.; Winter, R. K.; Gokel, G. W., Dianilides of dipicolinic acid function as synthetic chloride channels. *Chem. Commun.* **2010**, *46*, 2838-2840.
- 15 Carasel, I. A.; Yamnitz, C. R.; Winter, R. K.; Gokel, G. W., Halide ions complex and deprotonate dipicolinamides and isophthalamides: assessment by mass spectrometry and UV-visible spectroscopy. *J. Org. Chem.* **2010**, *75*, 8112-6.
- 16 Matulis, D.; Rouzina, I.; Bloomfield, V. A., Thermodynamics of cationic lipid binding to DNA and DNA condensation: Roles of electrostatics and hydrophobicity. *J. Am. Chem. Soc.* **2002**, *124*, 7331-7342.
- 17 Bennett, C. F.; Swayze, E. E., RNA targeting therapeutics: Molecular mechanisms of antisense oligonucleotides as a therapeutic platform. *Annu. Rev. Pharmacol. Toxicol.* **2010**, *50*, 259-293.
- 18 Perrin, D. D., Dissociation Constants of Organic Bases in Aqueous Solution, Butterworths, London, 1965; Supplement, 1972. 473 pp.
- 19 Fuhrhop, J.-H.; Wang, T., Bolaamphiphiles. *Chem. Rev.* **2004**, *104*, 2901-2937.
- 20 Drew, H.R.; Wing, R.M.; Takano, T.; Broka, C.; Tanaka, S.; Itakura, K.; Dickerson, R.E., Structure of a B-DNA dodecamer: Conformation and dynamics. *Proc. Natl. Acad. USA* **1981**, *78*, 2179-2183.
- 21 Braun, C.S.; Jas, G.S.; Choosakoonkriang, S.; Koe, G.S.; Smith, J.G.; Middaugh, C.R., The Structure of DNA within Cationic Lipid/DNA Complexes. *Biophys J.* **2003**, *84*, 1114-1123.

- 22 Isidro-Llobet, A.; Álvarez, M.; Albericio, F., Amino Acid-Protecting Groups. *Chem. Rev.* **2009**, *109*, 2455-2504.
- 23 Montalbetti, C.A.G.N.; Falque, V., Amide bond formation and peptide coupling. *Tetrahedron* **2005**, *61*, 10827-10852.
- 24 Rasband, W.S. ImageJ 1.47v. U. S. National Institutes of Health, Bethesda, Maryland, USA, (1997-2015) Available at: <http://imagej.nih.gov/ij/> (Accessed: 21st October 2015).
- 25 Landschulz, W. H.; Johnson, P. F.; McKnight, S. L., The leucine zipper: a hypothetical structure common to a new class of DNA binding proteins. *Science* **1988**, *240*, 1759-1764.
- 26 King, J.L.; Jukes, T.H., Non-Darwinian Evolution. *Science* **1969**, *164*, 788-798.
- 27 Philips, D.M. (Ed.), Histones and Nucleohistones 1971 (Plenum Publishing, New York), p. 225.
- 28 Giancotti, V.; Fonda, M.; Crane-Robinson, C., Tyrosine fluorescence of two tryptophan-free proteins: histones H1 and H5. *Biophys. Chem.* **1977**, *6*, 379-383.
- 29 Anton, I. A.; Frampton, J., Tryptophans in *myb* proteins. *Nature* **1988**, *336*, 719.
- 30 Frampton, J.; Leutz, A.; Gibson, T. J.; Graf, T., DNA-binding domain ancestry. *Nature* **1989**, *342*, 134.
- 31 Kanei-Ishii, C.; Sarai, A.; Sawazaki, T.; Nakagoshi, H.; He, D. N.; Ogata, K.; Nishimura, Y.; Ishii, S., The Tryptophan Cluster: A Hypothetical Structure of the DNA-binding Domain of the *myb* Protooncogene Product. *J. Biol. Chem.* **1990**, *265*, 19990-19995.
- 32 Zargarian, L.; Le Tilly, V.; Jamin, N.; Chaffotte, A.; Gabrielsen, O. S.; Toma, F.; Alpert, B., Myb-DNA recognition: role of tryptophan residues and structural changes of the minimal DNA binding domain of c-Myb. *Biochemistry* **1999**, *38*, 1921-1929.
- 33 Saikumar, P.; Murali, R.; Reddy, E. P., Role of tryptophan repeats and flanking amino acids in Myb-DNA interactions. *Proc. Natl. Acad. Sci. USA* **1990**, *87*, 8452-8456.
- 34 Tahirov, T. H.; Sato, K.; Ichikawa-Iwata, E.; Sasaki, M.; Inoue-Bungo, T.; Shiina, M.; Kimura, K.; Takata, S.; Fujikawa, A.; Morii, H.; Kumasaka, T.; Yamamoto, M.; Ishii, S.; Ogata, K., Mechanism of c-Myb-C/EBP beta cooperation from separated sites on a promoter. *Cell* **2002**, *108*, 57-70.
- 35 Huang, J.; Zhao, Y.; Liu, H.; Huang, D.; Cheng, X.; Zhao, W.; Taylor, I. A.; Liu, J.; Peng, Y. L., Substitution of tryptophan 89 with tyrosine switches the DNA binding mode of PC4. *Sci. Rep.* **2015**, *5*, 8789. doi: 10.1038/srep08789.
- 36 Masaki, T.; Norio, H.; Toshihisa, Y., Effect of oligopeptides on gene expression: comparison of DNA/peptide and DNA/peptide/liposome complexes *Int. J. Pharm.* **2004**, *269*, 71-80.
- 37 Baoling, C.; Wen, X.; Ran, P.; Chen, P., Design and characterization of a new peptide vector for short interfering RNA delivery. *J. Nanobiotechnol.* **2015**, *13*, 39.

- 38 Rajeswari, M. R.; Montenay-Garestier, T.; Hélène, C., Does tryptophan intercalate in DNA? A comparative study of peptide binding to alternating and nonalternating A-T sequences. *Biochemistry* **1987**, *26*, 6825-6831.
- 39 Werner, M. H.; Clore, M.; Fisher, C. L.; Fisher, R. J.; Trinh, L.; Shiloach, J.; Gronenborn, A. M., The solution structure of the human ETS1-DNA complex reveals a novel mode of binding and true side chain intercalation. *Cell* **1995**, *83*, 761-771.
- 40 Landolt-Marticorena, C.; Williams, K. A.; Deber, C. M.; Reithmeier, R. A. F., Non-random distribution of amino acids in the transmembrane segments of human type I single span membrane proteins. *J. Mol. Biol.* **1993**, *229*, 602-608.
- 41 Von Heijne, G., Membrane proteins: from sequence to structure. *Annu. Rev. Biophys. Biomol. Struct.* **1994**, *23*, 167-192.
- 42 Yao, W.; Wimley, W. C.; Gawrisch, K.; White, S. H., The Preference of Tryptophan for Membrane Interfaces. *Biochemistry* **1998**, *37*, 14713-14718.
- 43 Hu, J.; Barbour, L. J.; Gokel, G. W., The indole side chain of tryptophan as a versatile pi-donor. *J. Am. Chem. Soc.* **2002**, *124*, 10940-10941.
- 44 Abel, E.; Fedders, M. F.; Gokel, G. W., Vesicle formation from *N*-alkylindoles: implications for tryptophan-water interactions, *J. Am. Chem. Soc.* **1995**, *117*, 1265-1270.
- 45 Abel, E.; De Wall, S. L.; Edwards, W. B.; Lalitha, S.; Covey, D. F.; Gokel, G. W., The formation of stable vesicles from *N*- or 3-alkylindoles: possible evidence for tryptophan as a membrane anchor in proteins. *J. Org. Chem.* **2000**, *65*, 5901-5909.
- 46 Christensen, H. E.; Fairchild, E. J.; Lewis, R. J., Suspected carcinogens: a subfile of the NIOSH Toxic substances list, Vol. 2, 2nd Ed. Eds. National Institute for Occupational Safety and Health: Cincinnati, OH, Dec. 1976, 432 pp.
- 47 Smyth Jr., H. F.; Carpenter, C. P.; Well, C. S.; Pozzani, U. C.; Striegel, J. A., Range-Finding Toxicity Data: List VI. *AIHA J.* **1962**, *23*, 95-107.
- 48 Til, H. P.; Falke, H. E.; Prinsen, M. K.; Willems, M. I., Acute and subacute toxicity of tyramine, spermidine, spermine, putrescine and cadaverine in rats. *Food. Chem. Toxicol.* **1997**, *35*, 337-348.
- 49 Huang, Y.; Liu, Y.; Liu, Y.; Song, H.; Wang, Q., C ring may be dispensable for β -carboline: Design, synthesis, and bioactivities evaluation of tryptophan analog derivatives based on the biosynthesis of β -carboline alkaloids. *Bioorg. Med. Chem.* **2016**, *24*, 462-473.
- 50 Shin, C.; Seki, M.; Kakusho, T.; Takahashi, N., Dehydrooligopeptides. XV. Useful syntheses of dehydrodipeptides by the enzymatic coupling of α -dehydroglutamate with various α -amino acid amides using proteases. *Bull. Chem. Soc. Jpn.* **1993**, *66*, 2048-2053.
- 51 Kumar, R.; Rai, D.; Lown, J. W., Synthesis and In Vitro Cytotoxicity Studies of Novel L-Tryptophan-Polyamide Conjugates and L-Tryptophan Dimers Linked With Aliphatic Chains and Polyamides. *Oncol. Res.* **2003**, *14*, 247-265.

Chapter 5

Reversal of Tetracycline Resistance in *Escherichia coli* by Non-cytotoxic *bis*(Tryptophan)s

5.1. Introduction.

The current interest in anion binding molecules can hardly be overstated. Numerous reviews¹ of the area have appeared including two monographs.² Many of the anion binders derive from early work reported by Crabtree and coworkers³ who showed that arenes having *meta*-dicarboxylic acids, *e.g.* isophthalic acid, could form *bis*(amide)s that readily bound such spherical ions as chloride and bromide. The tris-arene hydrogen bond stabilization system was incorporated into a cryptand-like structure along with a crown ether and the combination functioned as a heteroditopic salt binder.⁴ Multiple hydrogen bonds are available for anion stabilization in cycles such as those known as calixpyrroles.⁵

In previous work, we prepared substituted *bis*(anilide)s of isophthalic and dipicolinic acid.⁶ These compounds were, like many tris-arenes, poorly soluble in water but certain of them formed channels in bilayer membranes.⁷ In other, unrelated work, we found that indole could function as an amphiphilic head group.⁸ Stable liposomes were formed from either 3- or *N*-substituted *n*-decyl- or *n*-octadecylindoles. The “head group” capability of tryptophan's indole is apparent in biology. The Leu-Trp repeats of gramicidin⁹ and the tryptophans present only at the membrane interfaces in the KcsA voltage gated potassium channel¹⁰ support this inference.

Previous work suggested that tryptophan could function effectively as an amphiphilic head group.¹¹ Our recent success with membrane active hydraphiles¹² and lariat ethers¹³ as antimicrobials and as synergists for antimicrobials¹⁴ led us to explore the biological activity of a range of tryptophan derivatives. The antibiotic health crisis¹⁵ encouraged us to survey the activity of the *bis*(tryptophan)s (BTs), which were originally patterned as anion binders. Surprisingly, several of these novel structures inhibit the growth of Gram-negative *Escherichia coli* K-12 and Gram-positive *Staphylococcus aureus*. Even more remarkable is that at sub-lethal concentrations, several BTs recover tetracycline's activity against tetracycline resistant *E. coli* (Tet^R *E. coli*) expressing the tetA efflux pump. Tetracycline activity was recovered by 16-fold. Four of the molecules reported here exhibited no cytotoxicity at the minimal inhibitory concentrations (MICs) against three mammalian epithelial cell lines. A membrane disruption based activity is hypothesized based on increased permeability of Gram-negative Tet^R *E. coli* bacterial cells by one of the BTs.

5.2. Results & Discussion.

Tryptophan occurs in proteins with the lowest frequency of the 20 genetically coded

amino acids.¹⁶ It is hydrophobic, electron rich, and it has an N-H donor residue that can stabilize anions by hydrogen bond interactions. Tryptophan is often found in transmembrane proteins at the bilayer interface.^{17,18} The frequent use of tryptophan and cationic residues in antimicrobial peptides¹⁹ encouraged us to design BTs to assess the minimal structural elements requisite for antibacterial properties.

We screened the BTs for biological activity because we anticipated that at least some of them could be amphiphiles and show membrane activity. We evaluated the antimicrobial function of BTs using Gram positive *Staphylococcus aureus* and two Gram negative *E. coli* strains: K-12 and tetracycline resistant *E. coli*.²⁰ Although the antimicrobial activity observed varied according to compound structure and organism, both potency and selectivity of bacterial membranes over mammalian membranes was documented.

5.2.1. Compounds studied. The compounds that are the focus of this report were prepared from diaminobenzenes or from α,ω -diaminoalkanes. They are shown in Figure 5.1. The amino acid, usually tryptophan, was *N*-Boc protected and the free carboxyl group was coupled with the appropriate diamine by using *N,N,N',N'*-tetramethyl-*O*-(1*H*-benzotriazol-1-yl)uronium hexafluorophosphate (HBTU). Four *meta*-phenylenediamine (*meta*-Ph) derivatives were prepared. They are shown in Figure 5.1 as **1-4**. Compound **1** has glycine side arms while **2** and **3** are *bis*(tryptophan) derivatives. The stereochemistry of the side arms in **2** and **3** varies: **2** = L,L and **3** = D,D. The diamine was acylated with 3-(3-indolyl)propanoic acid (IPA, sold as 3-indolepropionic acid) to form **4**. Compounds **5** and **6** are isomers of **2** but the arene is substituted *ortho* (**5**) or *para* (**6**).

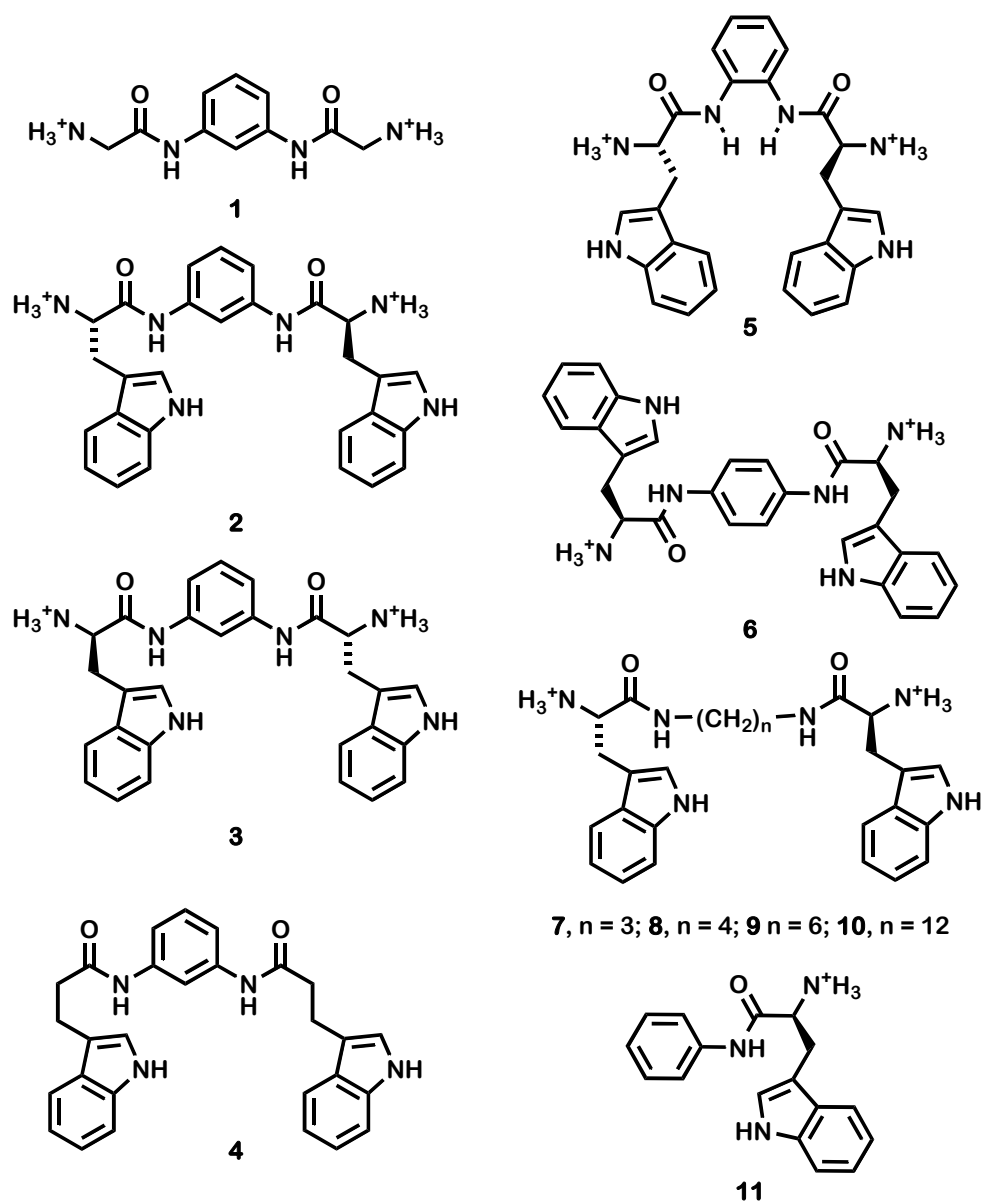


Figure 5.1. Chemical structures of compounds 1-11.

Compounds 7-11 are related to 2 but rather than using a *meta*-phenylenediamine as the spacer or connector chain, alkyl groups link the two L-tryptophans. The alkyl groups are propylene (7, C₃), butylene (8, C₄), hexylene (9, C₆), and dodecylene (10, C₁₂). Compound 11 comprises only a part of 2 and was intended to serve as a control. Note that chloride counter ions were used with all compounds except for the uncharged compound 4.

5.2.2. Bacteria used. Three strains of bacteria were the focus of this report. Two different strains of *E. coli* (Gram negative) were used. The laboratory strain of *E. coli*, K-12 (ATCC 700926), was used for preliminary MIC determinations. The tetracycline

resistant strain of *E. coli* (Tet^R) was prepared by transforming competent JM109 *E. coli* (Promega) with the pBR322 plasmid (Carolina Biologicals). This plasmid contains two resistance genes. The tetA gene expresses the tetracycline resistance TetA efflux pump²¹ and the amp^R gene expresses a β -lactamase enzyme²² that cleaves the four membered ring of penicillin derivatives. The resulting *E. coli*, which we designate Tet^R *E. coli*, is both tetracycline and ampicillin resistant. The TetA efflux pump belongs to the major facilitator superfamily (MFS), spans the cytoplasmic membrane, and transports tetracycline from the cell cytoplasm to the periplasmic space.²³ This active efflux utilizes the proton gradient as an energy source.²⁴

Gram-positive *S. aureus* (ATCC 29213) used for MIC study expresses the MFS type NorA efflux pump and is methicillin sensitive. MFS type efflux pumps are clinically relevant for resistance in both Gram positive and negative bacteria.²⁵ We therefore used these strains to determine the MIC values for BTs and to assess their ability to recover antimicrobial potency against resistant bacterial strains.

5.2.3. Antimicrobial activity. All minimum inhibitory concentration (MIC) values for compounds **1-11** were determined according to the methods prescribed by the National Committee for Clinical Laboratory Standards.²⁶ Essentially, the bacterium under study is grown to a specified optical density and added to antibiotic that is serially diluted by halves until the growth is inhibited by greater than 80%, detected spectroscopically. All the BTs were dissolved in DMSO and the solvent concentration was kept constant at 0.5% by volume in all experiments. We note that MIC concentrations are sometimes reported in $\mu\text{g}/\text{mL}$. For compound **10**, 10 μM corresponds to 6 $\mu\text{g}/\text{mL}$. We use μM here for convenience in comparisons. The MICs that are recorded in Table 5.1 represent at least two replicates of three trials each. A value of >128 μM recorded in the Table means that no growth inhibition was apparent at 128 μM so the MIC could be far higher.

Table 5.1: Minimal Inhibitory Concentrations (MICs)^a

Cpd	Link (AA) ^b	<i>E. coli</i> K12 (μM)	<i>E. coli</i> Tet ^R (μM)	<i>S. aureus</i> (μM)
1	<i>meta</i> -Ph (Gly)	>128	>128	>128
2	<i>meta</i> -Ph (L-Trp)	64	48 \pm 8	32
3	<i>meta</i> -Ph (D-Trp)	64	28 \pm 4	32
4	<i>meta</i> -Ph (IPA) ^c	>128	>128	>128
5	<i>ortho</i> -Ph (L-Trp)	64	56 \pm 8	32
6	<i>para</i> -Ph (L-Trp)	128	120 \pm 14	128
7	(CH ₂) ₃ (L-Trp)	>128	>128	>128
8	(CH ₂) ₄ (L-Trp)	>128	>128	>128
9	(CH ₂) ₆ (L-Trp)	>128	128	>128
10	(CH ₂) ₁₂ (L-Trp)	8	10 \pm 2	4
11	C ₆ H ₅ -L-Trp-NH ₂	>128	>128	>128

a. MIC resolution is in powers of 2 unless otherwise indicated by a range with \pm . b. Structure of both amino acids c. 3-(3-indolyl)propanoic acid.

5.2.4. *Comparison between K-12 E. coli and S. aureus.* The data in Table 5.1 show that 5 of the 11 compounds tested exhibited various levels of antimicrobial activity against *E. coli* and *S. aureus*. These compounds, **2**, **3**, **5**, **6**, and **10** are more active against Gram positive than Gram-negative bacteria. Indeed, the potency of **10** (MIC of 8 μM against K-12 *E. coli*) is twice that observed against *S. aureus* (4 μM). Most antibiotics are more potent against Gram-positive bacteria due to the absence of a secondary impermeable membrane.²⁷ Of course, a Gram-positive specific target is also possible as observed for daptomycin.²⁸

5.2.5. *Structural comparison.* The compounds studied fall into two categories: compounds having arenyl or alkyl spacers. The compounds having aromatic spacers are **5** (*ortho*), **1-4** (*meta*), and **6** (*para*). The alkylene spacers range from three to twelve methylenes in **7-10**. Compound **11** contains a single tryptophan (no spacer) and is intended to serve as a control.

The arylene BTs are more active antimicrobials than those having alkyl spacers except for **10** [(CH₂)₁₂ (L-trp)], the most potent compound against the three strains of bacteria tested. Note that **11**, the single Trp control, is essentially inactive (MIC > 128 μM). Compounds **1** and **2** are identical except that the two amino acids are glycine in the former and tryptophan in the latter. Compound **2** shows modest antimicrobial activity and **1** shows none (MIC > 128 μM) against all three bacteria. The activity of **2** was also lost when tryptophan was replaced by 3-(3-indolyl)propanoic acid (**4**). We

infer that both the charged ammonium moieties and the indoles in the tryptophan residues are critical for the activity of **2**, **3**, **5**, **6**, and **10**. The disposition of the side chains in otherwise identical compounds **2**, **5**, and **6** revealed that *ortho* and *meta* substitution produced similar toxicities to the three subject bacteria, but no essentially no activity was observed for *para*-phenylene bis(tryptophan) **6**.

A further comparison can be made between **2** and **3**, which differ only in the stereochemistry of the tryptophan residues. Both compounds showed similar activity against *E. coli* K-12 (64 μ M) and *S. aureus* (32 μ M). Compound **3**, in which the tryptophans have the uncommon D-configuration, was nearly twice as active (28 ± 4 μ M) as the naturally occurring isomer L-tryptophan analog (**2**, 48 ± 8 μ M) against *E. coli* Tet^R. Note that the MIC values in this case were narrowed from the power interval so that a closer comparison could be made. We speculate that although both **2** and **3** are similarly toxic to *E. coli* Tet^R, the D-tryptophans are metabolized less rapidly²⁹ and duration rather than potency is reflected in the different MICs.

The alkylene derivatives that approximate the molecular spacing of the tryptophans also show relatively low activity against all three bacteria. Thus, **7** and **8** are inactive. Compound **9** has a slightly longer spacer chain but is essentially inactive to all three bacterial strains. It is marginally more active against *E. coli* Tet^R than it is against the *E. coli* K-12 or *S. aureus*, but it is generally less active than **2** or **3** against all three bacteria. However, the greater antimicrobial activity of (CH₂)₁₂ (L-Trp) (**10**) compared to *meta*-Ph (L-trp) (**2**) and *meta*-Ph (D-trp) (**3**) could relate to overall separation of the ammonium or tryptophan residues. The separation of -NH₃⁺ groups in **10**, the most active BT, is ~ 21 Å (fully extended alkyl chain). In **2** and **3**, the separation is only ~ 12 Å. Of course, the phenylene BTs are more rigid than the alkyl BTs and the conformation of **10** in particular is currently unknown.

Amphiphiles are known to enhance the permeability of bacterial boundary layers.³⁰ Amphiphiles are also known to form aggregates in aqueous solution. An effort to detect aggregates of **10** was made by using dynamic light scattering (DLS). Compound **10** was deemed to be the most amphiphilic (bola-amphiphilic³¹) of the structures owing to the estimated maximal spacing of the amino groups. Solutions of **10**•(HCl)₂ at concentrations between 10 μ M and 1 mM were prepared and examined by dynamic light scattering methods. At the highest concentration, it appeared that some aggregates formed, but the counts were low and the results were considered inconclusive.

5.2.6. Cytotoxicity to mammalian cells. Our initial hypothesis was that antimicrobial activity resulted from membrane disruption. Membrane active compounds are often cytotoxic to mammalian cells.³² The survival of three mammalian epithelial cell lines

was assayed for **2**, **3**, **5**, and **10**. Inactive **6**, *para*-Ph (L-Trp) and **7**, (CH₂)₃ (L-Trp) were included as controls. The cell lines studied were human embryonic kidney (HEK-293), human cervix epithelial (Hela, ATCC CCL-2), and *Cercopithecus aethiops* kidney (Cos-7, ATCC CRL 1651). Cells were cultured for 24 h in 96-well plates and treated with media containing concentrations using [MIC] and [MIC]×2 determined previously for Tet^R *E. coli*. The number of surviving cells was determined using an XTT assay (Sigma-Aldrich); the results are represented as percent survival in Figure 5.2. Cells alone were used as controls and established 100% survival. The data represent two replicates of three trials and the error bars represent the standard deviation.

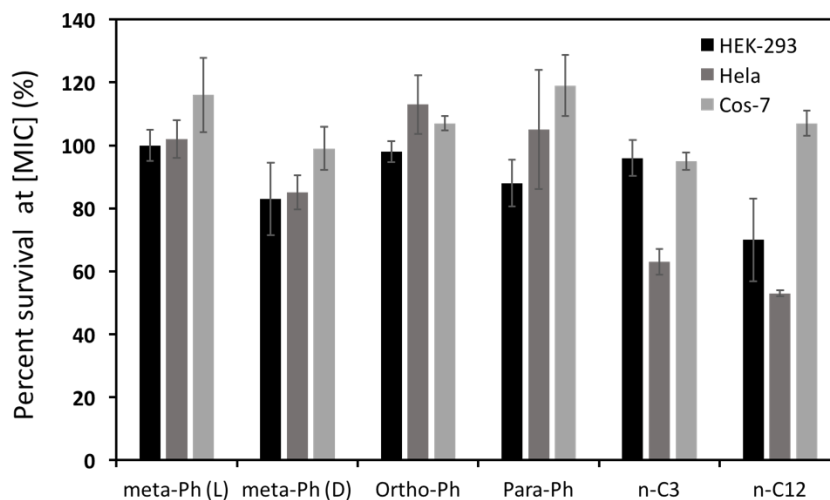


Figure 5.2. Cytotoxicity at the MIC concentration (against Tet^R *E. coli*) of *meta*-Ph (L-trp) (**2**, 28 μM), *meta*-Ph (D-trp) (**3**, 48 μM), *ortho*-Ph (L-trp) (**5**, 56 μM), *para*-Ph (L-trp) (**6**, 120 μM), (CH₂)₃ (L-trp) (**7**, 128 μM), and (CH₂)₁₂ (L-trp) (**10**, 10 μM) to HEK-293, HeLa and Cos-7 cells. Error bars represents the standard deviation in our results.

At MIC concentrations, arene-linked BTs **2**, **3**, **5**, and **6** showed ~100% survival against HEK-293, HeLa, or Cos-7 cells. Alkyl-linked **7** and **10** were minimally toxic to HEK-293 or Cos-7 cells, but were moderately toxic to HeLa cells. In general, the survival of Cos-7 cells was unaffected by the highest concentrations of all the compounds tested.

The survival of all three cell lines was unaffected by a two-fold increase in concentration of *meta*-Ph (L-trp) (**2**, 56 μM) and *ortho*-Ph (L-trp) (**5**, 112 μM), (Figure 5.3). In contrast, *meta*-Ph (D-trp) (**3**) at (96 μM) showed 62% survival for HEK-293 and 29% for HeLa cells. The *para*-Ph (L-trp) (**6**) at 240 μM, showed 61% survival for HEK-293 and 29% for HeLa cells. We note that the cytotoxicities for D-tryptophan (**3**) and *para*-Ph L-tryptophan (**6**) were observed at high concentrations: 96 μM and 240 μM respectively.

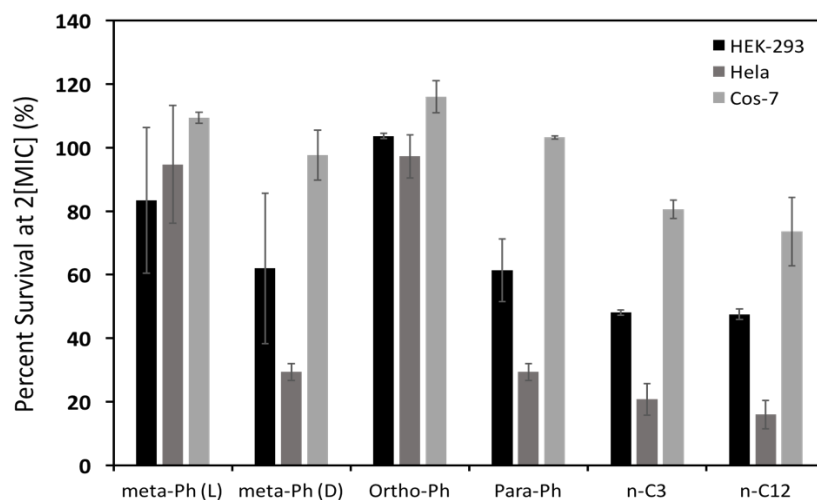


Figure 5.3. The graphs represents the cytotoxicity at twice the MIC concentration (against Tet^R *E. coli*) of *meta*-Ph (L-trp) (**2**, 56 μ M), *meta*-Ph (D-trp) (**3**, 96 μ M), *ortho*-Ph (L-trp) (**5**, 112 μ M), *para*-Ph (L-trp) (**6**, 240 μ M), (CH₂)₃ (L-trp) (**7**, 256 μ M) and (CH₂)₁₂ (L-trp) (**10**, 20 μ M) to HEK-293, HeLa and Cos-7 cells. Error bars represent the standard deviation in our results.

Two observations can be made from the data in Figure 5.3 concerning alkyl BTs **7** and **10**. First, **7** and **10** were more cytotoxic than phenylene BTs **2**, **3**, **5**, or **6**. At the MIC concentrations of (CH₂)₃ (L-trp) (**7**, 128 μ M) and (CH₂)₁₂ (L-trp) (**10**, 10 μ M), 80-100% survival was observed against HEK-293 and Cos-7 cells (Figure 5.2). At twice the MIC concentrations of **7** (256 μ M) and **10** (20 μ M), survival for HEK-293 and Cos-7 further decreased to 50-80% (Figure 5.3). We infer that alkyl-linked BTs may find use as antimicrobials, although this possibility was not pursued further as part of the present effort.

Second, the cytotoxicity of (CH₂)₃ (L-trp) (**7**) and (CH₂)₁₂ (L-trp) (**10**) was greater against HeLa cells than either HEK-293 and Cos-7 cell lines. The HeLa cells are adenocarcinoma involved cervical epithelial cells. The selectivity of (CH₂)₁₂ (L-trp) (**10**) at 20 μ M for HeLa cells over HEK-293 and Cos-7, suggests a potential application in cancer chemotherapy. While this is not the focus of the present report, we note that a (CH₂)₈ (L-Trp) analog of **10** prepared by Lown and co-workers showed promising cytotoxicity against 60 human cancer cell lines.³³

5.2.7. Recovery of antimicrobial activity against a resistant strain. The cytotoxicity of the compounds **2**, **3**, **5**, **6**, **7** and **10** was minimal at MIC concentrations. Next, we determined whether these compounds could be used at concentrations of $\frac{1}{2}$ MIC or lower to recover the activity of antibiotics against efflux pump expressing resistant

bacteria. At these lower concentrations there should be no cytotoxicity. In addition, at the half-MIC concentrations these compounds should not have any effect on bacterial growth. We hypothesized that if certain BTs increased membrane permeability, they could recover antimicrobial potency against efflux-based resistance. This hypothesis was tested with the Tet^R strain of *E. coli* prepared in our laboratory (see above).

We determined MICs for **2**, **3**, **5**, **6**, **7**, and **10** against Tet^R *E. coli*. Compounds **6** (*para*-Ph) and **7** (*n*-C₃) were also included as controls. The MICs against Tet^R *E. coli* were refined compared to the power series and are reported as a range in Table 5.1 (above). The MICs of tetracycline and ampicillin against Tet^R *E. coli* were 900 ± 100 μM and >1000 μM, respectively. For comparison, the MIC for tetracycline against non-resistant *E. coli* K-12 is ~3 μM. Ampicillin was used to maintain selective pressure for the expression of pBR322 plasmid. Ampicillin was omitted from experiments that contained tetracycline. Next, we determined the MIC of tetracycline when co-administered with **2**, **3**, **5**, **6**, **7**, or **10**. The results are recorded in Table 5.2. The results are represented as the MIC of tetracycline in the presence of the indicated BTs. The fold-recovery was determined by dividing the MIC of tetracycline when used alone by the MIC of tetracycline determined in the presence of our compounds.

Table 5.2. Recovery of tetracycline activity against Tet^R *E. coli*

Compounds Used	[Compound] μM	MIC [Tet] μM ^a	Fold Recovery	FIC ^c
None	0	900	n.a. ^b	n.a.
<i>meta</i> -Ph (L-Trp) (2)	24 [$\frac{1}{2}$ MIC]	56.25	16-fold	0.56
<i>meta</i> -Ph (L-Trp) (2)	12 [$\frac{1}{4}$ MIC]	112.5	8-fold	0.38
<i>meta</i> -Ph (L-Trp) (2)	14	112.5	8-fold	0.42
<i>meta</i> -Ph (D-Trp) (3)	14 [$\frac{1}{2}$ MIC]	112.5	8-fold	0.63
<i>meta</i> -Ph (D-Trp) (3)	7 [$\frac{1}{4}$ MIC]	225	4-fold	0.50
<i>ortho</i> -Ph (L-Trp) (5)	28 [$\frac{1}{2}$ MIC]	112.5	8-fold	0.63
<i>ortho</i> -Ph (L-Trp) (5)	14 [$\frac{1}{4}$ MIC]	225	4-fold	0.50
<i>para</i> -Ph (L-Trp) (6)	60 [$\frac{1}{2}$ MIC]	112.5	8-fold	0.63
<i>para</i> -Ph (L-Trp) (6)	30 [$\frac{1}{4}$ MIC]	225	4-fold	0.50
<i>para</i> -Ph (L-Trp) (6)	14	450	2-fold	0.62
<i>n</i> -C ₃ (L-Trp) (7)	60 [$\frac{1}{2}$ MIC]	112.5	8-fold	0.63
<i>n</i> -C ₃ (L-Trp) (7)	30 [$\frac{1}{4}$ MIC]	112.5	8-fold	0.38
<i>n</i> -C ₃ (L-Trp) (7)	5	450	2-fold	0.54
<i>n</i> -C ₁₂ (L-Trp) (10)	5 [$\frac{1}{2}$ MIC]	225	4-fold	0.75
<i>n</i> -C ₁₂ (L-Trp) (10)	2.5 [$\frac{1}{4}$ MIC]	450	2-fold	0.75

a. MIC is the observed inhibitory concentration of tetracycline in the presence of the indicated compound. MIC values represent two trials of two replicates each. MIC resolution is in powers of 2. b. 'n.a.' means not applicable. c. FIC is the fractional inhibitory concentration

Tetracycline activity was recovered by compounds **2**, **3**, **5**, **6**, **7** and **10** at $\frac{1}{2}$ and $\frac{1}{4}$ of its MIC values. This recovery of tetracycline potency was based on the concentration and the structure of the compounds used. The highest recovery of tetracycline activity was observed with *meta*-Ph (L-trp) (**2**). The MIC of tetracycline was decreased from 900 μM to 56.25 μM in the presence of 24 μM of compound **2**. At twice the concentration of compound **2** (48 μM), no cytotoxicity to HEK-293, HeLa, and Cos-7 cells was apparent (Figure 5.2). The $(\text{CH}_2)_{12}$ (L-trp) (**10**), most potent antimicrobial in the **1-10** group, showed only 2 to 4-fold recovery of tetracycline activity.

The fractional inhibitory concentration (FIC) is often used as a measure of synergism or antagonism in comparing two or more compounds.³⁴ The FIC is the sum of the fraction of the MIC for each compound used. Synergy is defined broadly as $\text{FIC} < 1$, or more conservatively as $\text{FIC} \leq 0.5$. Under the broad definition, all compounds tested can be said to have at least moderate synergy with tetracycline. All arene-based compounds fit the more conservative definition of synergy with FIC values of 0.5 or less at the tested concentrations. Compound **2** showed particularly high synergy with a FIC of 0.38. The shorter alkyl-linked compound **7** also had a FIC of 0.38, whereas the longer *n*-C₁₂ (L-trp) (**10**) did not show synergy below a FIC of 0.75.

Since the MICs of all the compounds tested were different, we chose a single concentration to compare the efficacies of different compounds in the expectation that if any trend was apparent, it would be revealed. We compared the ability of compounds **2**, **3**, **5** and **6** to recover tetracycline activity at 14 μM , which is much lower than the MIC observed with any arene-spacer based compounds. The alkyl-spacer based compounds (**3** and **12**) were compared at 5 μM , which is much lower than the MIC observed with either compound. It is apparent from the graph of Figure 5.4, that at 14 μM *meta*-Ph (L-Trp), **2**, is most effective at recovering tetracycline activity against Tet^R *E. coli*. The least effective synergists were those having *para*-Ph, **6**, or propylene (*n*-C₃), **7**, spacers. Clearly, regiochemistry and conformational mobility are contributors to the observed differences but the precise nature of the influence(s) is not known.

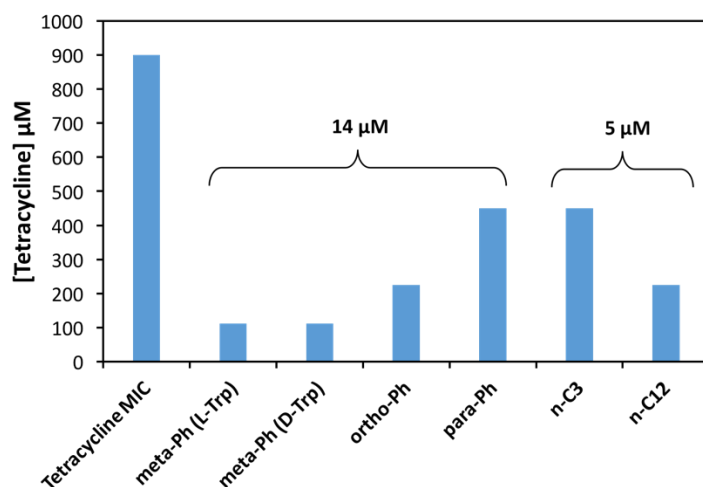


Figure 5.4. This graph compares the ability of *meta-ph* (L-trp) (**2**, 14 μM), *meta-ph* (D-trp) (**3**, 14 μM), *ortho-ph* (L-trp) (**5**, 14 μM), *para-ph* (L-trp) (**6**, 14 μM), $(\text{CH}_2)_3$ (L-trp) (**7**, 5 μM) and $(\text{CH}_2)_{12}$ (L-trp) (**10**, 5 μM) to recover tetracycline activity against Tet^R *E. coli*. MICs were reproduced three times and the resolution is in powers of 2.

5.2.8. Membrane permeability. Based on the MIC and toxicity studies, *meta-Ph* (L-trp), **2**, and $(\text{CH}_2)_{12}$ (L-trp), **10**, have emerged as compounds of interest for different reasons. The *meta-Ph* (L-trp), **2**, shows synergy against tetracycline resistant *E. coli*, without any cytotoxicity to three mammalian cell lines. Dodecylene BT, **10**, showed the greatest antimicrobial activity, but also exhibited cytotoxicity to HEK-293 and HeLa cells. In order for the BTs to exhibit toxicity to any of the microbes, it is essential for them to penetrate the bacterial membrane. In Gram-negative organisms, the boundary membrane consists of two layers although porins are present within them that could pass these relatively small molecules.

Figure 5.5 shows the results of a confocal microscopy study using *E. coli* Tet^R as the test organism. The study was designed to assess the membrane permeability and viability of the *E. coli* in the presence of BTs **2** and **10**. The three panels in Figure 5.5 show the bright field (BF) microscopic images (top row), the result when fluorescein diacetate (FDA) is present (middle row), and the presence of propidium iodide (PI, bottom row), if any. Propidium iodide does not normally pass through boundary membranes into bacteria or other cells. When it does, it intercalates in DNA, which leads to enhanced fluorescence. Fluorescein diacetate is incorporated into the cells during growth, but is not fluorescent. If the organism is or remains vital, the diester will be hydrolyzed and fluorescein will be observed by its fluorescence emission.

The membrane permeability and viability of *E. coli* Tet^R was observed for the microbe alone or in the presence of BTs **2** or **10**. Controls for the permeability/viability assay

were included for *E. coli* in the presence of a final concentration of 0.5% (v/v) DMSO (the vehicle for administration of BTs), and a final concentration of 0.1% (w/w) Triton X-100. We have recently demonstrated³⁵ that while small amounts of DMSO (e.g. 0.5% in media) do not alter biological activity, at higher concentrations and with certain organisms there is an effect. Thus, we never use more than 0.5% DMSO (v/v); the control is shown in the second column. Triton X-100 is a potent detergent, which is used at 0.1% or $\sim 1,670 \mu\text{M}$.

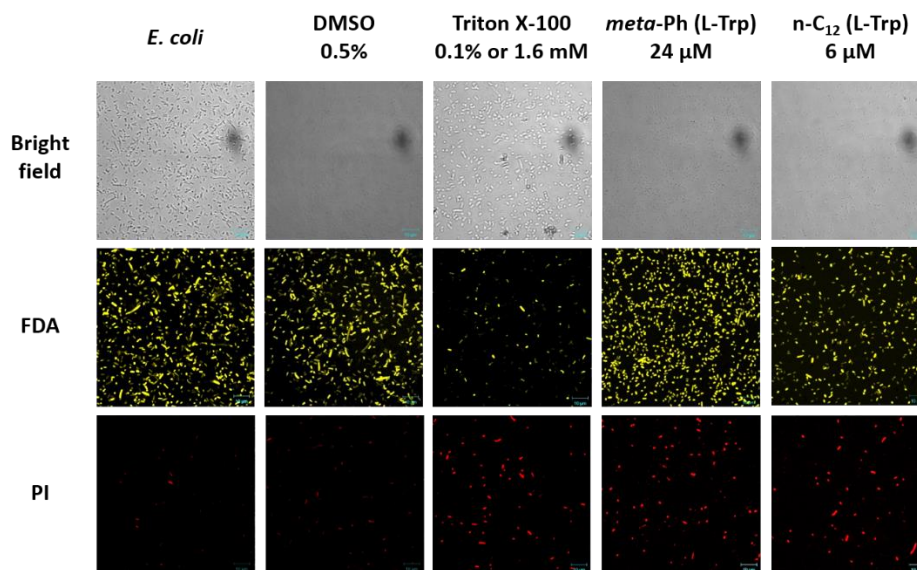


Figure 5.5: Tet^R *E. coli* cell membrane permeability by compounds **2** (*meta*-Ph (L-Trp)) and **10** (C₁₂-Trp) at $\sim \frac{1}{2}$ MIC and controls.

The images show that *E. coli* Tet^R alone or in the presence of 0.5% DMSO are vital. This is also the case when *E. coli* Tet^R is subjected to **2** at 24 μM or **10** at 6 μM . These concentrations were selected because each is $\frac{1}{2}$ the MIC value. The lower row of Figure 5.5 shows that propidium iodide does not infiltrate *E. coli* Tet^R in the absence of Triton X-100, **2**, or **10**. When Triton X-100 is the adjuvant, essentially all the cells are killed and the presence of PI may simply be part of the cellular detritus. Propidium iodide fluorescence is observed when **2** or **10** is added to the cells. This indicates that the membrane permeability has increased, yet cells remain vital at the concentrations tested (*cf.* FDA fluorescence).

A compound that inhibits bacterial growth and penetrates into the microbe's cytosol may also penetrate into mammalian cells. We therefore conducted a similar microscopic study with the human embryonic kidney (HEK-293) cell line. In this case, only compound **2** was studied. Its activity (MIC) against all three microbes ranged from 32-64 μM . The microscopic study was therefore conducted at 20 μM , a value well below any inhibitory concentration, and at 80 μM , a concentration above all three MIC

values. The 80 μM concentration was used to confirm the cytotoxicity of **2** and to establish the lack of serum inhibition. The results are shown in Figure 5.6.

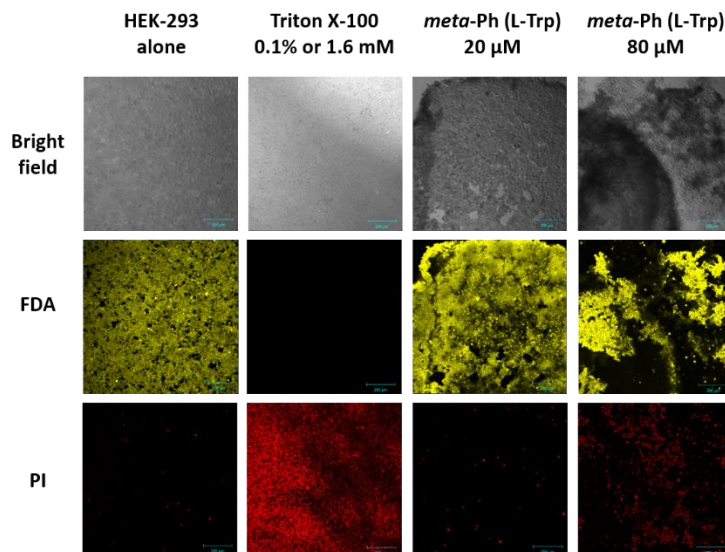


Figure 5.6. Mammalian cell permeability in HEK-293 in the presence of *meta*-Ph (L-Trp), **2**, at 20 μM and 80 μM .

Propidium iodide indicates an increase of the membrane permeability of HEK-293 cells and the FDA fluorescence reports cellular vitality. When Triton X-100 is administered at 0.1% ($\sim 1670 \mu\text{M}$), vitality is lost and a strong signal from propidium iodide reflects interaction of the dye with dispersed DNA. The results for **2** at 20 μM and 80 μM are interesting. At the lower concentration, a relatively low level of PI penetration is apparent and there is no loss of vitality. At 80 μM , there is considerable penetration of PI and some toxic effect is apparent.

These data indicate that at sub-lethal concentrations, *meta*-Ph (L-trp), **2**, increases the membrane permeability of *E. coli* cells, but shows no cytotoxicity or permeability alteration for HEK-293 mammalian cells. At higher concentrations, both cytotoxicity and membrane disruption are manifested.

5.3. Conclusion.

A series of nine *bis*(tryptophan) derivatives (BTs) and two control compounds was synthesized and tested for antimicrobial activity. The effect of arylene and alkylene linkers on the bacteriostatic activity of the compounds was assessed against two *E. coli* strains and a *S. aureus* strain. Structure-based studies revealed that in arylene-linked BTs the *meta* positioning of two tryptophans and the charge of the molecules are all crucial components to observe antimicrobial potency. Removal of any one property leads to loss of the antimicrobial activity. Antibacterial activity of alkylene-

linked BTs was observed only for the longest dodecylene spacer. The compounds were generally more active against Gram-positive *S. aureus* than Gram-negative *E. coli*. At sub-inhibitory concentrations the *meta*-phenylene linked BTs recovered the antibacterial activity of tetracycline against tetracycline-resistant *E. coli*. This apparent synergy may arise from the membrane activity of these compounds as revealed by confocal microscopy. Minimal cytotoxicity was observed for the arylene-linked BTs at MIC concentrations against three mammalian epithelial cell lines. Although many amphiphilic peptides have been previously reported, this study exemplifies a minimalist structure-based approach. The simplicity of the structures elaborated in this report notwithstanding, BTs effectively reversed efflux pump-mediated resistance. With additional mechanistic and structural studies, we seek to establish a strategy for combating efflux-based antibiotic resistance with membrane-active compounds.

5.4. Experimental Section.

5.4.1. Chemical synthesis and characterization.

The *tert*-butyl carbamate-protected (Boc-protected) amino acids were coupled to the diamine using a uronium-based coupling reagent HBTU in DMF with diisopropylethylamine. After workup and isolation of the desired boc-protected *bis*(amino acid) product, deprotection was carried out using hydrochloric acid dioxane/methanol and precipitated out with methylene chloride. All ¹H- and ¹³C-NMR spectra were determined at 300 and 75 MHz, respectively, in CDCl₃ unless otherwise specified.

General Procedure. The *tert*-butyl carbamate-protected (Boc-protected) amino acids and HBTU (2.1 equivalents) were dissolved in 10 mL anhydrous DMF with diisopropylethylamine (4.0 equivalents for the neutral diamines; 6.0 equivalents for diaminedihydrochlorides). The reaction was stirred overnight at room temperature under an argon atmosphere. The mixture was taken up in 75 mL ethyl acetate and washed with 1 M NaHSO₄ (2 x 75 mL), 5% NaHCO₃ (3 x 50 mL), and brine. The organic layer was dried by filtration through a MgSO₄/celite plug and the solvent removed *in vacuo*. The Boc-protected *bis*(amino acid) was used without further purification or was crystallized/precipitated from CH₂Cl₂/hexane. The deprotection was carried out by using 10 equivalents of HCl in dioxane/methanol and the product was obtained by precipitation and trituration with cold methylene chloride.

Di-*tert*-butyl ((1,3-phenylenebis(azanediyl))bis(2-oxoethane-2,1-diyl))dicarbamate (1a) was prepared according to the general procedure from 1,3-phenylenediamine (0.154 mg, 1.42 mmol) and Boc-Gly-OH. The product was obtained as a white powder (0.33 g, 55% yield), mp 95 °C (dec). ¹H-NMR: δ 1.44 (s, 18H, (CH₃)₃), 3.90 (d, 2H, αCH₂), 5.86 (m, 2H, Boc-NH), 7.12 (t, *J* = 7.2 Hz, 1H, phenyl H5),

7.23 (d, $J = 7.2$ Hz, 2H, phenyl H4, H6), 7.64 (s, 1H, phenyl H2), 8.92 (s, 2H, PhNHCO-). $^{13}\text{C-NMR}$ (75 MHz, CDCl_3): δ 28.27, 44.90, 80.28, 111.72, 116.02, 129.27, 138.00, 156.60, 168.52. HRMS (FAB⁺): calcd for ($\text{C}_{20}\text{H}_{30}\text{N}_4\text{O}_6$) 422.2165, found 422.2163.

2,2'-(1,3-Phenylenebis(azanediyl))bis(2-oxoethanaminium) chloride (1) was prepared according to the general procedure using **1a** (309 mg, 0.73 mmol). The product was obtained as a white powder (0.20 g, 94% yield), mp 310 °C (dec.). $^1\text{H-NMR}$ (D_2O): δ 3.88 (s, 4H, αCH_2), 7.14 (d, $J = 8.1$ Hz, 2H, phenyl H4, H6), 7.32 (t, $J = 8.1$ Hz, 1H, phenyl H5), 7.68 (s, 1H, phenyl H2). $^{13}\text{C-NMR}$ (D_2O): δ 40.92, 113.72, 117.97, 129.92, 136.99, 165.49. HRMS (FAB⁺): calcd for ($\text{C}_{10}\text{H}_{14}\text{N}_4\text{O}_2\text{Na}$) 245.1015, found 245.1014.

Di-tert-butyl ((2S,2'S)-(1,3-phenylenebis(azanediyl))bis(3-(1H-indol-3-yl)-1-oxopropane-2,1-diyl))dicarbamate (2a) was prepared according to the general procedure using 1,3-phenylenediamine (150 mg, 1.39 mmol) and Boc-L-Trp-OH. The product was obtained as a white powder (0.80 g, 85% yield), mp 148 °C (dec). $^1\text{H-NMR}$ ($\text{DMSO}-d_6$): δ 1.34 (s, 18H, $2(\text{CH}_3)_3$), 2.95-3.14 (ABX, 4H, $2\text{CH}_2\beta$), 4.39 (ABX, 2H, $2\text{CH}\alpha$), 6.90-7.12 (m, 6H, indole H5, indole H6, ArNH), 7.15-7.40 (m, 7H, indole H2, phenylene H4), phenylene H5, indole H7), 7.68 (d, $J = 7.7$ Hz, 2H, indole H4), 7.99 (s, 1H, phenylene H2). $^{13}\text{C-NMR}$ ($\text{DMSO}-d_6$): δ 28.07, 30.59, 55.67, 77.94, 109.85, 111.15, 114.34, 118.07, 118.54, 120.76, 123.71, 127.15, 131.24, 135.89, 139.16, 155.19, 171.11. HRMS (FAB⁺): calcd for ($\text{C}_{38}\text{H}_{44}\text{N}_6\text{O}_6\text{Na}$) 703.3220, found 703.3224.

(2S,2'S)-1,1'-(1,3-Phenylenebis(azanediyl))bis(3-(1H-indol-3-yl)-1-oxopropan-2-aminium) chloride (2) was prepared according to the general procedure using **2a** (313 mg, 0.46 mmol). The product was obtained as a white powder (0.24 g, 94% yield), mp 223 °C (dec). $^1\text{H-NMR}$ (CD_3OD): δ 3.33-3.53 (ABX, 4H, $2\text{CH}_2\beta$), 4.26 (ABX, 2H, $2\text{CH}\alpha$), 7.01 (t, $J = 7.4$ Hz, 2H, indole H5), 7.12 (t, $J = 7.0$ Hz, 2H, indole H6), 7.22 (s, 2H, indole H2), 7.26 (m, 2H, phenylene H4), 7.27 (m, 1H, phenylene H5), 7.38 (d, $J = 8.1$ Hz, 2H, indole H7), 7.67 (d, $J = 7.9$ Hz, 2H, indole H4), 7.93 (s, 2H, phenylene H2). $^{13}\text{C-NMR}$ (CD_3OD): δ 29.01, 55.68, 107.84, 112.61, 113.28, 117.54, 119.29, 120.35, 122.93, 125.73, 128.35, 130.32, 138.32, 139.60, 168.52. HRMS (FAB⁺): calcd for ($\text{C}_{28}\text{H}_{29}\text{N}_6\text{O}_2^+$) 481.2347, found 481.2356.

Di-tert-butyl ((2R,2'R)-(1,3-phenylenebis(azanediyl))bis(3-(1H-indol-3-yl)-1-oxopropane-2,1-diyl))dicarbamate (3a) was prepared according to the general procedure using 1,3-phenylenediamine (200 mg, 1.85 mmol) and Boc-D-Trp-OH. The product was obtained as a white powder (1.05 g, 84% yield), mp 141 °C (dec). $^1\text{H-NMR}$: δ 1.38 (s, 18H, $2(\text{CH}_3)_3$), 3.10-3.45 (ABX, 4H, $2\text{CH}_2\beta$), 4.62 (ABX, 2H, $2\text{CH}\alpha$), 6.90-7.23 (m, 6H, indole H5, indole H6, ArNH), 7.29-7.40 (m, 7H, indole H2, phenylene H4), phenylene H5, indole H7), 7.66 (d, $J = 7.0$ Hz, 2H, indole H4), 8.21 (s, 1H,

phenylene H2). ¹³C-NMR: δ 28.35, 28.98, 56.04, 80.49, 109.66, 111.63, 112.74, 116.83, 118.67, 119.35, 121.90, 123.79, 127.64, 129.34, 136.64, 138.14, 156.25, 171.58. HRMS (FAB⁺): calcd for (C₃₈H₄₄N₆O₆Na) 703.3220, found 703.3219.

(2*R*,2'*R*)-1,1'-(1,3-Phenylenebis(azanediyl))bis(3-(1*H*-indol-3-yl)-1-oxopropan-2-aminium) chloride (3) was prepared according to the general procedure using **3a** (440 mg, 0.65 mmol). The product was obtained as an off-white powder (0.23 g, 64% yield), mp 242 °C (dec). ¹H-NMR (CD₃OD): δ 3.33-3.53 (ABX, 4H, 2CH₂β), 3.65 (s, 6H, 2NH₃), 4.26 (ABX, 2H, 2CH_α), 7.01 (t, *J* = 7.4 Hz, 2H, indole H5), 7.12 (t, *J* = 7.0 Hz, 2H, indole H6), 7.22 (s, 2H, indole H2), 7.26 (m, 2H, phenylene H4), 7.27 (m, 1H, phenylene H5), 7.38 (d, *J* = 8.1 Hz, 2H, indole H7), 7.67 (d, *J* = 7.9 Hz, 2H, indole H4), 7.93 (s, 2H, phenylene H2). ¹³C-NMR (CD₃OD): δ 28.96, 55.67, 107.84, 112.58, 113.31, 117.55, 119.33, 120.32, 122.89, 125.76, 128.37, 130.28, 138.27, 139.56, 168.52. HRMS (FAB⁺): calcd for (C₂₈H₂₉N₆O₂⁺) 481.2347, found 481.2350.

***N,N'*-(1,3-Phenylene)bis(3-(1*H*-indol-3-yl)propanamide) (4)** was prepared according to the general procedure using 1,3-phenylenediamine (70 mg, 0.65 mmol) and indole-3-propionic acid. The product was obtained as a white powder (0.23 g, 78% yield), mp 154-156 °C. ¹H-NMR (CD₃OD): δ 2.76 (t, *J* = 7.6 Hz, 4H, 2COCH₂CH₂-indole), 3.18 (t, 7.6 Hz, 4H, 2COCH₂CH₂-indole), 7.04-7.39 (m, 9H, indole H5, indole H6, indole H2, phenylene H4, phenylene H6), 7.37 (d, *J* = 7.9 Hz, 2H, indole H7), 7.60-7.66 (m, 3H, indole H4, phenylene H5). ¹³C-NMR (CD₃OD): δ 21.81, 38.37, 111.71, 114.33, 116.43, 117.53, 118.72, 119.06, 121.83, 122.40, 127.52, 137.04, 139.11, 173.38. HRMS (FAB⁺): calcd for (C₂₈H₂₆N₄O₂Na) 473.1954, found 473.1945.

Di-*tert*-butyl ((2*S*,2'*S*)-(1,2-phenylenebis(azanediyl))bis(3-(1*H*-indol-3-yl)-1-oxopropane-2,1-diyl))dicarbamate (5a) was prepared according to the general procedure using 1,2-phenylenediamine (150 mg, 1.39 mmol) and Boc-L-Trp-OH. The product was obtained as a white powder (0.76 g, 80% yield), mp 129 °C (dec). Two hydrogen bonded conformations were observed spectroscopically, peaks for the major conformer are reported herein. ¹H-NMR: δ 1.50 (s, 9H, (CH₃)₃), 3.05-3.33 (ABX, 2H, βCH₂), 4.21 (ABX, 1H, αCH), 5.40 (d, *J* = 7.3 Hz, 1H, Boc-NH), 6.55-7.62 (m, 7H, ArH, ArNH), 8.98 (s, 1H, indole NH). ¹³C-NMR: δ 28.48, 28.84, 56.01, 80.53, 110.14, 111.55, 118.99, 119.65, 122.19, 123.45, 124.68, 126.10, 127.37, 129.33, 136.16, 155.71, 171.35. HRMS (FAB⁺): calcd for (C₃₈H₄₄N₆O₆Na) 703.3220, found 703.3218.

(2*S*,2'*S*)-1,1'-(1,2-Phenylenebis(azanediyl))bis(3-(1*H*-indol-3-yl)-1-oxopropan-2-aminium) chloride (5) was prepared according to the general procedure using **5a** (600 mg, 0.88 mmol). The product was obtained as a white powder (0.21 g, 43% yield), mp 201 °C (dec). Two hydrogen bonded conformations were observed spectroscopically, peaks for the major conformer are reported herein. ¹H-NMR

(CD₃OD): δ 3.35-3.65 (ABX, 2H, β CH₂), 4.58 (t, J = 6.9 Hz, 1H, α CH), 7.00-7.73 (m, 7H, ArH, ArNH). ¹³C-NMR (CD₃OD): δ 28.79, 55.74, 107.93, 112.56, 119.58, 120.36, 122.92, 125.81, 126.35, 127.36, 128.48, 130.99, 138.27, 169.44. HRMS (FAB⁺): calcd for (C₂₈H₂₉N₆O₂⁺) 481.2347, found 481.2359.

Di-tert-butyl ((2*S*,2'*S*)-(1,4-phenylenebis(azanediyl))bis(3-(1H-indol-3-yl)-1-oxopropane-2,1-diyl))dicarbamate (6a) was prepared according to the general procedure using 1,4-phenylenediamine (150 mg, 1.39 mmol) and Boc-L-Trp-OH. The product was obtained as a white powder (0.84 g, 89% yield), mp 167 °C (dec). ¹H-NMR (CD₃OD): δ 1.41 (s, 9H, (CH₃)₃), 3.19-3.36 (ABX, 2H, β CH₂), 4.47 (ABX, 1H, α CH), 6.98-7.12 (m, 3H, indole H5, indole H6, indole H2), 7.27-7.42 (m, 3H, indole H7, phenylene CH), 7.61 (d, J = 7.7 Hz, 1H, indole H4), 7.78 (s, 1H, indole NH). ¹³C-NMR (CD₃OD): δ 28.50, 29.26, 56.66, 80.52, 110.06, 111.90, 118.97, 119.50, 121.52, 122.07, 124.15, 128.14, 134.88, 137.26, 156.85, 172.14. HRMS (FAB⁺): calcd for (C₃₈H₄₄N₆O₆Na) 703.3220, found 703.3210.

(2*S*,2'*S*)-1,1'-(1,4-Phenylenebis(azanediyl))bis(3-(1H-indol-3-yl)-1-oxopropan-2-aminium) chloride (6) was prepared according to the general procedure using **6a** (475 mg, 0.70 mmol). The product was obtained as a white powder (0.36 g, 93% yield), mp 237 °C (dec.). ¹H-NMR (CD₃OD): δ 3.34-3.54 (ABX, 2H, β CH₂), 4.27 (ABX, 1H, α CH), 6.97-7.14 (m, 2 H, indole H5, indole H6), 7.24 (s, 1H, indole H7), 7.38 (d, J = 8.1 Hz, 1H, indole H7), 7.67 (d, J = 7.9 Hz, 1H, indole H4). ¹³C-NMR (75 MHz, CDCl₃): δ 28.93, 55.69, 107.90, 112.57, 119.33, 120.29, 121.88, 122.87, 125.72, 128.38, 135.61, 138.26, 168.33. HRMS (FAB⁺): calcd for (C₂₈H₂₈N₆O₂Na) 503.2171, found 503.2166.

Di-tert-butyl ((2*S*,2'*S*)-(propane-1,3-diylbis(azanediyl))bis(3-(1H-indol-3-yl)-1-oxopropane-2,1-diyl))dicarbamate (7a) was prepared according to the general procedure using 1,3-diaminopropane dihydrochloride (200 mg, 1.36 mmol) and Boc-L-Trp-OH. The product was obtained as a white powder (0.51 g, 58% yield). The compound was previously reported³³ and the spectra obtained matched those previously reported.

(2*S*,2'*S*)-1,1'-(Propane-1,3-diylbis(azanediyl))bis(3-(1H-indol-3-yl)-1-oxopropan-2-aminium) chloride (7) was prepared according to the general procedure using **7a** (380 mg, 0.59 mmol). The product was obtained as a white powder (0.30 g, 98% yield), mp 234 °C (dec). ¹H-NMR (CD₃OD): δ 1.40 (m, 2H, -CH₂CH₂NH-), 2.98 (m, 4H, -CH₂CH₂NH-), 3.22-3.65 (m, 4H, CH₂ β), 4.13 (ABX, 2H, CH α), 6.99-7.18 (m, 4H, indole H5, indole H6), 7.25 (s, 2H, indole H2), 7.39 (d, J = 6.4 Hz, 2H, indole H7), 7.69 (d, J = 4.7 Hz, 2H, indole H4), 8.30 (br, CONH). ¹³C-NMR (CD₃OD): δ 28.78, 29.39, 37.76, 55.27, 108.03, 112.62, 119.34, 120.22, 122.80, 125.71, 128.29, 138.02, 170.05. HRMS (FAB⁺): calcd for (C₂₅H₃₁N₆O₂⁺) 447.2503, found 447.2503.

Di-*tert*-butyl ((2*S*,2'*S*)-(butane-1,4-diylbis(azanediyl))bis(3-(1*H*-indol-3-yl)-1-oxopropane-2,1-diyl))dicarbamate (8a) was prepared according to the general procedure using 1,4-diaminobutane dihydrochloride (210 mg, 1.30 mmol) and Boc-L-Trp-OH. The product was obtained as a white powder (0.79 g, 92% yield). The compound was previously reported³³ and the spectra obtained matched those previously reported.

(*S*)-1-((4-((*R*)-2-ammonio-3-(1*H*-indol-3-yl)propanamido)butyl)amino)-3-(1*H*-indol-3-yl)-1-oxopropan-2-aminium chloride (8) was prepared according to the general procedure using **8a** (650 mg, 0.98 mmol). The product was obtained as a white powder (0.51 g, 97% yield), mp 204 °C (dec). ¹H-NMR (CD₃OD): δ 1.18 (m, 2H, -CH₂CH₂NH-), 3.05 (m, 2H, -CH₂CH₂NH-), 3.22-3.41 (ABX, 2H, CH₂β), 4.09 (ABX, 1H, CHα), 7.05-7.17 (m, 2H, indole H5, indole H6), 7.23 (s, 2H, indole H2), 7.40 (d, *J* = 7.9 Hz, 1H, indole H7), 7.66 (d, *J* = 7.9 Hz, 2H, indole H4), 8.25 (br, 1H, CONH). ¹³C-NMR (CD₃OD): δ 27.24, 29.06, 40.28, 55.40, 68.27, 108.29, 112.73, 119.38, 120.37, 123.00, 125.68, 128.51, 138.34, 170.13. HRMS (FAB⁺): calcd for (C₂₆H₃₃N₆O₂⁺) 461.2660, found 461.2668.

Di-*tert*-butyl ((2*S*,2'*S*)-(hexane-1,6-diylbis(azanediyl))bis(3-(1*H*-indol-3-yl)-1-oxopropane-2,1-diyl))dicarbamate (9a) was prepared according to the general procedure using 1,6-diaminohexane dihydrochloride (250 mg, 1.32 mmol) and Boc-L-Trp-OH. The product was obtained as a white powder (0.90 g, 99% yield). The compound was previously reported³³ and the spectra obtained matched those previously reported.

(2*S*,2'*S*)-1,1'-(Hexane-1,6-diylbis(azanediyl))bis(3-(1*H*-indol-3-yl)-1-oxopropan-2-aminium) chloride (9) was prepared according to the general procedure using **9a** (650 mg, 0.94 mmol). The product was obtained as a white powder (0.33 g, 62% yield), mp 193 °C (dec). ¹H-NMR (CD₃OD): δ 1.05 (m, 2H, aliphatic CH₂), 1.26 (m, 2H, aliphatic CH₂), 2.97-3.39 (m, 4H, -CH₂CH₂NH-, CH₂β), 4.06 (ABX, 2H, CHα), 7.02-7.15 (m, 2H, indole H5, indole H6), 7.20 (s, 1H, indole H2), 7.37 (d, *J* = 8.1 Hz, 1H, indole H7), 7.63 (d, *J* = 7.5 Hz, 2H, indole H4), 8.19 (br, CONH). ¹³C-NMR (CD₃OD): δ 27.38, 28.98, 29.85, 40.61, 55.29, 108.19, 112.64, 119.22, 120.27, 122.91, 125.52, 128.40, 138.26, 169.95. HRMS (FAB⁺): calcd for (C₂₈H₃₇N₆O₂⁺) 489.2973, found 489.2972.

Di-*tert*-butyl ((2*R*,2'*S*)-(dodecane-1,12-diylbis(azanediyl))bis(3-(1*H*-indol-3-yl)-1-oxopropane-2,1-diyl))dicarbamate (10a) was prepared according to the general procedure using 1,12-diaminododecane (250 mg, 1.25 mmol) and Boc-L-Trp-OH. The product was obtained as an off-white powder (0.93 g, 96% yield), mp 86 °C

(dec). ¹H-NMR: δ 1.08-1.34 (m, 22H, aliphatic CH₂), 1.41 (s, 18H, C(CH₃)₃), 2.99-3.32 (m, 8H, -CH₂CH₂NH-, CH₂β), 4.42 (ABX, 2H, CHα), 5.36 (br, 2H, Boc-NH), 6.03 (br, 2H, CONH), 6.95 (s, 2H, indole H2) 7.03-7.16 (m, 4H, indole H5, indole H6), 7.32 (d, *J* = 7.9 Hz, 2H, indole H7), 7.60 (d, *J* = 7.7 Hz, 2H, indole H4). ¹³C-NMR: δ 26.52, 28.16, 28.54, 28.99, 29.22, 29.28, 31.43, 39.38, 55.22, 65.72, 79.83, 110.12, 111.23, 118.60, 119.27, 121.81, 123.22, 127.26, 136.19, 155.44, 171.68. HRMS (FAB⁺): calcd for (C₄₄H₆₄N₆O₆Na) 785.4785, found 785.4792.

(S)-1-((12-((R)-2-Ammonio-3-(1H-indol-3-yl)propanamido)dodecyl)amino)-3-(1H-indol-3-yl)-1-oxopropan-2-aminium chloride (10) was prepared according to the general procedure using **10a** (715 mg, 0.92 mmol). The product was obtained as a white powder (0.56 g, 93% yield), mp 158 °C (dec). ¹H-NMR (CD₃OD): δ 1.08-1.34 (m, 22H, aliphatic CH₂), 2.99-3.38 (m, 8H, -CH₂CH₂NH-, CH₂β), 4.04 (ABX, 2H, CHα), 7.02-7.15 (m, 4H, indole H5, indole H6), 7.20 (s, 2H, indole H2), 7.37 (d, *J* = 7.9 Hz, 2H, indole H7), 7.62 (d, *J* = 7.9 Hz, 2H, indole H4). ¹³C-NMR (CD₃OD): δ 27.92, 28.98, 30.01, 30.43, 30.69, 30.77, 40.77, 55.29, 108.18, 112.62, 119.20, 120.24, 122.88, 125.51, 128.40, 138.25, 169.90. HRMS (FAB⁺): calcd for (C₃₄H₄₉N₆O₂⁺) 573.3912, found 573.3929.

(S)-tert-Butyl (3-(1H-indol-3-yl)-1-oxo-1-(phenylamino)propan-2-yl)carbamate (11a) was prepared according to the general procedure using aniline (200 mg, 2.15 mmol) and Boc-L-Trp-OH. The product was obtained as a white powder (0.65 g, 80% yield). The compound was previously reported³⁶ and the spectra obtained matched those previously reported.

(S)-3-(1H-Indol-3-yl)-1-oxo-1-(phenylamino)propan-2-aminium chloride (11) was prepared according to the general procedure using **11a** (350 mg, 0.92 mmol). The product was obtained as a white powder (0.17 g, 57% yield). The compound was previously reported³⁷ and the spectra obtained matched those previously reported.

5.4.2. Bacterial strains and antibiotics used. K-12 *E. coli* (ATCC 700926) and *S. aureus* (ATCC 29213) were acquired from ATCC. The *S. aureus* strain was used in the BSL-2 facility. K-12 *E. coli* was grown in L. B. Miller media (Sigma-Aldrich) and *S. aureus* was grown in cation adjusted MHII media (Sigma-Aldrich). Tet^R *E. coli* was made by transforming JM109 competent *E. coli* (Promega) with pBR322 plasmid (Carolina Biological) using the manufacturers protocol. Tet^R *E. coli* was grown in L. B. Miller media containing the 100 µg/mL Ampicillin. Ampicillin and tetracycline were obtained from Sigma-Aldrich and dissolved in autoclaved milli-Q water before use.

5.4.3. MICs and Synergy. MIC experiments were performed as described in the Clinical and Laboratory Standards Institute (CLSI) standard microdilution protocols.

Bacteria was grown overnight from one CFU in media without antibiotics. Tet^R *E. coli* was grown in media containing 100 µg/mL ampicillin. On the day of experiment, bacteria were knocked back to O.D. 600 nm = 0.550 in the same media. These exponential phase bacteria were then diluted in antibiotics free media to get 4 x 10⁸ CFU/mL. In a 96-well, plate either L.B. Miller or MHI media was added followed by serially diluted compounds **1-11**, tetracycline, or ampicillin. All the tryptophan based compounds were dissolved in DMSO and the final concentration of DMSO in each well was kept constant at 0.5% (v/v). For the combination experiments, first the BT or control was added to the media in the well followed by the antibiotics. The contents of the well were mixed before adding 20 µL of bacteria to get 4 x 10⁵ CFU/mL per well. The plates were incubated at 37°C, 200RPM for 24 hours before collecting results on the Biotek Cytation 3 plate reader. No more than three plates were stacked on top of each other at a time. Optical density of the wells was determined at λ=600 nm. Cells alone were considered as 0% inhibition and media alone was considered as 100% inhibition. Any inhibition greater than 80% was considered as the MIC. The results were reproduced three times before reporting.

5.4.4. Cytotoxicity to mammalian cells. HeLa (ATCC CCL-2) cells were acquired from ATCC. Cos-7 (ATCC CRL-1651) cells were donated by Dr. C. Dupureur and HEK-293 cells were donated by Dr. M. Nichols. Cell lines were regularly maintained in growth media containing DMEM (ATCC), 10% fetal bovine serum (FBS, ATCC) and 1% penicillin-streptomycin solution (ATCC). Adherent HEK-293, Hela and Cos-7 cells were trypsinized using 0.25% (w/v) trypsin-EDTA (Sigma-Aldrich), suspended in a fresh media and diluted to get a concentration of 3 x 10⁵ cells/ml. Cells were seeded in a 96-well plate (100 µL/well) to get 3 x 10⁴ cells/well. The plates were incubated for 24 hours at 5% CO₂ and 37°C to reach a confluency of 80-90%.

In a sterile 1.5 mL micro-centrifuge tube, compounds **2, 3, 5, 6, 7** and **10** (0.5% DMSO) were mixed with assay media (DMEM + 10% FBS) and serially diluted by 2-fold each to get 2[MIC], [MIC], ½[MIC] and ¼[MIC] concentrations. A control containing 0.5% DMSO was also prepared. After 24 hours, the spent media in the 96-well plate containing HEK-293, Hela and Cos-7 cells (90% confluency) was replaced with 100 µL media containing the compounds **2, 3, 5, 6, 7** and **10** at various concentrations. The cells were incubated at 37°C and 5% CO₂ for 24 hours before performing XTT assay (Sigma-Aldrich). The XTT assay was performed according to the manufacturer's protocol. After 24 hours of treatment with compounds, the media was replaced with PBS and 25 µL XTT was added to each well. The XTT assay works by the reduction of tetrazolium compound by alive cells to the colored soluble formazan product. The absorbance of the product was measured at 450 nm (XTT) and 690 nm (background). Percent survival was calculated by comparing the average absorbance of cells treated with compounds **2, 3, 5, 6, 7**, and **10** to that of cells alone.

Two replicates for each treatment were determined. Average percent survival and standard deviation were calculated.

5.4.5. Membrane permeability. To test the membrane permeability of the Tet^R *E. coli*, the bacteria was first grown overnight from one CFU in media containing 100 µg/mL Ampicillin at 37°C and 200RPM. Tet^R *E. coli* was then knocked back to O.D. 600 nm = 0.550 before use. In a sterile test, cells were added followed by either compounds 2 or 10 at half-MIC concentrations and incubated at 37°C and 200 RPM. The concentration of DMSO was kept constant at 0.5% -by volume in each case. After 30 minutes of incubation, the cells were washed by centrifugation at 3000xg for 5 minutes and re-suspended in sterile phosphate buffered saline (PBS). Propidium iodide (30 µM, Thermo-Fischer) and fluorescein diacetate (60 µM, Sigma-Aldrich) were added to the Tet^R *E. coli* cells in the PBS, mixed by vortexing and incubated at 37°C and 200RPM. After 30 minutes, the cells were washed again by centrifugation at 3000xg for 5 minutes. The pellet was suspended in a fresh PBS, loaded onto a clean glass slide, covered with a cover slip and observed under Zeiss LSM 700 confocal microscope.

To test the permeability of HEK-293 cells, the cells were cultured in growth medium as described above. HEK-293 (90% confluent) were then seeded in a 96-well plate to get 30,000 cells/well. After 24 hours of incubation at 37 °C and 5% CO₂, the spent media was replaced with media (DMEM and 10% FBS) containing compound 2 at either 20 µM or 80 µM. The 80 µM concentration was used to confirm the cytotoxicity of the compound 2 and to make sure that serum did not inhibit its activity. Triton X-100 at 0.1%-by volume (1670 µM) and DMSO 0.5% (v/v) were also used as controls. After 2 hours of incubation, spent media was replaced with PBS containing propidium iodide (30 µM) and fluorescein diacetate (60 µM) and incubated at 37 °C and 5% CO₂. After 2 hour of incubation, the spend media was replaced with fresh PBS and the cells were observed under Zeiss LSM 700 confocal microscope. The images were reported without any alterations. The gain and the intensity in all the images were kept constant.

5.5. References.

- 1 (a) Hargrove, A. E.; Nieto, S.; Zhang, T.; Sessler, J. L.; Anslyn, E. V., Artificial receptors for the recognition of phosphorylated molecules. *Chem. Rev.* **2011**, *111*, 6603-6782. (b) See Chapter 4, Reference 2.
- 2 (a) Bowman-James, K.; Bianchi, A.; García-Espana, E., *Anion Coordination Chemistry*. Eds.; Wiley VCH: New York, 2012, 574 pp. (b) Sessler, J. L.; Gale, P. A.; Cho, W.-S., *Anion Receptor Chemistry*. Royal Society of Chemistry: Cambridge, 2006; 413 pp.

- 3 (a) Kavallieratos, K.; de Gala, S. R.; Austin, D. J.; Crabtree, R. H., Readily Available Non-preorganized Neutral Acyclic Halide Receptor with an Unusual Nonplanar Binding Conformation. *J. Am. Chem. Soc.* **1997**, *119*, 2325-2326. (b) Kavallieratos, K.; Bertao, C. M.; Crabtree, R. H., Hydrogen Bonding in Anion Recognition: A Family of Versatile, Nonpreorganized Neutral and Acyclic Receptors. *J. Org. Chem.* **1999**, *64*, 1675-1683.
- 4 Koulov, A. V.; Mahoney, J. M.; Smith, B. D., Facilitated transport of sodium or potassium chloride across vesicle membranes using a ditopic salt-binding macrobicycle. *Org. Biomol. Chem.* **2003**, *1*, 27-29.
- 5 (a) Gale, P. A.; Sessler, J. L.; Král, V., Calixpyrroles. *Chem. Commun.* **1998**, 1-8. (b) Park, I.-W.; Yoo, J.; Kim, B.; Adhikari, S.; Kim, S. K.; Yeon, Y.; Haynes, C. J. E.; Sutton, J. L.; Tong, C. C.; Lynch, V. M.; Sessler, J. L.; Gale, P. A.; Lee, C.-H., Oligoether-Strapped Calix[4]pyrrole: An Ion-Pair Receptor Displaying Cation-Dependent Chloride Anion Transport. *Chem. Eur. J.* **2012**, *18*, 2514-2523.
- 6 Carasel, I. A.; Yamnitz, C. R.; Winter, R. K.; Gokel, G. W., Halide ions complex and deprotonate dipicolinamides and isophthalamides: assessment by mass spectrometry and UV-visible spectroscopy. *J. Org. Chem.* **2010**, *75*, 8112-8116.
- 7 Yamnitz, C. R.; Negin, S.; Carasel, I. A.; Winter, R. K.; Gokel, G. W., Dianilides of dipicolinic acid function as synthetic chloride channels. *Chem. Commun.* **2010**, *46*, 2838-2840.
- 8 (a) Abel, E.; De Wall, S. L.; Edwards, W. B.; Lalitha, S.; Covey, D. F.; Gokel, G. W., Aggregate formation from 3-alkylindoles: amphiphilic models for interfacial helix anchoring groups. *Chem. Commun.* **2000**, 433-434. (b) Abel, E.; De Wall, S. L.; Edwards, W. B.; Lalitha, S.; Covey, D. F.; Gokel, G. W., The formation of stable vesicles from N- or 3-alkylindoles: possible evidence for tryptophan as a membrane anchor in proteins. *J. Org. Chem.* **2000**, *65*, 5901-5909.
- 9 Ketchum, R. R.; Hu, W.; Cross, T. A., High-resolution conformation of gramicidin A in a lipid bilayer by solid-state NMR. *Science* **1993**, *261*, 1457-1460.
- 10 Doyle, D. A.; Cabral, J. M.; Pfuetzner, R. A.; Kuo, A.; Gulbis, J. M.; Cohen, S. L.; Chait, B. T.; MacKinnon, R., The structure of the potassium channel: molecular basis of K⁺ conduction and selectivity. *Science* **1998**, *280*, 69-77.
- 11 Abel, E.; Fedders, M. F.; Gokel, G. W., Vesicle formation from N-alkylindoles: implications for tryptophan-water interactions, *J. Am. Chem. Soc.* **1995**, *117*, 1265-1270.
- 12 (a) Leevy, W. M.; Donato, G. M.; Ferdani, R.; Goldman, W. E.; Schlesinger, P. H.; Gokel, G. W., Synthetic hydrophile channels of appropriate length kill *Escherichia coli*. *J. Am. Chem. Soc.* **2002**, *124*, 9022-9023. (b) Leevy, W. M.; Gokel, M. R.; Hughes-Strange, G.; Schlesinger, P. H.; Gokel, G. W., Structure and Medium Effects on Hydrophile Synthetic Ion Channel Toxicity to the Bacterium *E. coli*. *New J. Chem.* **2005**, *29*, 205-209. (c) Leevy, W. M.; Gammon, S. T.; Levchenko, T.; Daranciang, D. D.; Murillo, O.; Torchilin, V.; Piwnica-Worms, D.; Huettner, J. E.; Gokel, G. W., Structure-Activity Relationships, Kinetics, Selectivity, and Mechanistic Studies of Synthetic Hydrophile Channels in Bacterial and Mammalian Cells. *Org. Biomol. Chem.* **2005**, *3*, 3544-3550.

- 13 Leevy, W. M.; Weber, M. E.; Gokel, M. R.; Hughes-Strange, G. B.; Daranciang, D. D.; Ferdani, R.; Gokel, G. W., Correlation of bilayer membrane cation transport and biological activity in alkyl-substituted lariat ethers. *Org. Biomol. Chem.* **2005**, *3*, 1647-1652.
- 14 (a) Atkins, J. L.; Patel, M. B.; Cusumano, Z.; Gokel, G. W., Enhancement of antimicrobial activity by synthetic ion channel synergy. *Chem. Commun.* **2010**, *46*, 8166-7. (b) Patel, M. B.; Garrad, E. C.; Stavri, A.; Gokel, M. R.; Negin, S.; Meisel, J. W.; Cusumano, Z.; Gokel, G. W., Hydraphiles enhance antimicrobial potency against *Escherichia coli*, *Pseudomonas aeruginosa*, and *Bacillus subtilis*. *Bioorg. Med. Chem.* **2016**, In Press (doi:10.1016/j.bmc.2016.04.058)
- 15 (a) Center for Disease Control and Prevention, Antibiotic resistance threats in United States, 2013. (b) World Health Organization, Antimicrobial resistance global report and surveillance, 2014.
- 16 King, J.L.; Jukes, T.H., Non-Darwinian Evolution. *Science* **1969**, *164*, 788-798.
- 17 Landolt-Marticorena, C.; Williams, K. A.; Deber, C. M.; Reithmeier, R. A. F., Non-random distribution of amino acids in the transmembrane segments of human type I single span membrane proteins. *J. Mol. Biol.* **1993**, *229*, 602-608.
- 18 Von Heijne, G., Membrane proteins: from sequence to structure. *Annu. Rev. Biophys. Biomol. Struct.* **1994**, *23*, 167-192.
- 19 Chan, D. I.; Prenner, E. J.; Vogel, H. J., Tryptophan- and arginine-rich antimicrobial peptides: structures and mechanisms of action. *Biochem. Biophys. Acta* **2006**, *1758*, 1184-1202.
- 20 Boucher, H. W.; Talbot, G. H.; Bradley, J. S.; Edwards, J. E.; Gilbert, D.; Rice, L. B.; Scheld, M.; Spellberg, B.; Bartlett, J., Bad bugs, no drugs: No ESKAPE! An update from the Infectious Disease Society of America. *Clin. Infect. Dis.* **2009**, *48*, 1-12.
- 21 Sapunarcic, F., Levy, S.B.; Substitutions in the interdomain loop of the Tn10 TetA efflux transporter alter tetracycline resistance and substrate specificity, *Microbiol.* **2005**, *151*, 2315-2322.
- 22 Bolivar, F.; Rodriguez, R. L.; Greene, P. J.; Betlach, M. C.; Heyneker, H. L.; Boyer, H. W.; Crosa, J. H.; Falkow, S., Construction and characterization of new cloning vehicles. II. A multipurpose cloning system. *Gene* **1977**, *2*, 95-113.
- 23 Thanassi, D. G.; Suh, G. S. B.; Nikaido, H., Role of outer membrane barrier in efflux-mediated tetracycline resistance of *Escherichia coli*. *J. Bacteriol.* **1995**, *177*, 998-1007.
- 24 Levy, S. B., Active efflux mechanisms for antimicrobial resistance. *Antimicrob. Agents Chemother.* **1992**, *36*, 695-703.
- 25 Sun, J.; Deng, A.; Yan, A., Bacterial multidrug efflux pumps. *Biochem. Biophys. Res. Commun.* **2014**, *453*, 254-267.
- 26 NCCLS, Methods for Dilution Antimicrobial Susceptibility Tests for Bacteria that grow Aerobically. *National Committee for Clinical Laboratory Standards* **2000**, *5th Edition*, M7-A5.
- 27 Nikaido, H., Preventing of drug access to bacterial targets: permeability barrier and active efflux. *Science* **1994**, *264*, 382-388.

- 28 Straus, S. K.; Hancock, R. E. W., Mode of action of the new antibiotic for Gram-positive pathogens daptomycin: Comparison with cationic antimicrobial peptides and lipopeptides. *Biochem. Biophys. Acta* **2006**, *1758*, 1215-1223.
- 29 Vig, B. S.; Lorenzi, P. J.; Mittal, S.; Landowski, C. P.; Shin, H.; Mosberg, H. I.; Hilfinger, J. M.; Amidon, G. L., Amino Acid Ester Prodrugs of Floxuridine: Synthesis and Effects of Structure, Stereochemistry, and Site of Esterification on the Rate of Hydrolysis. *Pharm. Res.* **2003**, *20*, 1381-1388.
- 30 (a) Lambert, P. A.; Hammond, S. M., Potassium fluxes, first indications of membrane damage in micro-organisms. *Biochem. Biophys. Res. Commun.* **1973**, *54*, 796-799. (b) Hancock, R. E. W., Peptide Antibiotics. *Lancet* **1997**, *349*, 418-422.
- 31 Fuhrhop, J.-H.; Spiroski, D.; Boettcher, C., Molecular monolayer rods and tubules made of α -(L-lysine), ω -(amino) bolaamphiphiles. *J. Am. Chem. Soc.* **1993**, *115*, 1600-1601.
- 32 (a) Shai, Y., Mode of action of membrane active antimicrobial peptides. *Biopolymers* **2002**, *66*, 236-48. (b) Shai, Y.; Makovitzky, A.; Avrahami, D., Host defense peptides and lipopeptides: modes of action and potential candidates for the treatment of bacterial and fungal infections. *Curr. Protein Pept. Sci.* **2006**, *7*, 479-86.
- 33 Kumar, R.; Rai, D.; Lown, J. W., Synthesis and In Vitro Cytotoxicity Studies of Novel L-Tryptophan-Polyamide Conjugates and L-Tryptophan Dimers Linked With Aliphatic Chains and Polyamides. *Oncol. Res.* **2003**, *14*, 247-265.
- 34 Berenbaum, M. C., What is synergy? *Pharmacol. Rev.* **1989**, *41*, 93-141.
- 35 Negin, S.; Gokel, M. R.; Patel, M. B.; Sedinkin, S. L.; Osborn, D. C.; Gokel, G. W., The Aqueous Medium-Dimethylsulfoxide Conundrum in Biological Studies, *RSC Adv.* **2015**, *5*, 8088-8093.
- 36 Huang, Y.; Liu, Y.; Liu, Y.; Song, H.; Wang, Q., C ring may be dispensable for β -carboline: Design, synthesis, and bioactivities evaluation of tryptophan analog derivatives based on the biosynthesis of β -carboline alkaloids. *Bioorg. Med. Chem.* **2016**, *24*, 462-473.
- 37 Shin, C.; Seki, M.; Kakusho, T.; Takahashi, N., Dehydrooligopeptides. XV. Useful syntheses of dehydrodipeptides by the enzymatic coupling of α -dehydroglutamate with various α -amino acid amides using proteases. *Bull. Chem. Soc. Jpn.* **1993**, *66*, 2048-2053.